INFRARED PHOTOMETRY AND POLARIMETRY OF BLAZARS

Paul Anthony Holmes

Presented for the degree of Doctor of Philosophy
at the University of Edinburgh

September, 1984.

This thesis is my own
composition, except where
specifically indicated in the text

September, 1984

Abstract.

A sample of blazars has been studied with infrared photometry and polarimetry in the J,H & K wavebands, using the U.K.I.R.T. in Hawaii. The objects observed for this thesis are part of an ongoing monitoring programme, for which a total of 35 objects have now been studied, many for the first time with infrared polarimetry. These results have been analysed statistically and several important correlations have emerged.

Wavelength-dependent polarization has been observed in some objects, and our observations show, for the first time at infrared wavelengths, a correlation between the strength of wavelength-dependence and the polarization degree. This result, together with an analysis of night to night variations in total and polarized flux, allow us to formulate a phenomenological model for these objects. Luminosity calculations suggest that relativistic beaming is important in the most luminous objects. The exotic polarization behaviour of OJ 287, which was observed in January 1983, is explained in terms of a relatively simple two-component model.

The properties of blazars as a class are reviewed and brief histories of the individual objects are given. The results of our observations are described in detail in chapters 4 & 5. Computer simulations were performed to determine the polarization properties of various distributions of magnetic field and electron energies, and the results tabulated. Current models for the spectral and polarization properties of blazars are described in some detail. The implications of the results presented in this thesis upon these models are also discussed.

Acknowledgements.

I wish to thank Peter Brand for being an excellent superviser and friend throughout the course of my research, and for introducing me to the exciting world of blazars. Thanks are also due to my co-workers Chris Impey and Perry Williams for their help and encouragement during my trips to Hawaii. Chris was an amusing and eccentric co-observer, and Perry was invaluable as a proficient telecope driver.

For my first two years, Steve Heathcote was a patient and indispensible wizard, being a willing help and bottomless source of wisdom in many subjects.

I am grateful to Susan Hooper for her flawless typing, not only of parts of this thesis, but also of many documents, papers, tables etc. Thanks also to Marjory Fretwell for her superb illustrations.

Thanks are due to Colin Aspin, Mark Toner and Peter Meadows for help with producing the hard copy. Colin, for a cable, Mark, for an extra pair of hands and Peter, for coffee and sandwiches.

I would like to thank Drs Gerry Gilmore and John Peacock for reading the first draft of this thesis, and whose comments helped to tidy up the presentation considerably.

Finally, I am very grateful to the Robert Cormack Bequest Fund for the award of a studentship, without whose continued support this work would not have been possible.

CONTENTS

Chapter 1. Introduction.

1.1 Discovery.

BL Lacertae objects (BL Lacs) have been the subject of much study since 1968 when John Schmitt (1968) identified the "variable star" BL Lacertae with the unusual radio source VRO 42.22.01. MacLeod and Andrew (1968) made observations of this radio object with the 46-meter telescope at the Algonquin Radio Observatory, and discovered an unusual spectrum. The double-bumped spectrum at centimeter wavelengths suggested the presence of two components which become optically thick at different frequencies. They found a few percent polarization, and a rotation measure that was consistent with VRO 42.22.01 being an extragalactic object.

Rapid variations at radio wavelengths were observed by several authors (e.g. Andrew et al. 1969). The optical spectrum was shown to be featureless, with neither emission nor absorption lines (Oke, Neugebauer & Becklin, 1969) and also a relatively high degree of linear polarization was observed by Visvanathan (1969). The image is non-stellar on Palomar Sky Survey plates, and Miller, French and Hawley (1978) demonstrated that BL Lac lies at the nucleus of an elliptical galaxy with an emission line redshift of $z=0.0695$.

1.2 Review of Characteristics.

Since the identification of BL Lac as an unusual extragalactic object, many more objects have been found with similar characteristics, and are classified, after the prototype, as BL Lacertae Objects. The number of BL Lac and BL Lac-like objects known is rapidly increasing with time. The review by Stein, O'Dell and Strittmatter (1976)

(SOS) contains 32 objects, and the review of highly polarized extragalactic objects by Angel and Stockman (1980) (AS) contains 56 objects. More than 80 BL Lac objects are now known (Hewitt & Burbidge 1980; SOS; AS). The main properties of BL Lac objects are now briefly described.

1.2.1 Radio Properties.

All BL Lac objects are radio-emitters. Selection techniques favour radio-emitters as most BL Lacs have been found by identifications with accurate radio positions of flat spectrum radio sources. Despite the selection effects, it appears that radio-quiet BL Lacs are very rare. The few BL Lacs that have been selected by optical methods are also strong radio-emitters. In his thesis, Impey (1981) describes an optical search technique based on high linear polarization. Several possible candidates emerged although none have yet been convincingly demonstrated to be radio-quiet BL Lac objects. It is possible that the lack of known radio-quiet BL Lacs is not a selection effect, as BL Lacs are intrinsically stronger emitters at radio frequencies than at optical frequencies compared with quasars (Weiler & Johnson 1980; Sramek & Weedman 1980).

Angel and Stockman (1980) list 19 highly polarized quasars with strong emission lines. Only one of these, 2225-055 (PHL 5200), is radio-quiet. There is some doubt, however, as to whether this object may be classified as a BL Lac-like object, since it has a constant polarization (p=4%) and no observed flux variability.

Most BL Lac objects have a very compact radio core coincident with a bright optical nucleus (Weiler and

Johnston 1980). In his sample of 27 BL Lac objects, Wardle (1978) found approximately 50% had extended structure (10-200 arc seconds) at centimeter wavelengths. 2 objects have extended double structure, although none have been found with the classic double-lobed structure.

The radio spectra of BL Lacs differ from those of quasars. BL Lacs have a typical spectral index of $\alpha \simeq 0$ ($\alpha = -d \ln S_\nu / d \ln \nu$) and remain optically thick up to approximately millimeter wavelengths (O'Dell et al. 1978; Smith 1984) whereas quasars tend to have $\alpha \simeq 0.2$ below 5 GHz and be optically thin above 10 GHz (Kellerman and Pauliny-Toth 1972).

One of the most striking features of BL Lac objects is the variability of radio flux. BL Lacs show both (i) a larger amplitude and (ii) more rapid flux variability than quasars, indicating that they are an extremely active sub-set of the quasar phenomemon.

1.2.2 Optical/Infrared Properties.

The continuity of flux and polarization properties from optical to infrared wavelengths indicates that the observed radiation originates from the same physical emission region. The optical/infrared continua of BL Lac objects may be well approximated by a power-law (see section 4.6) implying a non-thermal origin. Similar to the radio flux, the optical/infrared flux is highly variable on short timescales. Archival flux changes of $\Delta m \sim 5$ magnitudes have been recorded for some objects. There has been marginal evidence for periodicity at varying timescales, from minutes to days, although such periodocity has never been positively confirmed. Similar behaviour is seen in OVV quasars and the varia-

tions seen in "normal" quasars and Seyfert nuclei are only 10-20%.

The continuum shape remains fairly constant throughout large variations in flux. Short term variations in spectral slope have, however, been observed in some objects (e.g. 2254+074, $\Delta\alpha \sim 0.6$ in one hour; Tapia et al. 1976). The small number of sub-millimeter observations available reveal little deviation from a simple interpolation between radio and infrared fluxes. There is some continuity between radio and optical/infrared properties. Simultaneous outbursts in these two wavelength regimes have been observed in several objects. The timescale of variations at radio wavelengths is usually much longer than for the shorter wavelengths, however, and the radio linear polarization is seldom as high as 10%.

1.2.3 Polarization.

The property of BL Lac objects (and OVV quasars) that distinguishes them from other active extragalactic objects is their high and variable degree of linear polarization. Mechanisms that can produce high degrees of polarization are discussed in section 9.2. There is a distinct bi-modal distribution in the polarization properties of extragalactic objects, with a pronounced dip between 2-3% (Stockman 1978). The vast majoriy of quasars have polarizations of $p_{opt} \leqslant 2\%$. It is reasonable, then, to consider those extragalactic objects with polarizations $p_{opt} \geqslant 5\%$ (say), including OVV quasars and BL Lac objects, as one class of object.

One of the original "defining" characteristics of BL Lac objects was the lack of spectral lines. As observations

improved, weak spectral features were discovered in objects previously thought to have none, and the definition was relaxed. The similarities between the properties of OVV quasars (which have strong emission lines) and BL Lac objects (which do not) suggest that they may indeed belong to the same class of object. Spiegel (Angel and Stockman 1980) suggested the name "Blazar" for this class, the name adopted throughout this thesis.

Although the degree of linear polarization is high (up to 44%, Impey, Brand & Tapia 1982), the circular polarization is undetectable or present at only a few tenths of a percent (Stein, O'Dell & Strittmatter 1976, and references therein). Near the spectral maximum, circular polarization has been observed in excess of 1%, although it has been suggested that the conversion of linear to circular polarization dominates the intrinsic contribution (ibid.).

Faraday effects are very small. Observations of AO 0235+164 by Ledden and Aller (1979) (see section 8.5.1) at two radio wavelengths ($\lambda\lambda$ 8.0,14.5 cms) rule out all frequency-dependent effects, such as Faraday rotation, since the rotation varies inversely as the square of the frequency ($\Delta\theta \propto \nu^{-2}$). The lack of observed Faraday rotation in an object sets limits on the ratio of thermal to relativistic electrons in the source, since the rotation outside the source (in the intergalactic medium or in our galaxy $|b^{II}| > 25$) is small. The lack of observed Faraday rotation is some sources sets limits of $n_e / n_{rel} < 10^{-4}$ (Wardle 1977).

1.2.4 Summary of Properties.

At the Pittsburgh Conference (Wolfe 1978), much discussion was devoted to the problem of the defining characteristics of BL Lac objects. With so heterogeneous a sample, it is difficult to find properties common to all objects.

One of the original defining characteristics was the absence of emission lines. As observations improved, this condition was relaxed to "weak or no emission lines". The bi-modal distribution of the polarization degree in extra-galactic sources indicates a natural dividing line between "normal" quasars and the more active OVV quasars and BL Lac objects. As discussed in sub-section 1.2.3, the name "blazar" will be used for this class of object throughout this thesis.

A safe definition of blazars, therefore, could be "highly polarized, rapidly variable, non-thermal extra-galactic sources". The common properties of blazars may be summarized as follows.

(i) A high and variable degree of linear polarization with very little or no circular polarization.

(ii) Rapid timescales of variability of flux and polarization properties at all frequencies.

(iii) Non-thermal radiation from radio to optical frequencies.

(iv) Power-law flux distributions, most noticeably at infra-red frequencies.

(v) Usually a featureless spectrum.

(vi) Rotations of polarization position angle at all frequencies.

(vii) Usually a star-like image, although some objects have extended structure, and some are embedded in elliptical galaxies.

In many respects, blazars are similar to quasars, but there are distinguishing features. The primary differences are:

(i) The majority of objects classed as blazars are BL Lac objects, which, unlike quasars, have weak or no emission lines.

(ii) Blazars usually have steeper optical and flatter radio continua than quasars.

(iii) Blazars are, by definition, more highly polarized than quasars.

(iv) Variability in blazars at radio and optical/infrared frequencies is usually more rapid and of a larger amplitude than quasar variability.

There is a continuity of properties from BL Lacs, through highly-polarized and normal quasars, to Seyferts and N galaxies, and yet there is no widely accepted physical explanation for the primary differences between blazars and quasars listed above. Neither is it certain where we should draw the line between these different classes of object, and what the physical significance is of doing so. For example, is the absence of emission lines in BL Lacs more significant than the bimodal distribution in polarizations? Suggestions have been made by several authors to explain these differences.

Altchuler & Wardle (1975) have suggested that the more variable BL Lacs are young quasars which have not yet

ejected much material from the core. They find that the "average" polarization of blazars (meaning a vector average of all the observations) is small, although the individual observations show much higher polarizations, whereas the non-BL Lac type sources tend to have a much more strongly polarized constant component. For the 4 BL Lacs studied, the large amplitude variations and absence of steep spectrum components indicate that these objects are extremely young and have yet to develop extended non-variable structures.

There has been much speculation upon the reason for the absence of spectral lines in BL Lac objects, and these are discussed in SOS. It is possible that the non-thermal continuum completely dominates the emission line flux. However, many BL Lacs have been observed at well below peak brightness with still no spectral features, which tends to argue against such an explanation. Another possibility is that there is insufficient ultraviolet radiation to excite the surrounding gas. The observed steepness and curvature (see section 4.6) in the flux distribution support this. The ultraviolet cut-off needs to be rather severe to make the Ly α and Hβ lines undetectable. It is not known if such a cutoff is a general feature of BL Lacs.

A third possibility is a lack of gas surrounding the source. There is clearly not a total absence of material, as many BL Lacs are known to have weak spectral features, although in several cases, these are due to host or intervening galaxies.

Perhaps the most commonly-hypothesised explanation of the differences between blazars and quasars is beaming

towards the observer. This has been discussed by several authors (e.g Blandford & Rees 1978; Schwartz & Ku 1983). Relativistic beaming along the line of sight can produce several effects that are seen in blazars, such as flux boosting, rapid variations and large amplitude swings of position angle (see discussion in 4.4.7). Blandford & Rees (1978) point out that beaming may suppress emission lines. Another obvious consequence is that extended double radio structure should not be seen in blazars, which is indeed the case. There may, however, be a problem with space density arguments. The probability of a suitable orientation varies as the square of the bulk Lorentz factor of the jet, although there will be a strong selection effect in favour of such sources. The quantitative details depend critically upon the luminosity function of blazars, which is unknown. Schwartz & Ku (1983) estimate the local volume density of BL Lac objects, based on Einstein X-ray observations, which they find to be the same order of magnitude as the local densities of Seyfert galaxies and optically selected quasars. They argue that this indicates that orientation is not solely responsible for the differences between quasars and BL Lac objects.

The primary disinction between blazars and quasars is that of polarization degree. If the mechanism for producing polarization is the same in these two classes of object, namely synchrotron radiation, then we may infer either (a) a more ordered magnetic field in blazars, giving rise to an intrinsically higher polarization degree or (b) a depolarizing mechanism present in quasars. If difference is

correct, then we can envisage a mechanism such as turbulence causing the magnetic field lines to "tangle" in the synchrotron emitting region. Alternatively, there may be a depolarizing mechanism extrinsic to the emitting region. Two depolarizing mechanisms have been considered by Stockman (1978), namely Faraday depolarization and scattering.

When light traverses a medium with an embedded magnetic field, B, the position angle of polarization will rotate ($\Delta\theta \propto \nu^{-2} B$). Since we observe over a finite bandwidth, there will be a certain amount of "cancellation" or depolarization. Stockman considers two types of scattering mechanisms: scattering from dust and from free electrons. While the mechanisms mentioned above could undoubtedly cause depolarization, there is some doubt as to whether quasars actually do produce polarization by the synchrotron process, as suggested in the previous paragraph.

Stockman, Moore & Angel (1983) discuss the origin of polarization in quasars. They point out that, while the highly polarized quasars (HPQs) are consistent with the canonical synchrotron hypothesis, this is by no means certain for "normal" quasars (or LPQs). They argue that it is unlikely that LPQs are simply depolarized or diluted HPQs, since LPQs lack significant polarimetric variations, which are the hallmark of HPQs and blazars. The consider electron and dust scattering, and also stable but disordered synchrotron emission. They conclude that only "dust scattering from a disk or oblate cloud produces the correct polarization characteristics of the LPQs", i.e. lack of variab-

ility, alignment with radio lobe structure, and a weak wavelength-dependence ($dp/d \ln \nu > 0$).

We see from the above discussion that, while blazars and "normal" quasars have several characteristics in common, there may be fundamental physical differences. The distinction may be relatively simple: for example, LPQs may have more dust and gas surrounding the emitting regions than blazars, thus causing depolarization, scattering and emission lines. It is unknown whether the differences are relatively "superficial" or whether blazars and normal quasars represent two distinct classes of object. Ultimately, analysis of complete sample of all classes of AGN will provide the answer to this question.

1.3 The Monitoring Programme.

The first observations in the monitoring programme made in December 1979. All observations were made using the 3.8 meter United Kingdom Infrared Telescope on Mauna Kea and the Brand/Impey polarimeter, and are described in chapter 2. At the beginning of the programme, very little infrared polarimetry work had been done on BL Lac objects. The primary purpose of monitoring these objects was to establish a sufficiently large database for a statistical analysis of the various properties. The secondary thrust of the programme was to observe unusual objects in more detail. If an object was undergoing a flare or exhibited unusual polarization properties, for example, it was observed every night of the current observing run, and two objects were observed with multiwavelength photometry and polarimetry also. Two papers resulted from these multiwavelength coll-

aborations: AO 0235+164 (Impey, Brand & Tapia 1982) and OJ 287 (Holmes et al. 1984c, hereafter H+13; see also chapter 5).

Four data papers have also resulted from our programme, namely Impey et al. 1982, 1984 (hereafter papers I & II respectively) and Holmes et al. 1984 a,b (hereafter papers III & IV respectively). The blazars observed were chosen primarily from the two aforementioned reviews. There was clearly a bias towards the more interesting objects (the brighter, more variable and more highly polarized objects). However, a total of 35 blazars have now been observed at least once in our programme, and this number represents more than 50% of those attainable from UKIRT.

This thesis attempts to answer, at least in part, the question posed at the end of section 1.2. Ideally, complete samples are required to enable astronomers to determine the different natures of blazars and quasars as separate classes of object. It will be some time before it is possible to compile a complete sample of objects so heterogeneous as blazars. This thesis presents the data from the monitoring programme, and also offers a phenomenological description of the behaviour of blazars at infrared wavelengths.

Chapter 2. Observations.

2.1 Description of Observations.

All the infrared observations reported here were carried out on the 3.8 meter United Kingdom Infrared Telescope (UKIRT) on Mauna Kea, Hawaii, using a photovoltaic Indium Antimonide (InSb) detector and a rotating HR polaroid followed by a Lyot depolarizer. All the data were collected in three runs in November 1982, January 1983 and January 1984. Of the first run, only 25th November was not lost to cloud. Of the 6 consecutive nights in January 1983, only half a night was lost to cloud; the weather was otherwise excellent. The final run in January 1984 lost the first night to cloud and freezing fog. Of the 5 remaining nights in the final run, there were some problems with telescope windshake and atmospheric transparency, and consequently, poorer photometric accuracy.

24 blazars were observed photometrically, 18 of which were observed polarimetrically also, several of these for the first time in the infrared. A total of 9 objects was observed quasi-simultaneously with three-colour (J,H,K) photometry and polarimetry. The f/35 chopping secondary was used with a chopping frequency of 7-8 Hz. The instrumental sensitivity was calculated several times per night. Broad band filters were used and their effective wavelengths were J(1.25 microns), H(1.65 microns), K(2.2 microns) and L(3.4 microns).

Analyser efficiency and position angle zero point were redetermined each time the polarimeter was mounted on the telescope. Photometric offset magnitudes were calculated

by observing photometric standards near the zenith, and correcting for atmospheric extinction. Flux calibrations have taken into account the effect of differing flux distributions of the objects and calibrators in the broad pass bands.

The polarimetry was calibrated using nearby unpolarized stars. For the first two runs, the instrumental polarization (calculated at least twice per night),of less than half a percent, was repeatable over the run to better than one quarter percent. For the last run, the calculation was made twice per night, with the exception of 9th and 10th January. Only one determination was made on 9th January and polarimetric standard observations were spoilt by cloud on 10th January. The instrumental polarization for this run was, on average, $\beta \leqslant 0.4\%$, repeatable to a quarter percent.

The "patchiness" of the interstellar medium makes the extinction difficult to determine accurately. Estimates of the interstellar extinction correction were taken from maps of reddening derived from HI and galaxy counts (Burstein and Heiles 1982), and by using the extinction values of Savage and Mathis 1979. Seven objects required significant correction ($A_K \geqslant 0.03$) and only seven objects required no correction at all. See Table 2.1.

2.2 Procedure.

In this section observational procedure is briefly described. Fuller details of the equipment used and observing procedures are given by Impey (Thesis 1981).

2.2.1 Polarimeter.

The polarimeter was mounted on the telescope, for

each of the three runs, in the configuration shown in figure 2.1. The instrumental polarization was greatly improved over the previous runs in the monitoring programme by including a Lyot depolarizer in the optical system. A Lyot depolarizer consists of a thick phase plate of many waves retardation followed by a second plate twice as thick as the first with its reference axis set at 45° to the first. Such a depolarizer is ideal for use with broad band filters as it averages over wavelength. The polarimeter consists of a sheet of HR polaroid rotated by a stepper motor. The offset angle is defined as that angle, measured North through East, between the polaroid transmission axis and due North. This angle was estimated at the telescope and used in the on-line reduction. The angle was calculated exactly by comparison with results from polarimetric standards.

2.2.2. Crossed Polaroids Test.

This test is performed to determine the analyser efficiency. A second sheet of HR polaroid is inserted and remains fixed while the analyser rotates. HR polaroid has an efficiency of almost 100% for shorter wavelengths, but this drops to ~88% for the K waveband.

2.2.3. Dichroic Mirror.

A dichroic mirror was placed in the beam as shown in figure 2.1. Optical light is transmitted through to the Scanco TV system, which is used for finding and guiding. The infrared beam is reflected through the variable filter and aperture wheels onto the InSb detector.

2.2.4. Detector and Cryostat.

The detector is a 0.5 mm piece of a photoconductive

material called Indium Antimonide. It has a high impedance and two values of feedback resistor. The high resistance is generally used for observations of blazars, except for the longer wavelength (L) observations of the brighter objects, since the signal amplitude is proportional to the feedback resistance. Low resistance is used for observing bright standard stars.

The detector and preamp circuitry are mounted inside a dewar maintained at cryogenic temperatures, in order to reduce the detector noise.The inner and outer jackets of the cryostat are filled with liquid Nitrogen (T=77 K) and pumping of the inner jacket reduces the temperature to T $\sim$ 65 K. Another method of reducing the detector noise is a technique called flashing. This has become a standard technique although the mechanism is not well understood. It has been found that shining a torch onto the detector through the largest aperture and shortest wavelength filter reduces the noise by a factor of $\sim$3.

2.2.5. Chopping and Nodding.

Because the object signal is often very much smaller than the sky signal for faint sources such as blazars, the technique of star/sky chopping is used. Chopping alternately flicks the signals from a) sky and b) star and sky onto the detector by moving the optic axis. This can be done by either focal plane chopping, by vibrating the dichroic, or by a chopping secondary. On UKIRT, the latter method is used, the secondary now being driven electronically. A phase sensitive detector (p.s.d.) is used to subtract the sky signal from the signal of star and sky. The output of the

p.s.d. is then a D.C. voltage, which goes to a V-F converter. The output is a series of pulses which is converted to a count rate and then to an instrumental magnitude.

This sky subtraction is only a first appoximation, as it takes no account of sky brightness gradients. This effect is removed by beam switching, or "nodding". Nodding centres the detector on two different positions (reference beams) to remove sky gradients and telescope asymmetries. The beam is switched normally every 10 seconds or so. The value of the sky brightness which is then subtracted is the average value of the sky brightness in the two reference beams.

2.2.6. Focus and Beam Profiles.

Best infrared focus was normally slightly different from the best optical focus. Clearly, for a small detector, the best possible focus is essential. Thermal changes within the dome will alter the focus and this was therefore checked at least twice per night.

Beam profiles were checked at the beginning of every night. Normally, little or no adjustment was needed after the first night of each run, but on the third run in January 1984, significant adjustments of the dewar were required each night.

Beam profiles were taken by letting a bright star drift through each beam. Profiles should have steep sides and a plateau, otherwise signal can be lost by small deviations in guiding and centring, leading to systematic errors if a different part of the detector is used for object and standard.

TABLE 2.1 Interstellar Extinction

Galactic coordinates calculated from:

$$\sin b'' = \sin\delta \cos 62.6 - \cos\delta \sin 62.6 \sin(\alpha - 282.25)$$

$$\cos b'' \cos(l'' - 33.^{\circ}0) = \cos\delta \cos(\alpha - 282.25^{\circ})$$

$$\sin\delta = \cos b'' \sin(l'' - 33.^{\circ}0) \sin 62.6 + \sin b'' \cos 62.6$$

E(B-V) values from Burstein and Heiles (1982).

R_λ (= $A_\lambda/E(B-V)$) are tabulated in Savage & Mathis (1979).

Values used: $R_J = 0.87$, $R_H = 0.63$, $R_K = 0.38$, $R_L = 0.16$

OBJECT	GAL. COORDS. l"	b"	E(B-V)	A_J	A_H	A_K
0215	162	-54.5	∿0.02	0.02	0.01	0
0219	140	-17	0.09	0.08	0.06	0.03
0235	157	-39	0.09	0.08	0.06	0.03
0422	194	-39	0.07	0.06	0.04	0.03
0735	202	+18	0.09	0.08	0.06	0.03
0736	217	+11	0.14	0.12	0.09	0.05
0752	195	+25	0.03	0.03	0.02	0.01
0754	211	+19	∿0.02	0.02	0.01	0
0808	221	+19	∿0.02	0.02	0.01	0
0818	235	+13	0.09	0.08	0.06	0.03
0829	221	+24	0.03	0.03	0.02	0.01
0912	197	+43	∿0.02	0.02	0.01	0
1253	305	+57	0.02	0.02	0.01	0
1418	98	+58	0.03	0.03	0.02	0.01
2200	93	-10	0.40	0.35	0.25	0.15

0048-097, 0420-014, 1147+245, 1156+295, 1215+303, 1219+285, and 1308+326 required no correction.

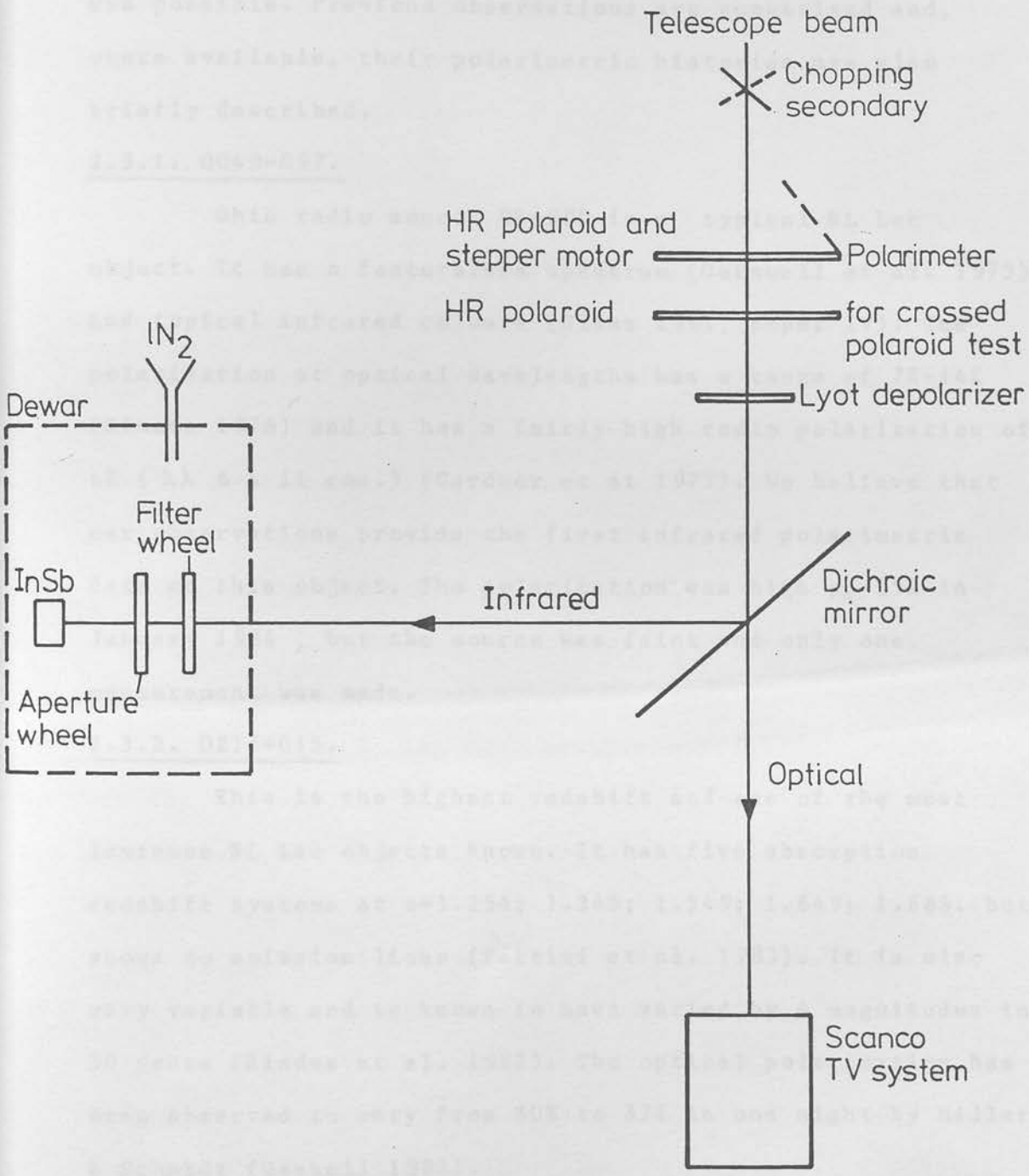

Figure 2.1 Schematic Diagram of the Polarimeter System.

2.3 Objects.

All the objects observed in the three runs are described in the following sub-sections. For some of the brighter, better-studied objects, some attempt at modelling was possible. Previous observations are summarised and, where available, their polarimetric histories are also briefly described.

2.3.1. 0048-097.

Ohio radio source OB-080 is a typical BL Lac object. It has a featureless spectrum (Carswell et al. 1973) and typical infrared colours (Glass 1981; paper IV). The polarization at optical wavelengths has a range of 7%-14% (Kinman 1976) and it has a fairly high radio polarization of 6% ($\lambda\lambda$ 6 & 11 cms.) (Gardner et at 1975). We believe that our observations provide the first infrared polarimetric data on this object. The polarization was high p_K=15% in January 1984 , but the source was faint and only one measurement was made.

2.3.2. 0215+015.

This is the highest redshift and one of the most luminous BL Lac objects known. It has five absorption redshift systems at z=1.254; 1.345; 1.549; 1.649; 1.686. but shows no emission lines (Pettini et al. 1983). It is also very variable and is known to have varied by 4 magnitudes in 30 years (Blades et al. 1982). The optical polarization has been observed to vary from 30% to 37% in one night by Miller & Schmidt (Gaskell 1982).

We observed 0215+015 on 10th and 12th January in 1983. Although the polarization was high (16%-17%), the

object was faint (H=13) which precluded further observation. There was no evidence for variability over a timescale of two days. It was observed again in January 1984, and showed pronounced wavelength-dependence (see figures 7.1). p_K was constant, to within errors, on each of the four consecutive nights. The position angles θ_K showed a rotation of $\Delta\theta \simeq 10^\circ$ on 3 consecutive nights.

2.3.3. 0219+428.

3C 66A has a highly tentative redshift of z=0.444, identified from an MgII emission feature (Miller et al. 1978). The optical polarization has been observed to vary form 3% to 15.5%, and the optical flux by 1.25 magnitides (Zekl et al. 1981).

We observed it on 3 consecutive nights in January 1983 and found no evidence for variability in flux or position angle. Wavelength-dependence of $(dp/d\lambda > 0)$ was seen on the first two nights but was absent on the third.

2.3.4. 0235+164.

AO 0235+164 has two absorption redshift systems at z=0.524 and z=0.852 (Rieke et al. 1976) and is very variable in flux and polarization from radio to optical wavelengths (Spinrad & Smith 1975). There have been several outbursts (e.g. Impey, Brand & Tapia 1982) and during two there was evidence for correlated radio/optical activity (Ledden, Aller & Dent 1976; Balonek & Dent 1980). The optical polarizaton has a range of 5%-44% (Angel and Stockman 1980) and from 2%-36% in the infrared (Paper I; Impey, Brand & Tapia 1982). Although there was no evidence for flux variability in January 1983, this object brightened by about 1 magnitude

between 25th November and 8th January.

There was a strong wavelength-dependence of polarization in November, with p increasing with frequency, but this dependence was absent in January 1983. There appeared to be stochastic changes in the polarization behaviour from night to night, the position angle remaining relatively stable whilst the polarization degree varied by a factor of two between 8th and 9th January 1983. Between the two observing runs in November and January, there was a rotation in position angle of approximately 70° and a steepening of the spectral index from 1.1 to 1.6. When observed again in the January 1984 run, the object had dimmed and the polarization dropped to 3-4%, with a 40° rotation in successive nights (7th-8th January).

2.3.5. 0420-014.

Ohio Radio Source OF-035 (also OA 129) was identified by Bolton & Wall (1970). It has an emission line redshift of z=0.915 (ibid.) and an absorption line redshift of z=0.633 (Miller, French & Hawley 1978), with a high and variable optical polarization (ibid.). The source was too faint for accurate polarimetry in January 1984, and it was observed in 3-colour photometry on one night only.

2.3.6. 0422+004.

One of the lesser studied BL Lac objects, 0422+004 is an Ohio Radio Source OF 038 with no published redshift. It has an optical polarization range of 6%-22% (Angel et al. 1978) and an archival variability of 1.5 magnitudes (Kinman 1976). We believe these observations provide the first infrared polarimetric data on this object.

Two nights observations showed the source to have dimmed $\Delta m=0.3$ with an increase in polarization p =13.6%-19.8%. No rotation in position angle was observed. This object was observed again in the final run. The polarization had dropped to around 6% and the position angle changed to $\theta \sim 40^{\circ}$ from the January 1983 value of $\theta \sim 166^{\circ}$.

2.3.7. 0735+178.

This object has an absorption redshift of z=0.424 and a high and variable polarization in the infrared (papers I & II). It has undergone several outbursts with subsequent steep declines and has twice been observed to rise to maximum brightness from deep minima on very short timescales (Zekl et al. 1981). 0735+178 sometimes exhibits wild fluctuations in polarization and brightness but occasionally shows periods of stability with $p \sim 22\%$ (Angel et al. 1978; paper I).

Five nights observing in January 1983 showed relative stability of flux, polarization and position angle. Paper I reported that polarization increased towards shorter wavelengths, but such behaviour was not observed in this run. A large rotation of position angle was observed between November 1982 and January 1983, $\Delta\theta \sim 80^{\circ}$.

It was observed again on 3 consecutive nights in January 1984. It exhibited significant wavelength-dependence, with polarization increasing with frequency (as previously noted) esp. on 9th January (p_K =3.8%, p_J =8.3%).

The position angle remains fairly stable ($\theta \sim 24^{\circ}$), except for a sudden rotation with wavelength on 11th January ($\theta_K=8^{\circ}$, $\theta_{J,H}$ =25°). See figures 7.2. Such behaviour is

consistent with the two superposed component model discussed in chapter 5.

2.3.8. 0736+017.

This object is a BL Lac-like object as it has variable optical polarization 0%-6% (Moore & Stockman 1980) and strong Hα and Hβ optical emission lines. Our January 1983 data are the first infrared polarimetric observations. One year later, the polarization had dropped from 7% to 3% and the position angle had rotated from 44^{o} to 144^{o}.

2.3.9. 0752+258.

OI 287 (also VR 25.07.04) was identified by Wills (1976), and has an emission line redshift of z=0.446 (Wills and Wills 1976) Stockman (1978) observed it on 3 occasions and found no evidence for variability. This object qualifies for inclusion in our monitoring programme as a highly polarized quasar (Stockman 1978). It was observed for one night only on the final run, and was too faint to make polarimetry or further photometry worthwhile.

2.3.10. 0754+100.

This Ohio Radio Source OI 090.4 has a range in optical polarimetry of 3%-26%, and has been observed to vary from 5%-10% polarization in only 4 hours (Angel et al. 1978). The infrared polarization is also variable (2%-19%) (papers I & II). It has an archival variability of Δ m=2.5 mag and given the rapid variability of polarization, it would be surprising if rapid flux variations were not eventually observed. During the January 1983 observing run, only small fluctuations in flux and polarization were seen and the position angle remained fairly stable. By January 1984,

the flux had halved, the position angle had rotated through $\Delta\theta \sim 60^{\circ}$, but the polarization degree remained roughly constant at $p \sim 9\%$.

2.3.11. 0808+019.

A relatively little-studied object, 0808+019 is a flat spectrum radio variable (Browne and McEwan 1972). Spectral features have been observed (Strittmatter et al. 1974). It has a high and variable optical polarization (p=4%-14%) with no preferred position angle (Kinman 1976). It was observed photometrically for one night in the final run, in one waveband only, as it was barely above threshold detectability.

2.3.12. 0818-128.

OJ-131 is a flat spectrum source identified with a blue polarized source by Tapia et al. (1977). It has a very high and variable optical polarization (9%-36%) (see paper II) and a flux variability of $\Delta m=2.9$ mag (Craine et al. 1978). Similar to 0752+258, three-colour photometry on one night in the final run showed this object to be too faint for further observation.

2.3.13. 0829+046.

This Parkes and Ohio Source has an optical polarization range of p=1.7%-22% (Zekl et al. 1981) and an archival magnitude range of $\Delta m=3.6$ (Weiler & Johnson 1980). There is no published redshift data. Our observations, which are the only infrared polarimetry data for this object, reveal a high and variable polarization, and variable flux. 0829+046 was observed on 3 consecutive nights in January 1983. The object brightened by $\Delta m \sim 0.5$ mag corresponding to an incr-

ease in the polarization by a factor of two, and a small rotation in position angle of $\Delta\theta \sim 10^{\circ}-15^{\circ}$. This behaviour is consistent with a variable component turning on. This variable component is a highly-polarized power-law source, with $p \sim 30\%$ and $\theta \sim 109^{\circ}$, and a spectral index $\alpha = 0.86$. See discussion and diagram in section 4.2.

In the January 1984 observations of this object, the flux had dropped by more than a factor of 2. Between 7th and 10th January 1984, the position angle rotated through $\Delta\theta \sim 50^{\circ}$, the polarization dropped from 9.4% to 6.1% (cf. January 1983 p= 14%), while the flux remained almost constant.

2.3.14. 0851+202.

OJ 287 is perhaps the best studied and the most rapidly variable BL Lac object known. It has shown large amplitude (Δ m > 4 mag) and rapid (Δt<1 hour) variability at radio, infrared and optical wavelengths (Visvanathan & Elliot 1973; Véron & Véron 1975; Wolstencroft, Gilmore & Williams 1982; Valtaoja et al. 1982). The optical polarization has a range of 0.4%-29% (see chapter 5; Angel & Stockman 1980). It has a tentative emission line redshift of z=0.306 (Miller, French & Hawley 1978) identified from a single O III line.

Periods of wavelength-dependent polarization have been observed by Kikuchi et al. (1976) but there was no evidence for it in the data of paper II. The data presented in paper III, together with simultaneous optical polarimetry, exhibit exotic polarization behaviour and variable flux, including a remarkable 80° rotation between the V & I

wavebands. This behaviour may be explained in terms of two superposed synchrotron components (see chapter 5). Our data reveal large variations in flux and polarization properties, with the flux decreasing by 7% in one hour from a peak brightness which corresponded to a minimum in the polarization degree.

We observed OJ 287 again in January 1984, and found it in a relatively low luminosity state. There was marginal evidence for wavelength-dependence ($\overline{P}_K$=10.4%, $\overline{P}_{H,J}$ =12.5%) with small variations from night to night (see figure 7.3). The polarization gradually increased with time, and the position angles were relatively stable, $\Theta \simeq 113^{\circ} \pm 9^{\circ}$. Analysis of the internight variations shows a result very similar to that of 0829+046 (paper III). The source dims by $\Delta m \sim 0.25$ mag consistent with a shallow-sloped non-thermal source turning off. The variation in flux is too small to give accurate polarization properties for the variable component. Despite fluctuations in flux (Δm=0.3 from 8th-10th), the colours remained remarkably constant (J-H = 0.86 ± 0.01, H-K = 0.86 ± 0.02).

2.3.15. 0912+297.

This object was identified by Wills & Wills (1976), and at 14.7% has one of the highest radio (λ 3.7 cm) polarizations yet seen in a BL Lac object (Wardle 1978). It was observed on one night with JHK photometry and polarimetry. There was marginal evidence for wavelength-dependence of polarization, and it has a stable position angle. The infrared spectral index α =0.7 was distinctly different from that of α =0.99 (paper II) observed in April 1981 and α =1.8

(paper II) observed in in April 1980. The January 1984 observations showed no significant changes in flux, and no polarimetry was taken.

2.3.16. 1156+295.

This is a strong-lined quasar at a redshift z=0.728 (Schmidt 1978) with an optical polarization of up to 28% (D. Wills, personal communication). Our observations in January 1983 show the highest infrared polarization yet at p=18%, although the source was too dim to make further polarimetry worthwhile.

2.3.17. 1215+303.

ON 325 is a typical BL Lac object, having no spectral features and an archival variability of more than 3 magnitudes (Zekl et al. 1981). Optical polarimetry reveals a range of 4%-17% and a variable position angle (ibid.) Our observations show a high polarization, p_J=13% with a relatively shallow spectrum.

2.3.18. 1219+285.

ON 231 (W Com Ber) is also a typical BL Lac, with no published redshift, an archival vaiability of 4 magnitudes, and a high and variable polarization, p=2%-10% (Zekl et al. 1981). This object was observed for one night only in the final run.

2.3.19. 1253-055.

3C279 is an OVV quasar with many strong emission lines and a redshift z=0.538 (Burbidge et al. 1977). It is the most variable extragalactic object known with an archival magnitude range of 6.7 magnitudes, and at peak brightness is one of the most luminous objects in the Universe.

The polarization in January 1983 was high at p_K=14.5% but the source was too faint to make further polarimetry worthwhile.

2.3.20. 1308+326.

This object has two redshift systems, z_{em}=0.996 and z_{abs}=0.879, both identified from Mg II lines (Miller, French & Hawley 1978). It has an archival variability of 5.8 (Zekl et al. 1981). The polarimetry ranges are 0%-28% in the optical (ibid.) and 7%-20% at infrared wavelengths (paper I). Although the object was highly polarized at $p_K \sim 17.6\%$, it was too faint for further polarimetry. The object was only marginally brighter in January 1984 and no polarimetry was taken.

2.3.21. 1418+546.

1418+546 was confirmed a BL Lac object by Craine et al. (1978), and has an archival variability of $\Delta m \sim 4.8$ mag (paper I). The infrared polarization has been seen to vary from 9% to <1% in just 3 months, with a maximum of p_K=18%.

2.3.22. 2200+420.(BL Lac).

This prototype object is one of the best studied of all blazars, and its properties have been reviewed by Stein et al. (1976) and Miller (1978). The non-thermal sources lie at the centre of a giant elliptical galaxy at z=0.0695. It is highly variable in flux and polarization on short time-scales (Angel et al 1978; paper II). Wavelength- dependent polarization has been seen on more than one occasion (Angel & Stockman 1980; Puschell & Stein 1980), but is usually absent.

It was observed on two nights, on 9th November 1982 and 9th January 1983. The polarization rose from 9% to 12% while the flux dropped by more than one magnitude. In November, the infra-red position angle was $\theta \sim 100^{\circ}$ with a rotation of $\Delta\theta \sim 80^{\circ}$ between the two dates.

Chapter 3. Reduction and Methods.

3.1 Polarimetry reduction.

In order to describe an electromagnetic wave we need to know its intensity, frequency, direction of propagation, orientation, and how these vary with time. The electric vector is chosen to specify the orientation. The orientational characteristics of this vector in time and space are termed the polarization of the wave.

The degree of polarization is defined as being the ratio of polarized to total flux.

$$p = \frac{I_{pol}}{I_{tot}} = \frac{I_{max} - I_{min}}{I_{max} + I_{min}}$$

where I_{max} and I_{min} are respectively the maximum and minimum intensities transmitted through a polarizer at differing orientations.

There are four Stokes parameters which describe the state of polarization of an electromagnetic wave. The most general state is elliptical polarization, which is caused by a superposition of two oscillations

$E_1 = \mathcal{E}_1 e^{i\phi_1}$ and $E_2 = \mathcal{E}_2 e^{i\phi_2}$ ($\mathcal{E}_1 \mathcal{E}_2$ real)

where $\underline{E}$ is the electric vector given by

$$\underline{E} = (\hat{\underline{x}} E_1 + \hat{\underline{y}} E_2) e^{-i\omega t}$$

The Stokes parametres are then defined by

$$I \equiv \mathcal{E}_1^2 + \mathcal{E}_2^2 \qquad Q \equiv \mathcal{E}_1^2 - \mathcal{E}_2^2$$

$$U \equiv 2\mathcal{E}_1\mathcal{E}_2 \cos(\phi_1 - \phi_2) \qquad V \equiv 2\mathcal{E}_1\mathcal{E}_2 \sin(\phi_1 - \phi_2)$$

For 100% polarized light $I^2 = U^2 + Q^2 + V^2$.

The parameter V represents circular polarization which, for blazars, is undetectable or present at only a few tenths of one per cent. It was assumed to be zero throughout.

Mueller calculus provides a method of calculating the effects upon the Stokes parameters of the passage of a beam of light through an optical element. The resultant parameters are then calculated by matrix operations. The Mueller calculus for the optical system described in section 2.2 is detailed in Impey (1981, Thesis). The reduction software, written by Malcolm Stewart and Chris Impey, is outlined below.

(a) The polarimeter was rotated in 45° steps, and 8 scans of the object recorded. (b) For a polaroid followed by a dichroic, Mueller calculus gives a functional form (Impey 1981, Clarke & Grainger 1971) of

$$I \propto 1 + A \cos 2\phi + B \sin 2\phi + C \qquad 3.1$$

for the observed intensity for a given position of the polaroid.

[where I=observed intensity
ϕ =position angle of the polaroid major axis

and $A = \beta \cos 2\alpha + p \cos 2\theta$ 3.2

$B = \beta \sin 2\alpha + p \sin 2\theta$

where (β, α) and (p, θ) are the instrumental and object polarization and position angle respectively ; C contains terms in $\cos\phi$ and $\sin\phi$ which are included as a diagnostic of the systematic errors and the noise in an individual observation. For a perfect polarimeter C=0].

The observed intensity is then plotted (on-line) against and A & B are then determined by a least squares fit to the 8 point plot. The instrumental parameters are calculated by observing and unpolarized standard. p and θ are then calculated for each object.

(c) The effective retardance of the dichroic is determined by observing a polarized standard, and the instrumental

sensitivity by observing a photometric standard.

(d) The errors in p and θ take into account 3 factors. (i) An error associated with the goodness of fit to the functional form in 3.1. (ii) An error associated with the signal to noise. For faint objects, the degree of polarization will be systematically overestimated, since the probability distribution of the true values of p is not Gaussian, although this effect only becomes important at very low signal to noise (S/N < 2). This effect has been considered by Vinokur (1965) and by Wardle & Kronberg (1974). For the results described here, the signal to noise is generally large, and the corrections required are negligible. (iii) A equivalent photon error associated with the fluctuations in the current from the detector. The largest error is then adopted as the error associated with an observation.

The on-line reduction program at Mauna Kea gave immediate estimates for p and θ and their assocaited errors. The data files were later edited for glitches, coadded and analysed on the Edinburgh VAX computer. The final results are tabulated in section 4.1.1.

3.2 Photometry Reduction.

The Mauna Kea computer provides on-line instrumental magnitudes and estimates of the error due to noise. Photometric standard stars were observed several times during the night, in order to calculate an accurate offset magnitude. The magnitudes of the blazars are then calculated from the instrumental and offset magnitudes, correcting for airmass (see Table 3.1) using the equations

$$M(\text{offset}) = M(\text{standard}) - M(\text{inst.}) + (a-1)e$$

and

$$M(\text{blazar}) = M(\text{offset}) + M(\text{inst.}) - (a-1)e$$

where a is the airmass and where e is the extinction (in magnitudes) per unit airmass, shown in Table 3.1.

This magnitude was then corrected for galactic extinction (described in section 2.1). The resultant magnitude was then converted into a flux density (S_ν) using the zero magnitude flux densities shown in Table 3.1.

The formal error due to noise in the signal was usually of the order of 1% or 2%. The error in the resultant magnitude was usually dominated by a factor associated with the repeatability of offset magnitudes of standard stars. This factor includes any variations in the sky transparency and also any fluctuations in the detector sensitivity.

It was found that peak signal was lost on crossing the meridian, due to a slight tilt in the detector. Care was taken, therefore, to ensure that magnitudes were calculated using photometric standards observed on the same side of the meridian.

3.3. Methods

3.3.1. Spearman Rank Test.

The standard parametric correlation test assumes that the variables are normally distributed. This is not necessarily a good assumption when dealing with polarization parameters, and so we use the non-parametric Spearman Rank Correlation Coefficients throughout.

The s.r.c.c. (r_S) is calculated from

$$r = 1 - \frac{6\sum^{N} (x_i - y_i)^2}{(N^3 - N)} \qquad \text{(Conover 1971)} \qquad 3.3$$

where there are N data pairs. The values (x_i, y_i) represent the ranks of the variables for the ith pair.

$$1 \leqslant x_i \leqslant N$$
$$1 \leqslant y_i \leqslant N$$

A high value of r_S indicates significant correlation. It is possible, however, that an apparent correlation occurs when both variables correlate with a third variable. We test for this using the Spearman Partial Rank Correlation Coefficient (Macklin 1982).

For 3 variables (X,Y,Z), we wish to test the Null Hypothesis that the (X-Y) correlation arises entirely from the (X-Z) and (Y-Z) correlaions separately. The S.P.R.C.C. is defined as

$$r_{XY,Z} = \frac{r_{XY} - r_{XZ}\, r_{YZ}}{[(1-r_{XZ}^2)(1-r_{YZ}^2)]^{1/2}} \qquad 3.4$$

where r_{ij} is the Spearman coefficient for the correlation between the two variable ij. The significance level is defined by

$$D = \frac{1}{2}(N-4)\ \ln\left(\frac{1+r_{XY,Z}}{1-r_{XY,Z}}\right) \qquad 3.5$$

$D_{XY,Z}$ is distributed normally about zero with unit variance, for large N, and describes the level of confidence with which we may reject the Null Hypothesis.

TABLE 3.1 Photometry reduction data

Extinction per unit airmass e

$e_J = 0^m.15, \quad e_H = 0^m.08, \quad e_K = 0^m.12, \quad e_L = 0^m.16$

Zero magnitude flux densities S (0)

$S_J(0) = 1520$ mJy

$S_H(0) = 980$ mJy

$S_K(0) = 620$ mJy

Photometric Standard Stars

	K	H	J
HD 1160	7.04	7.05	7.06
G1 105.5	6.525	6.635	7.295
HD 40335	6.45	6.47	6.55
BD 0^o 1694	4.585	4.825	5.735
HD 84800	7.35	7.535	7.595
HD 22686	7.185	7.19	7.195
G1 406	6.08	6.12	6.25
G1 299	7.64	7.915	8.43
HD 106965	7.315	7.335	7.38
HD 105601	6.685	6.715	6.82
HD 77281	7.03	7.05	7.11

3.3.2 Chi-square Fitting

We wish to calculate the value of Chi-square (χ^2) for fitting data points to a line, taking into account errors in both co-ordinates. Assume that the points (x_i, y_i) have Gaussian-distributed errors (σ_x, σ_y). The perpendicular distance (l_i) of (x_i, y_i) from the line $y = mx + c$ is given by

$$l_i = (y_i - mx_i - c)/(1 + m^2)^{\frac{1}{2}} \qquad 3.6$$

Let us define a set of axes $\bar{x}$, $\bar{y}$ which have the measured point as the origin. See figure 3.1. The probability that the measured point originated in an area dA around $(\bar{x}, \bar{y})$ (in the new frame) is given by $p(\bar{x}, \bar{y})\, dA$, where

$$p(\bar{x}, \bar{y}) = \frac{1}{2\pi\sigma_x\sigma_y} \exp -\tfrac{1}{2}\left\{\frac{\bar{x}^2}{\sigma_x^2} + \frac{\bar{y}^2}{\sigma_y^2}\right\} \qquad 3.7$$

We assume that the measured point originated on a line with slope m, so that

$$p(\bar{x}, \bar{y}) = \frac{1}{2\pi\sigma_x\sigma_y} \exp -\tfrac{1}{2}\left\{\frac{\bar{x}^2}{\sigma_x^2} + \frac{(m\bar{x} + k)^2}{\sigma_y^2}\right\} \qquad 3.8$$

where $k = \sqrt{1 + m^2}$

The probability, $p(l)dl$, that the measured point originated anywhere on a line at a distance l to l + dl is given by the line integral of $p(\bar{x}, \bar{y})$, so that

$$p(l) = \int_{-\infty}^{\infty} p(\bar{x}, \bar{y})\, ds = 1 + m^2 \int_{-\infty}^{\infty} p(\bar{x}, \bar{y})\, d\bar{x} \qquad 3.9$$

Since

$$\frac{ds}{dx} = \sqrt{1 + m^2}$$

therefore

$$p(1) = \frac{\sqrt{1 + m^2}}{2\pi\sigma_x\sigma_y} \int_{-\infty}^{\infty} \exp - \tfrac{1}{2} \left\{ \frac{\bar{x}^2}{\sigma_x^2} + \frac{(m\bar{x} + k)^2}{\sigma_y^2} \right\} d\bar{x} \qquad 3.10$$

Now $$\left\{ \frac{\bar{x}^2}{\sigma_x^2} + \frac{(m\bar{x} + k)^2}{\sigma_y^2} \right\} = a^2 (\bar{x} + b)^2 + q^2 \qquad 3.11$$

where $a^2 = 1/\sigma_x^2 + m^2/\sigma_y^2$

$b = mk/a^2 \sigma_y^2$

$q^2 = k^2/\sigma_y^2 - a^2 b^2$

$= k^2/(\sigma_y^2 + m^2 \sigma_x^2)$

We recognise the identity

$$\int_{-\infty}^{\infty} \exp - \tfrac{1}{2} \left[a^2 (\bar{x} + b)^2 \right] d(\bar{x} + b) = \frac{\sqrt{2\pi}}{a} \qquad 3.12$$

So that

$$p(1) = \frac{\sqrt{1 + m^2}}{2\pi\sigma_x\sigma_y} \cdot \frac{\sqrt{2\pi}}{a} \exp - \tfrac{1}{2} \frac{k^2}{(\sigma_y^2 + m^2 \sigma_x^2)} \qquad 3.13$$

If σ_1 is the Gaussian error is 1 then the probability density, p(1), is also given by

$$p(1) = \frac{1}{\sqrt{2\pi}\,\sigma_1} \exp - \tfrac{1}{2} \cdot \frac{1^2}{\sigma_1^2} \qquad 3.14$$

By comparison, then,

$$\sigma_1 = \frac{\sigma_x \sigma_y a}{\sqrt{1+m^2}}$$

$$= \frac{\sigma_y^2 + m^2 \sigma_x^2}{1 + m^2} \qquad 3.15$$

$\sum_i 1i^2/\sigma_{1i}^2$ is χ^2 distributed with n - 2 degrees of freedom (m, c are fixed).

From equations 3.6 and 3.15 we see that

$$\chi^2 = \sum_i 1i^2/\sigma_{1i}^2 = \sum_i \frac{(y_i - mx_i - c)^2}{\sigma_y^2 + m^2 \sigma_x^2} \qquad 3.16$$

3.3.3 Two-Component Fitting

We wish to calculate the polarization and spectral properties of two superposed components. Firstly, we consider the polarization properties of two superposed power law spectra, and secondly, we derive the formulae for spectral curvature resulting from superposing two spectra.

(i) Consider two power-law components with spectral indices α_1 and α_2. Let each component have wavelength-independent polarization properties. The resultant Stokes parameters are given by

$$\begin{aligned} S &= S_1 + S_2 \\ Q \equiv pS\cos 2\theta &= p_1 S_1 \cos 2\theta_1 + p_2 S_2 \cos 2\theta_2 \\ U \equiv pS\sin 2\theta &= p_1 S_1 \sin 2\theta_1 + p_2 S_2 \sin 2\theta_2 \end{aligned} \qquad 3.17$$

where (S, p_1, θ), (S_1, p_1, θ_1) and (S_2, p_2, θ_2) are the flux, polarization degree and position angle of the resultant radiation, and components 1 and 2 respectively. (See Figure 3.2).

The resultant polarization, p, is then given by

$$p = \frac{\sqrt{(\Sigma Q)^2 + (\Sigma U)^2}}{S} \qquad 3.18$$

so that

$$S^2 p^2 = (p_1 S_1)^2 + (p_2 S_2)^2 + 2 p_1 S_1 p_2 S_2 (\cos 2\theta_1 \cos 2\theta_2 + \sin 2\theta_1 \sin 2\theta_2),$$

$$\therefore \quad p^2 = \frac{p_1^2 + p_2^2 (S_2/S_1)^2 + 2 p_1 p_2 (S_2/S_1) \cos 2\xi}{(1 + S_2/S_1)^2} \qquad 3.19$$

where $\xi \equiv \theta_1 - \theta_2$.

The resultant position angle, θ, is then given by

$$\tan 2\theta = \frac{\Sigma U}{\Sigma Q} = \frac{p_1 \sin 2\theta_1 + p_2 \sin 2\theta_2}{p_2 \cos 2\theta_2 + p_2 \cos 2\theta_2} \qquad 3.20$$

The frequency-dependence enters in the factor S_2/S_1. The cross-over frequency, ν_o, is defined as the frequency at which $S_2 = S_1$. For two power-law spectra, we have

$$S_1 = k_1 \nu^{-\alpha_1} \qquad S_2 = k_2 \nu^{-\alpha_2}$$

At ν_o, $S_1 = S_2 = k_1 \nu_o^{-\alpha_1} = k_2 \nu_o^{-\alpha_2}$

so that $$k_2/k_1 = \nu_o^{-(\alpha_1 - \alpha_2)}$$

Generally

$$\frac{S_2}{S_1} = \frac{k_2}{k_1} \nu^{-(\alpha_2 - \alpha_1)} = (\nu/\nu_o)^{\alpha_1 - \alpha_2} \qquad 3.21$$

(ii) Local spectral index, α, is defined by

$$\alpha \equiv - d \ln S_\nu / d \ln \nu$$

Therefore, for two superposed spectra of index α_1, α_2 respectively, the resultant local spectral index, α_1 is given by

$$\alpha(S_1 + S_2) = - \frac{d \ln (S_1 + S_2)}{d \ln \nu} \cdot (S_1 + S_2)$$

$$= - \frac{d(S_1 + S_2)}{d \ln \nu} \qquad \text{since } dx \equiv x \, d \ln x$$

$$= -\frac{dS_1}{d\ln\nu} - \frac{dS_2}{d\ln\nu} = -\frac{S_1 d\ln S_1}{d\ln\nu} - \frac{S_2 d\ln S_2}{d\ln\nu}$$

$$= S_1\alpha_1 + S_2\alpha_2$$

Therefore $\alpha = \delta_1\alpha_1 + \delta_2\alpha_2$

where $\delta_1 \equiv S_1/(S_1 + S_2)$ and $\delta_2 \equiv 1 - \delta_1$ 3.22

Differentiate equation 3.22 with respect to $\ln\nu$, to give

$$\frac{d\alpha}{d\ln\nu} = \delta_1\frac{d\alpha_1}{d\ln\nu} + \delta_2\frac{d\alpha_2}{d\ln\nu} - A$$

where $A \equiv -\alpha_1\frac{d\delta_1}{d\ln\nu} - \alpha_2\frac{d\delta_2}{d\ln\nu}$

Now $\frac{d\delta_1}{d\ln\nu} = \delta_1\frac{d\ln\delta_1}{d\ln\nu} = \delta_1|\alpha - \alpha_1|$

So that $A = \alpha_1\delta_1|\alpha_1 - \alpha| + \alpha_2\delta_2|\alpha_2 - \alpha|$

Substituting for α and δ_2 from equations 3.22 gives

$$A = (\delta_1 - \delta_1^2)(\delta_1^2 - 2\alpha_1\alpha_2 + \alpha_2^2)$$

$$= \delta_1\delta_2(\alpha_2 - \alpha_1)^2$$

So that $\frac{d\alpha}{d\ln\nu} = \delta_1\frac{d\alpha_1}{d\ln\nu} + \delta_2\frac{d\alpha_2}{d\ln\nu} - \delta_1\delta_2(\alpha_2 - \alpha_1)^2$ 3.23

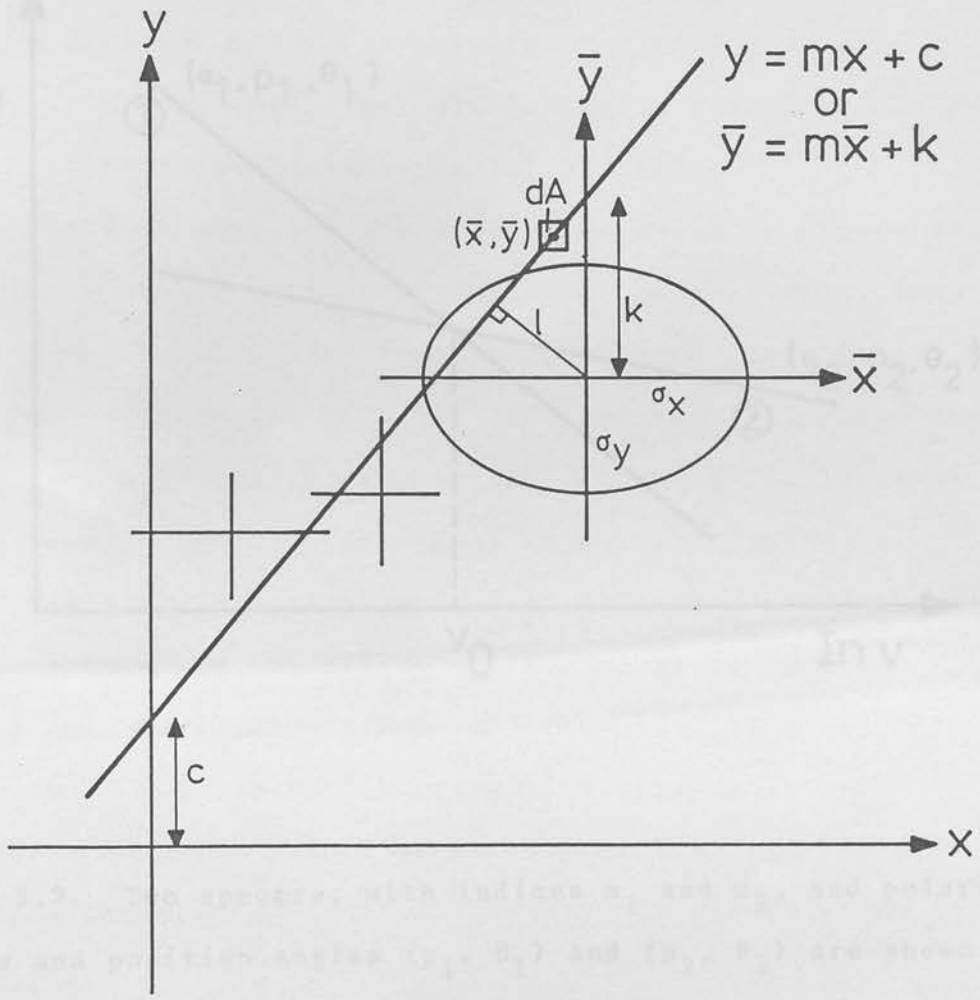

Figure 3.1. Data points (x_i, y_i) are assumed to have Gaussian errors. The best-fit line is shown as y = mx + c, or as $\bar{y}$ = m$\bar{x}$ + k, where the data point is the origin.

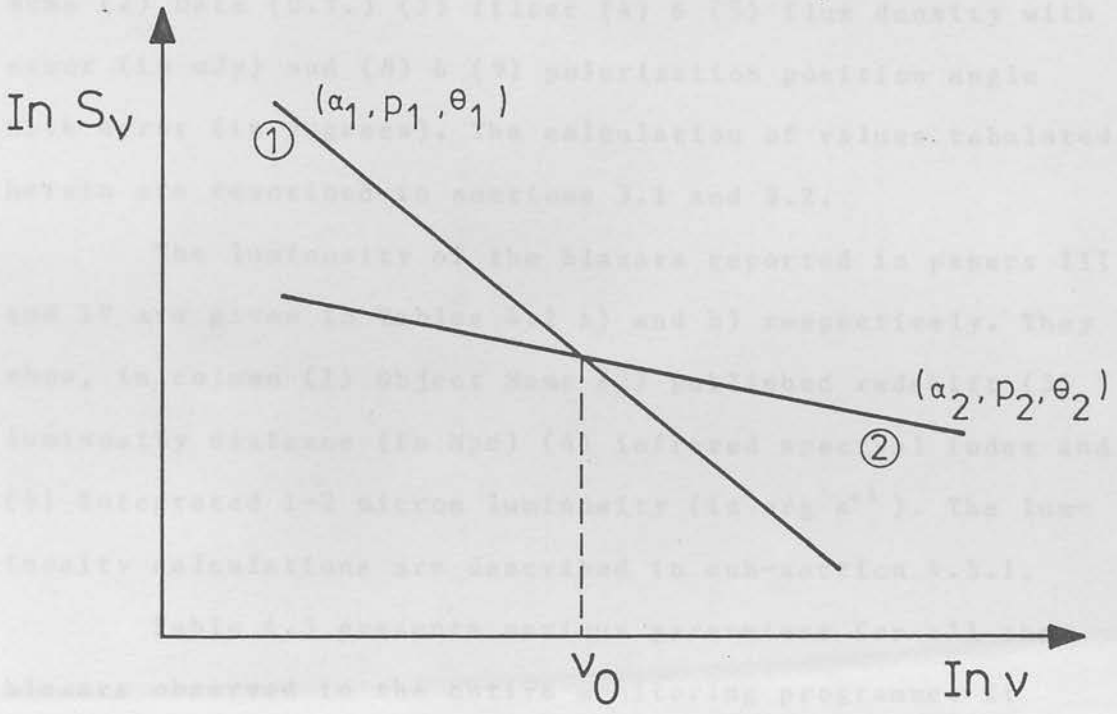

Figure 3.2. Two spectra, with indices α_1 and α_2, and polarization degrees and position angles (p_1, θ_1) and (p_2, θ_2) are shown at their "cross-over" frequency ν_o.

Chapter 4. Results.

4.1 Tabulated Results.

In this section, the tabulated results of the monitoring programme are presented. The flux and polarization data reported in papers III and IV are given in Tables 4.1 a) and b) respectively. They show, in column (1) Object Name (2) Date (U.T.) (3) filter (4) & (5) flux density with error (in mJy) and (8) & (9) polarization position angle with error (in degrees). The calculation of values tabulated herein are described in sections 3.1 and 3.2.

The luminosity of the blazars reported in papers III and IV are given in Tables 4.2 a) and b) respectively. They show, in column (1) Object Name (2) published redshift (3) luminosity distance (in Mpc) (4) infrared spectral index and (5) integrated 1-2 micron luminosity (in erg s^{-1}). The luminosity calculations are described in sub-section 4.3.1.

Table 4.3 presents various parameters for all the blazars observed in the entire monitoring programme. It shows in column (1) Object Name (2) redshift (3) & (4) Maximum and mean log 1-2 micron luminosity respectively (5) & (6) maximum and mean polarization degrees respectively (7) polarization range (8) position angle range and (9) mean 1-2 micron spectral index.

The large rotations with time of the polarization position angle which are common in blazars result in an ambiguous value for $\Delta\theta$ (i.e. $\Delta\theta = (\theta_2 - \theta_1) \pm 180^\circ n$; n=0,1,2,..). In all cases, the minimum inferrable position angle range was adopted (column 8).

TABLE 4.1 (a)

Flux and Polarization Properties of the Blazars in the Sample.

OBJECT	DATE	w/b	F_ν (mJy)	$\sigma(F_\nu)$	p%	σ(p%)	θ^0	$\sigma(\theta^0)$
0215+015	10 Jan 83	K	8.6	0.2	15.9	3.6	145	7
		H	6.2	0.1	17.4	1.1	145	2
		J	4.2	0.1	–		–	
	12 Jan 83	K	8.6	0.2	–		–	
		H	6.3	0.1	–		–	
		J	4.6	0.1	–		–	
0219+428	8 Jan 83	K	14.6	0.4	16.5	1.5	17	3
		H	11.6	0.2	18.2	1.6	25	2
		J	8.6	0.2	22.5	4.8	20	6
	9 Jan 83	K	12.5	0.1	15.7	1.1	23	2
		H	10.9	0.4	16.2	1.2	27	2
		J	7.1	0.1	20.8	3.9	24	5
	10 Jan 83	K	13.9	0.2	15.6	1.4	24	3
		H	10.9	0.1	15.4	1.0	22	2
		J	8.3	0.1	14.5	2.1	28	4
0235+164	25 Nov 82	K	5.8	0.1	14.7	2.0	26	4
		H	3.9	0.1	17.6	3.2	40	5
		J	3.2	0.1	23.8	2.6	31	3
	8 Jan 83	K	16.3	0.4	17.8	1.8	106	3
		H	11.6	0.2	13.5	0.7	103	1
		J	6.6	0.1	18.1	1.5	103	2
	9 Jan 83	K	15.9	0.2	8.5	1.2	117	5
		H	10.8	0.4	7.1	2.3	116	9
		J	6.3	0.1	–		–	
	10 Jan 83	K	14.3	0.3	6.9	1.5	107	7
		H	10.0	0.1	9.6	2.8	111	9
		J	6.1	0.1	7.1	3.5	114	14
	12 Jan 83	K	15.4	0.3	11.6	0.4	105	1
		H	10.8	0.2	11.5	2.2	105	6
		J	7.0	0.2	16.2	2.2	109	4
0422+004	8 Jan 83	K	15.7	0.5	13.6	1.3	166	3
		H	11.7	0.2	–		–	
		J	8.4	0.2	–		–	
	12 Jan 83	K	11.9	0.2	19.8	1.5	164	3
		H	8.6	0.2	13.7	1.6	168	3
		J	6.1	0.2	–		–	
0735+178	25 Nov 82	K	28.1	0.6	13.2	6.4	21	6
		H	21.4	0.2	20.8	0.4	7	1
		J	15.1	0.3	19.8	1.0	9	2
	7 Jan 83	K	21.5	0.2	14.2	1.1	136	8
		H	17.5	0.6	12.6	1.4	135	8
		J	11.5	0.4	14.6	2.9	141	10
	8 Jan 83	K	22.7	0.6	12.4	1.2	129	3
		H	16.9	0.3	11.3	0.7	133	2
		J	11.2	0.2	11.8	1.2	136	3

OBJECT	DATE	w/b	F_ν(mJy)	$\sigma(F_\nu)$	p%	σ(p%)	θ^0	$\sigma(\theta^0)$
0735+178 (cont.)	9 Jan 83	K	22.3	0.2	13.7	1.3	137	3
		H	17.7	0.7	12.7	1.5	138	3
		J	10.6	0.2	17.0	1.4	127	2
	10 Jan 83	K	20.9	0.4	10.8	1.3	131	4
		H	15.5	0.2	14.2	1.2	131	2
		J	11.3	0.1	12.6	0.6	134	1
	12 Jan 83	K	21.9	0.4	12.2	0.8	141	2
		H	16.3	0.3	12.0	1.5	132	4
		J	11.9	0.3	10.0	2.0	135	6
0736+017	10 Jan 83	K	6.6	0.1	7.3	4.3	44	19
		H	4.6	0.1	–		–	
		J	3.2	0.1	–		–	
0754+101	8 Jan 83	K	18.4	0.5	8.7	1.1	169	4
		H	13.3	0.3	8.9	1.4	179	5
		J	9.1	0.2	10.2	0.6	177	2
	9 Jan 83	K	15.9	0.2	6.2	1.2	0	7
		H	11.9	0.4	8.4	1.0	176	4
		J	8.7	0.2	6.2	1.8	176	9
	11 Jan 83	K	18.4	0.4	8.5	0.8	4	3
		H	13.7	0.2	5.3	1.0	163	5
		J	10.2	0.1	10.2	2.5	179	7
0829+046	10 Jan 83	K	21.3	0.4	7.8	0.2	130	1
		H	15.4	0.2	7.4	0.9	129	4
		J	10.5	0.1	6.7	2.3	118	10
	11 Jan 83	K	31.4	0.6	13.8	1.0	116	2
		H	23.3	0.2	13.8	0.9	114	2
		J	16.7	0.2	16.2	0.5	114	1
	12 Jan 83	K	28.6	0.6	14.0	0.8	129	2
		H	19.9	0.4	13.6	0.5	122	1
		J	14.0	0.4	12.1	1.0	122	2
0851+202	25 Nov 83	K	32.2	0.6	9.1	0.4	6	2
		H	24.2	0.2	9.1	0.5	10	2
		J	17.3	0.3	8.7	1.3	10	4
	7 Jan 83	K	88.8	0.8	9.4	0.3	99	1
		H	77.1	2.8	9.2	0.2	78	1
		J	60.0	2.2	8.3	0.9	71	3
	8 Jan 83	L	183.3	5.0	–		–	
		K	133.2	3.6	3.5	0.3	78	4
			123.7	3.4				
		H	103.6	1.9	2.6	0.2	71	2
			98.0	1.8				
		J	77.6	1.4	1.5	0.2	98	3
			74.8	1.4				
	9 Jan 83	L	168.7	3.4	–		–	
		K	121.4	1.2	6.8	0.6	111	3
		H	85.4	3.1	4.6	0.1	114	1
		J	67.0	1.2	4.4	0.4	116	3
	10 Jan 83	L	159.6	4.8	–		–	
		K	106.8	1.9	5.7	0.4	114	2

OBJECT	DATE	w/b	F_ν (mJy)	$\sigma(F_\nu)$	p%	σ(p%)	θ^0	(θ^0)
0851+202 (cont.)	10 Jan 83	H	80.8	0.8	4.4	0.1	120	1
		J	62.2	0.6	3.6	0.3	119	2
	11 Jan 83	L	152.5	3.1	–		–	
		K	101.0	1.8	10.2	0.3	109	1
		H	75.0	0.8	8.4	0.3	107	1
		J	58.3	0.5	8.4	0.3	109	1
	12 Jan 83	L	173.4	1.7	–		–	
		K	113.9	2.1	6.4	0.2	120	1
		H	87.7	1.6	6.0	0.2	118	1
		J	67.0	1.8	6.1	0.3	118	1
0912+297	12 Jan 83	K	7.7	0.2	10.5	1.9	175	6
		H	6.4	0.1	12.1	1.0	179	2
		J	5.2	0.2	13.5	2.8	0	6
1156+295	9 Jan 83	K	3.5	0.1	18.2	5.6	64	10
		H	2.6	0.1	–		–	
		J	1.8	0.1	–		–	
1253-055	11 Jan 83	K	3.9	0.1	14.5	3.5	49	8
		H	2.5	0.1	–		–	
		J	1.8	0.1	–		–	
1308+326	12 Jan 83	K	3.2	0.1	17.6	3.0	136	6
		H	2.0	0.1	–		–	
		J	1.3	0.1	–		–	
1418+546	11 Jan 83	K	13.4	0.3	7.6	2.8	92	12
		H	10.1	0.2	–		–	
		J	7.4	0.2	–		–	
2200+420	25 Nov 83	K	66.1	1.2	9.0	1.7	103	6
		H	–		5.8	1.0	99	5
		J	45.9	0.9	6.2	1.9	99	9
	9 Jan 83	K	24.0	0.2	–		–	
		H	21.4	0.8	–		–	
		J	14.0	0.3	–		–	

TABLE 4.1b Flux and Polarization data for the Blazars in this sample.

OBJECT	DATE	FILTER	F_ν(mJy)	$\sigma(F_\nu)$	p%	σ(p%)	θ^0	$\sigma(\theta)^0$
0048-097	9 Jan	K	4.1	.1	15.1	2.9	143.9	5.6
		H	3.2	.1				
		J	2.2	.1				
0215+015	8 Jan	K	8.9	.3	21.3	2.7	59.6	3.6
		H	6.7	.1				
		J	4.7	.2				
	9 Jan	K	8.6	.3	21.2	2.6	68.3	3.6
		H	6.5	.1	27.2	1.3	68.4	1.4
		J	4.6	.1	29.9	1.9	68.6	1.8
	10 Jan	K	9.4	.2	20.3	.9	79.3	1.3
		H	6.4	.1	24.6	.8	75.7	.9
		J	5.1	.1	25.1	1.1	73.8	1.2
	11 Jan	K	8.8	.4	21.3	1.5	78.3	2.1
		H	6.4	.3				
		J	4.6	.2				
0219+425	8 Jan	K	7.9	.2	11.0	1.7	28.7	4.6
		H	5.6	.2				
		J	5.2	.2				
0235+164	7 Jan	K	7.4	.7	4.7	1.9	23.3	11.4
		H	4.9	.4				
		J	3.1	.3				
	8 Jan	K	8.1	.2	3.1	1.6	63.8	15.2
		H	5.2	.2				
		J	3.1	.2				
	11 Jan	K	9.5	.6				
		H	7.1	.4				
		J	4.3	.2				
0420-014	9 Jan	K	1.6	.1				
		H	1.2	.1				
		J	0.8	.1				
0422+004	8 Jan	K	11.2	.3				
		H	8.3	.2	5.2	2.5	27.1	13.6
		J	5.5	.2				
	9 Jan	K	12.6	.4	5.8	1.3	42.0	6.5
		H	9.2	.2	7.3	.3	46.7	1.2
		J	6.6	.2	6.8	.9	33.7	3.7
0735+178	7 Jan	K	12.3	1.0	5.4	.9	23.4	4.7
		H	9.0	.7				
		J	6.2	.5	5.2	1.6	21.6	8.7
	9 Jan	K	13.4	.4	3.8	1.6	19.5	11.7
		H	9.5	.2	8.1	1.0	21.1	3.5
		J	6.3	.2	8.3	1.1	26.6	3.6
	10 Jan	K	13.7	.3	4.8	.9	25.4	5.0
		H	10.0	.2	5.2	.9	23.5	4.9
		J	6.6	.1	6.9	1.1	29.7	4.6
	11 Jan	K	12.8	.6	3.2	1.4	8.5	12.1
		H	9.1	.5	6.0	.3	24.8	1.5
		J	6.5	.3	5.7	1.2	25.8	5.9

OBJECT	DATE	FILTER	F_ν(mJy)	$\sigma(F_\nu)$	p%	σ(p)%	θ^0	$\sigma(\theta)^0$
0736+017	8 Jan	K	5.7	.1	3.0	2.8	143.7	27.0
		H	3.6	.1				
		J	2.6	.1				
0752+258	10 Jan	K	1.6	.1				
		H	1.1	.1				
		J	0.8	.1				
0754+100	7 Jan	K	8.1	.7	8.9	3.0	51.7	9.7
		H	5.9	.5				
		J	4.1	.3				
0808+019	10 Jan	K	0.3	0.1				
0818-128	8 Jan	K	3.6	.1				
		H	2.4	.1				
		J	1.8	.1				
0829+046	7 Jan	K	12.8	1.2	9.4	1.0	111.3	3.1
		H	9.4	.8				
		J	6.6	.6				
	10 Jan	K	11.1	.2	6.1	2.6	64.3	12.0
		H	7.6	.2				
		J	5.2	.1				
	11 Jan	K	10.6	.5				
		H	7.9	.4				
		J	5.2	.3				
0851+202	7 Jan	K	22.5	1.8	8.8	.9	128.8	2.8
OJ 287		H	16.4	1.3	9.3	.5	131.2	1.5
		J	11.5	1.0	10.1	.5	126.7	1.3
	8 Jan	K	28.9	.9	9.6	1.0	107.2	3.0
		H	21.2	.2				
		J	15.1	.6	13.3	2.2	95.6	4.8
	9 Jan	K	25.8	.8	11.1	.6	114.0	1.6
		H	18.3	.4	13.0	.8	114.8	1.8
		J	13.1	.4	12.9	1.6	117.2	3.5
	10 Jan	K	21.7	.4	11.1	.6	116.4	1.7
		H	15.0	.3	12.8	.2	109.7	.5
		J	10.4	.2	14.7	1.0	112.8	1.9
	11 Jan	K	22.9	1.5	11.4	.6	107.4	1.5
		H	16.6	.8	14.7	.8	109.1	1.6
		J	11.6	.5	10.9	2.5	99.7	6.6
0912+297	11 Jan	K	7.9	.4				
		H	6.4	.4				
		J	5.1	.3				
1147+245	9 Jan	K	8.0	.2	2.9	1.4	171.8	13.7
		H	6.1	.2				
		J	4.5	.1				

OBJECT	DATE	FILTER	F_ν(mJy)	$\sigma(F_\nu)$	p%	σ(p)%	θ^0	$\sigma(\theta)^0$
1215+303	10 Jan	K	14.1	.3				
		H	11.9	.2				
		J	9.4	.2				
	11 Jan	K	13.2	.7	10.4	.7	165.7	2.0
		H	10.7	.5				
		J	9.1	.4	12.8	1.6	169.4	3.6
1219+285	10 Jan	K	9.2	.2				
		H	6.6	.2				
		J	4.8	.1				
1253-055	10 Jan	K	4.2	.1				
		H	2.9	.1				
		J	1.7	.1				
1308+326	10 Jan	K	3.7	.1				
		H	2.1	.1				
		J	1.7	.1				

TABLE 4.2(a)

Luminosity of Blazars in the current sample.

Object	z	d(Mpc)	α_{IR}	$L_{1-2\mu m}$ (erg s^{-1})
0215+015	1.686	6740	1.11	4.3×10^{46}*
0219+428	0.444	1780	0.94	4.8×10^{45}*
0235+164	0.852	3410	1.61	2.2×10^{46}
0735+178	0.424	1700	1.25	6.6×10^{45}
0736+017	0.191	760	1.30	3.7×10^{44}*
0851+202	0.306	1220	0.96	2.1×10^{46}*
1156+295	0.729	2920	1.22	3.2×10^{45}
1253-053	0.538	2150	1.32	1.9×10^{45}
1308+326	0.996	3980	1.59	6.0×10^{45}
2200+420	0.069	276	0.65	6.0×10^{44}

* indicates highest luminosity observed.

TABLE 4.2(b)

Luminosity of Blazars in the current sample.

Object	z	d(Mpc)	α_{IR}	$L_{1-2\mu m}$ (erg s^{-1})
0215+015	1.686	6740	1.07	4.6×10^{46}*
0219+428	0.444	1780	0.74	2.6×10^{45}
0235+164	0.852	3410	1.40	1.2×10^{46}
0420-014	0.915	3660	1.19	2.3×10^{45}*
0735+178	0.424	1700	1.30	4.0×10^{45}
0736+017	0.191	760	1.37	3.1×10^{44}
0752+258	0.446	1780	1.17	5.2×10^{44}*
0851+202	0.306	1220	1.16	4.2×10^{45}
1253+055	0.538	2150	1.45	2.0×10^{45}
1308+326	0.996	3980	1.45	6.8×10^{45}

* indicates highest luminosity observed.

TABLE 4.3

Various parameters for all of the blazars observed in the monitoring programme.

Name	z	1-2 μm lum. max	1-2 μm lum. min	polarization max	polarization mean	polarization range	P.A. range	mean IR sp. index
(1)	(2)	(3)	(4)	(5)	(6)	(7)	(8)	(9)
0048	-	-	-	15.1	15.1	-	-	1.07
0215	1.686	46.66	46.65	29.9	20.3	14.0	85	1.13
0219	0.444	45.68	44.57	22.5	14.2	11.5	11	0.91
0235	0.852	46.68	46.20	36.2	12.5	33.1	136	1.81
0306	-	-	-	3.6	2.9	1.4	69	-
0420	0.915	45.36	45.36	-	-	-	-	1.19
0422	-	-	-	19.8	11.0	14.6	60	1.18
0735	0.424	46.36	45.79	32.6	17.0	29.4	79	1.20
0736	0.191	44.57	44.53	7.3	5.2	4.3	80	1.34
0752	0.446	44.72	44.72	-	-	-	-	1.17
0754	-	-	-	18.9	8.5	16.6	123	1.04
0818	-	-	-	21.4	13.3	15.4	37	0.89
0829	-	-	-	16.2	10.6	10.1	66	1.23
0851	0.306	46.32	45.73	19.7	11.4	18.2	124	1.02
0912	-	-	-	13.5	10.4	8.4	55	0.88
1147	-	-	-	14.8	12.5	11.9	63	1.21
1156	0.729	46.98	46.30	18.2	12.2	14.6	136	1.20
1215	-	-	-	12.8	11.6	-	-	0.70
1219	-	-	-	-	-	-	-	1.17
1253	0.538	45.88	45.27	16.2	13.8	6.5	49	1.46
1308	0.996	46.51	45.82	20.1	13.7	12.9	100	1.09
1335	-	-	-	-	-	-	-	1.70
1400	0.244	45.08	44.39	-	-	-	-	1.20
1418	-	-	-	17.9	10.9	17.0	128	1.01
1514	0.049	44.68	44.06	7.4	5.8	4.6	45	0.86
1538	-	-	-	-	-	-	-	0.92
1641	0.595	46.45	45.87	16.2	11.8	12.9	64	1.60
1652	0.034	44.49	44.49	-	-	-	-	0.36
1727	0.055	43.90	43.46	-	-	-	-	1.00
1749	-	-	-	-	-	-	-	2.00
1921	0.353	45.65	45.30	13.9	13.9	-	-	1.50
2155	0.170	45.84	45.34	3.0	2.0	2.0	17	0.35
2200	0.069	45.62	44.58	15.1	9.0	10.9	100	1.28
2223	1.404	46.71	46.56	16.3	12.6	10.8	85	1.50
2254	-	-	-	17.4	17.4	-	-	-

4.2 Internight Variations.

4.2.1. Variation Models.

If internight variations in the total and polarized fluxes are due to an increased/decreased contribution from a polarized source ($p \leqslant 75\%$) then

$$\Delta I_{pol} \leqslant 75\% \ \Delta I_{tot} \qquad 4.1$$

This inequality is represented by the shaded area in figure 4.1 (see also section 4.5)

If $\Delta I_{pol} > 75\% \ \Delta I_{tot}$ (Area 2) 4.2

or $\Delta I_{pol} / \Delta I_{tot} < 0$ (Area 3) 4.3

then a more sophisticated model is required; for example, a change in the degree of alignment of the magnetic field, or two or more polarized components rotating relative to another while varying in flux.

Högbom (1979) has shown that most astrophysical fields are essentially tangled. However, Laing (1980) suggests that these fields may be compressed or stretched to form "local alignment" along the line if sight, to produce regions of high polarization. It is therefore possible to populate area 2 (figure 4.1) by the increased flux in a jet, for example, convecting the field to increased alignment. Area 3 may be populated by (a) an OJ 287-type two-component model, or (b) tangling/untangling a magnetic field. Such a field, given a twist, will decrease alignment and so decrease polarization degree, while increasing the local field density and, therefore, total flux.

4.2.2. Observations.

The observations presented in this thesis extend the database of papers I & II to 148 data pairs. We examine the

relation between variations in total and polarized flux from night-to-night in the J,H,K wavebands.

Figure 4.1 shows a plot of ΔI_{pol} ($\equiv p_2 I_2 - p_1 I_1$) against ΔI_{tot} ($I_2 - I_1$). The data plotted in this figure are all the data of this monitoring programme, up to and including January 1983, but excluding that of OJ 287 (January 1983). It is reasonable to exclude this data on two grounds. Firstly, the object was very bright and this strongly effects any correlation. Secondly, the behaviour of OJ 287 was extremely unusual and was clearly inconsistent with an aligned sub-units model. The remaining data, 110 data pairs, show a very strong correlation between internight changes in total and polarized fluxes. A Spearman Rank correlation coefficient of $r_S = 0.473$ allows us to reject the null hypothesis (that the flux changes are unrelated) at the 99.95% conidence level, although large values of ($\chi^2/N = 2.7$) indicates significant scatter of the data from the best-fit line.

Of these 110 data points, only 8 lie beyond 2σ of the shaded area. The data are thus consistent with internight variations produced by sub-units polarized at $p \sim 18\%$. This value is derived from the best-fit line as described by the Pearson least-squares fit.

A similar analysis was performed for the data including that of January 1984. We find a Spearman coefficient of $r_S = 0.496$ for 33 data points, i.e. correlated at >> 99.9% confidence level. These data are consistent with internight variations being produced by turning on/off sub-units polarized at $p \sim 16\%$. If the variable component is

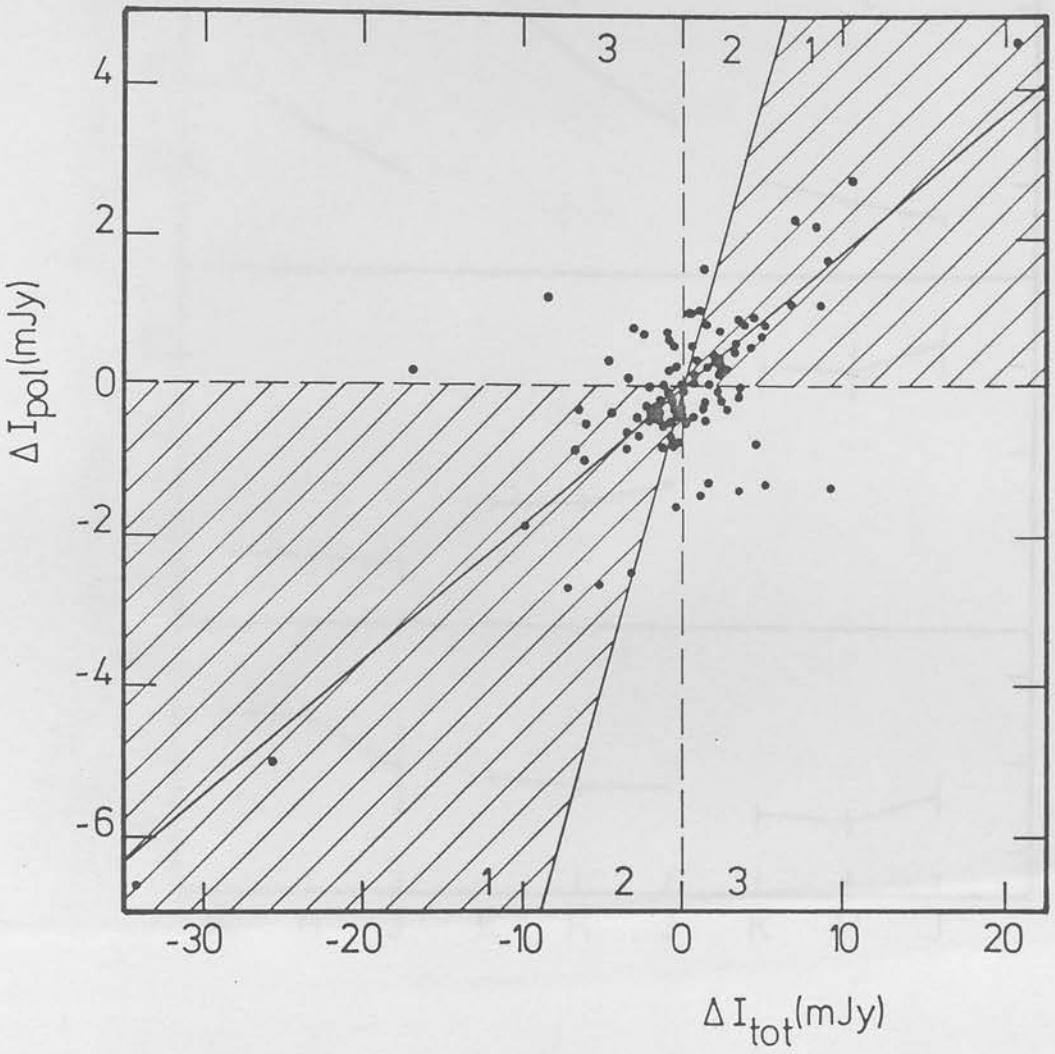

Figure 4.1 Internight variations in the total and polarized flux, except for OJ 287 (January 1983) and BL Lac (May 1981). BL Lac has been omitted for convenience of graph presentation, but is included in the data analysis. Only the shaded area may be populated by objects that vary by "turning on/off" polarized flux.

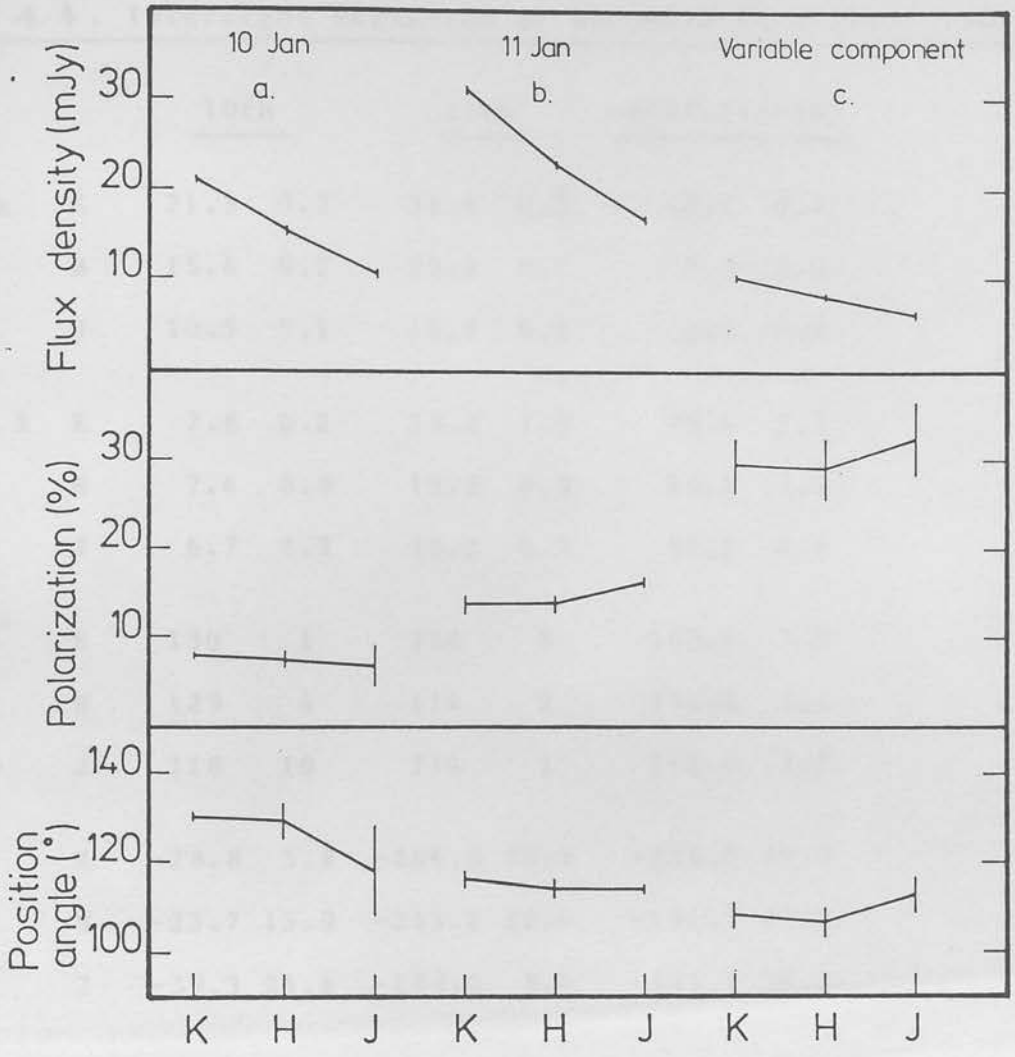

Figure 4.2 Polarization properties of 0829+046 on 10th and 11th January 1983 and of the variable component.

TABLE 4.4. Internight Variation of 0829+046 in January 1983

		10th		11th		diff.(11-10)	
Flux	K	21.3	0.2	31.4	0.3	10.1	0.4
	H	15.4	0.2	23.3	0.2	7.9	0.3
	J	10.5	0.1	16.7	0.2	6.2	0.2
Pol %	K	7.8	0.2	13.8	1.0	29.4	3.3
	H	7.4	0.9	13.8	0.9	29.1	3.7
	J	6.7	2.3	16.2	0.5	32.5	4.4
θ^0	K	130	1	116	2	108.4	3.0
	H	129	4	114	2	106.8	3.4
	J	118	10	114	1	112.6	3.7
Q	K	-28.8	5.8	-266.8	30.3	-238.0	30.9
	H	-23.7	15.9	-215.2	22.4	-191.5	27.5
	J	-39.3	24.6	-188.0	9.4	-141.7	26.3
U	K	-163.6	5.8	-341.5	30.3	-177.9	30.9
	H	-111.5	15.9	-239.0	22.4	-127.5	27.5
	J	-58.3	24.6	-201.0	9.4	-142.8	26.3

not aligned to the underlying component, then we require $p>16\%$. This is significantly different from the typical blazar polarization of $p \sim 11\%$ (see section 4.4.5).

4.2.3. 0829+046.

Detailed internight polarization behaviour can only be accurately evaluated for individual objects with large ($\Delta m > 0.5$ mag) internight flux variations. In 1983, 0829+046, brightened by $\Delta m=0.5$ from 10th to 11th January, with a corresponding increase in polarization by a factor of two. The data is shown in Table 4.4. The p,θ values are transformed into Stokes parameters using

$$U = p \sin 2\theta \qquad 4.4$$
$$Q = p \cos 2\theta$$

We assume that the increase in flux may be described as a single ("variable") component being superposed on the "underlying component" (10th Jan.). The properties of the variable component are then described by the difference in Stokes parameters between the two nights. The data can, therefore, be understood in terms of:

(i) a relatively shallow ($\alpha = 0.86$, cf. $\alpha(10th) = 1.25$)

(ii) highly polarized ($p \sim 30\%$, cf. $p(10th) = 8\%$)

(iii) wavelength-independent ($\theta \sim 109^\circ$) source turning on.

See figure 4.2 and Table 4.4.

4.3 Luminosity.

4.3.1 Calculation of Infrared Luminosity.

The near-infrared luminosity is calculated assuming a) cosmological redshifts and b) isotropic emission. We further assume a Friedmann model with cosmological constant $\Lambda = 0$, $H_0 = 75$ km s^{-1} Mpc^{-1} , and $q_0 = 1$. Choosing $q_0 = 0$ would

increase the luminosity by a factor $\sim(1+z/2)^{\alpha}$ (Mattig 1958). The luminosity in the rest frame of the blazar is given by:

$$L(\nu) = 4\pi d^2 (1+z)^{-1} F(\nu/(1+z)) \qquad 4.5$$

where $d=cz/H_o$ is the luminosity distance, and $F(\nu/(1+z))$ is the flux in the blazar rest frame, and is calculated from

$$F(\nu/(1+z))=F(\nu)(1+z)^{\alpha} \qquad 4.6$$

where α is the near-infrared spectral index ($\alpha \equiv -d \ln F_\nu / d \ln \nu$) and $F(\nu)$ is the integrated flux density from 1 to 2 microns. The $(1+z)^{\alpha}$ term corrects for the fact that the K-band samples a different part of the energy spectrum.

The infrared luminosity is taken to be the integrated luminosity density from 1 to 2 microns. These luminosities are lower limits as they are calculated using the J,H,K waveband fluxes only.

4.3.2 Variability-Luminosity Models.

In this sub-section, we consider three, model-dependent inequalities relating the minimum timescales of variability with luminosity.

(i) Elliot and Shapiro (1974) argue for a variability--luminosity criterion of the form

$$\log t_{min} \text{ (secs)} > \log L \text{ (erg s}^{-1}\text{)} - 43.1 \qquad 4.7$$

This assumes that the main interaction between the infalling matter and outgoing radiation is electron scattering, and that the timescale of variability is the light travel time across the Schwarzschild radius. Therefore, we have that the luminosity (L) of the object must satisfy the inequality

$$L \leqslant L_{Edd} = 4\pi GMm_p c/\sigma_T \qquad 4.8$$

$$= 1.3 \times 10^{38} (M/M_\odot) \text{ erg s}^{-1}$$

where M = mass of the black hole
L_{Edd} = Eddington luminosity
m_p = mass of the proton
σ_T = Thomson cross-section.

For black hole accretion, we expect the minimum timescales of variation to be greater than the light travel time across the Schwarzschild radius.

$$t_{min} > \frac{2GM}{c^3} = 0.98 \times 10^{-5} \ (M/M_\odot) \text{ sec} \qquad 4.9$$

Eliminating $(M/M_\odot)$ from these equations yields equation 4.7 Violation of the criterion implies one or more of the following:-

The source is (a) not steady, (b) radiating above the Eddington limit, (c) non-isotropic or (d) relativistically beamed.

(ii) Abramowicz and Nobili (1982) point out that periodic variations can only occur on longer timescales, equal to the rotation period of the inner edge of a disc accreting onto a maximally rotating black hole. They find a similar variability-luminosity criterion of the form

$$\log t_{min} > \log L - 43.1 + \log(\tau / \lambda) \qquad 4.10$$

where τ is a dimensionless, model-dependent parameter which depends upon the location of the region which provides the periodic time variation, and λ is also a dimensionless parameter, equal to the luminosity in units of the Eddington luminosity.

Abramowicz, Calvani & Nobili (1980) have shown that geometrically thick accretion discs are capable of radiating at many times (up to ~ 100) the Eddington limit. This is because the radiation is highly beamed in a long narrow vortex along the axis of rotation (see sub-section 8.5.3 (ii)).

Relativistic beaming, however, invalidates these criteria by reducing the luminosity requirement by factors of up to $\gamma^{-(3+\alpha)}$ (Blandford and Konigl 1979) or, more usually, $\gamma^{-(2+\alpha)}$ (Scheuer & Readhead 1979) where γ is the bulk Lorentz factor of the emitting material.

(iii) Fabian and Rees (1978) describe a variability criterion, assuming that luminous outbursts cannot occur on timescales shorter than the light crossing time of the emitting region. Moreover, if the electron scattering optical depth, τ_{es}, through this region exceeds unity, the photons diffuse out on a timescale τ_{es} times larger than the light crossing time.

Assuming a mass to energy conversion efficiency of η, they find an inequality of the form

$$L \leqslant 2*10^{41} \ (\eta/0.1) \ t_{min} \quad \text{erg s}^{-1} \qquad 4.11$$

4.3.3 Observations.

Several objects in the monitoring programme have been seen to violate the Elliot and Shapiro spherical accretion criterion, namely BL Lac, 0235+164, 1308+326, and 3C 446 (reported in papers I and II) for their 1 to 10 micron integrated luminosities.

The timescale of variability in the object's rest frame is defined throughout as

$$t_{min} = 10\% \ (\Delta t/(1+z)) \ (L/\Delta L) \qquad 4.12$$

In January 1983, 0J 287 was observed to flare by $\sim$7% in just one hour. The integrated 1 to 10 micron luminosity violates the Elliot and Shapiro criterion although not the Abramowicz and Nobili limit for a massive rotating black hole. This implies that we are looking at radiation

emanating from near the throat of a geometrically thick accretion disc, or, at least, not by uniform spherical accretion.

The integrated 1 to 2 micron luminosity of OJ 287, together with the Fabian and Rees criterion, requires an efficiency of $\eta \geqslant 20\%$, which approaches the limit even for matter falling onto a maximally rotating black hole ($\eta \simeq 42\%$, Lynden-Bell 1978).

4.4 Correlations.

The data tabulated in section 4.1.3 (table 4.3) are the results for the whole monitoring programme. We have now observed approximately half of all known blazars, mostly with infrared polarimetry, many for the first time. This constitutes a sufficiently large sample for meaningful statistical analysis, and several important correlations have emerged.

Various parameters for each object observed in the programme are presented in the table. It shows in columns (1) Name (2)redshift (3) & (4)maximum and mean 1 to 2 micron luminosity respectively, (5) & (6)the maximum and mean polarization degrees respectively, (7)the polarization range (8) the position angle range and (9)the mean infrared spectral index. See section 4.1 for method of calculation of parameters.

Relationships are investigated using the non-parametric Spearman rank and partial rank correlation coefficients, described in section 3.3.1. The correlations are described in the following sub-sections and the interpretation is discussed in sub-section 4.4.7

4.4.1 Position Angle Range and Luminosity.

A correlation between maximum luminosity and position angle range is evident from our data set. This unexpected relationship was first reported in paper II, and later confirmed in papers III and IV. For 14 objects we find a Spearman coefficient of $r_S=0.574$ (98% confidence interval). In paper III, the partial rank test did not allow rejection of the null hypothesis at better than the 1 sigma level ($D_{\theta L,N}=1.03$, cf. $D_{\theta N,L}=1.57$). The updated and expanded data set presented in table 4.3, however, yields the following coefficients.

$r_{\theta L}=0.574$ $\quad r_{\theta L,N}=0.419$ $\quad D_{\theta L,N}=1.411$

$r_{\theta N}=0.569$ $\quad r_{\theta N,L}=0.410$ $\quad D_{\theta N,L}=1.378$

$r_{LN}=0.477$ $\quad r_{LN,\theta}=0.223$ $\quad D_{LN,\theta}=0.718$

The value $D_{\theta L,N}=1.411$ allows to reject the null hypothesis at the 92% confidence level. This is only marginally significant, as correlations at this level can so easily occur spuriously. We would point out, therefore, that a 92% confidence level is not conclusive, but merely suggestive. However, this luminosity and position angle relationship has been observed three times in our data, which argues for its reality. We find no other third parameter which suggests that the $L^{max}-\Delta\theta$ correllation may not be intrinsic. For example, similar partial rank tests yield $D_{L\theta,z}=1.908$ and $D_{L\theta,\alpha}=1.712$.

A further triple correlation shows that the position angle rotations are more likely to be correlated with maximum, rather than mean, luminosity (i.e. $r_{L\,\Delta\theta}=0.530$ cf. $r_{L^m\Delta\theta}=0.574$). See figures 4.3.

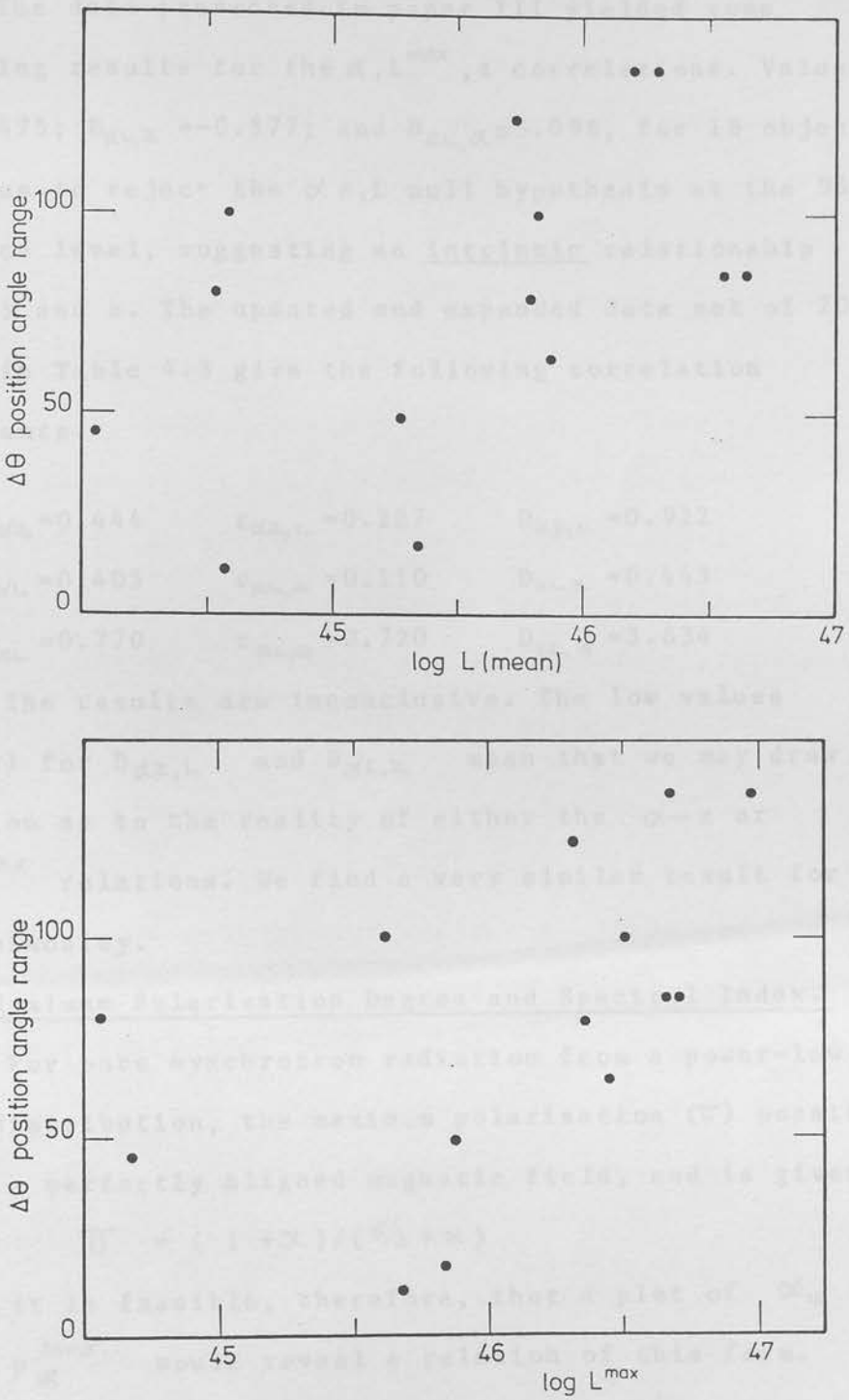

Figure 4.3 a) & b) Position angle range ($\Delta\theta$) versus log mean ($\bar{L}$) and maximum (L^{max}) 1-2 micron luminosities respectively.

4.4.2 Redshift and Spectral Index

The data presented in paper III yielded some interesting results for the α, L^{max}, z correlations. Values of $D_{\alpha z,L} = 1.475$; $D_{\alpha L,z} = -0.577$; and $D_{zL,\alpha} = 5.098$, for 18 objects allowed us to reject the $\alpha z,L$ null hypothesis at the 95% confidence level, suggesting an intrinsic relationship between α and z. The updated and expanded data set of 20 objects in Table 4.3 give the following correlation coefficients.

$r_{\alpha z} = 0.444$	$r_{\alpha z,L} = 0.227$	$D_{\alpha z,L} = 0.922$
$r_{\alpha L} = 0.405$	$r_{\alpha L,z} = 0.110$	$D_{\alpha L,z} = 0.443$
$r_{zL} = 0.770$	$r_{zL,\alpha} = 0.720$	$D_{zL,\alpha} = 3.634$

The results are inconclusive. The low values (i.e. <1) for $D_{\alpha z,L}$ and $D_{\alpha L,z}$ mean that we may draw no conclusion as to the reality of either the $\alpha - z$ or $\alpha - L^{max}$ relations. We find a very similar result for the mean luminosity.

4.4.3. Maximum Polarization Degree and Spectral Index.

For pure synchrotron radiation from a power-law energy distribution, the maximum polarization (Π) possible is from a perfectly aligned magnetic field, and is given by

$$\Pi = (1 + \alpha)/(5/3 + \alpha) \qquad 4.13$$

It is feasible, therefore, that a plot of α_{IR} against p_{IR}^{max} would reveal a relation of this form.

A strong correlation between mean infrared spectral index and maximum polarization for 14 objects was reported in paper I. The expanded data set of 17 objects in paper II showed a somewhat diluted correlation, with a Spearman coefficient $r_S = 0.68$. The further expanded and updated sample

of 22 objects presented in paper III is shown in figure 4.4a. As the number of objects in the sample and the number of observations have increased, so the correlation has faded. The total data set for 24 objects is shown in figure 4.4b. It appears as though a second population is emerging from the observations, where p_{IR}^{max} and $\bar{\alpha}_{IR}$ are anti-correlated. It is more feasible, however, that the majority of blazars in our sample have typical spectral indices in the range $\alpha = 1.2 \pm 0.4$, and a maximum infrared polarization in the range $p^{max} = 12\text{-}24\%$. The apparent correlation in the early data was probably largely due to the fortuitous inclusion of extreme objects, such as 0235+164, 0306+102, and 2155-052. We find no significant correlation for p_{IR}^{max}, $\bar{p}$, or Δp with $\bar{\alpha}_{IR}$.

It is also interesting to note that p_{IR}^{max} is unrelated to the range of position angles ($\Delta\theta$). These two parameters depend only upon the magnetic field geometry; polarization varies with the degree of field alignment, whereas position angle range depends upon field rotations only. So we see that for the magnetic field in the emitting region, the degrees of maximum alignment and rotation are not strongly correlated.

We do find, however, that the range of polarizations and $\Delta\theta$ are correlated at the 99.5% confidence interval ($r_s = 0.535$ for 22 points). The Spearman partial rank coefficients show that this relationship may be due entirely to a strong correlation of each parameter with the number of observations.

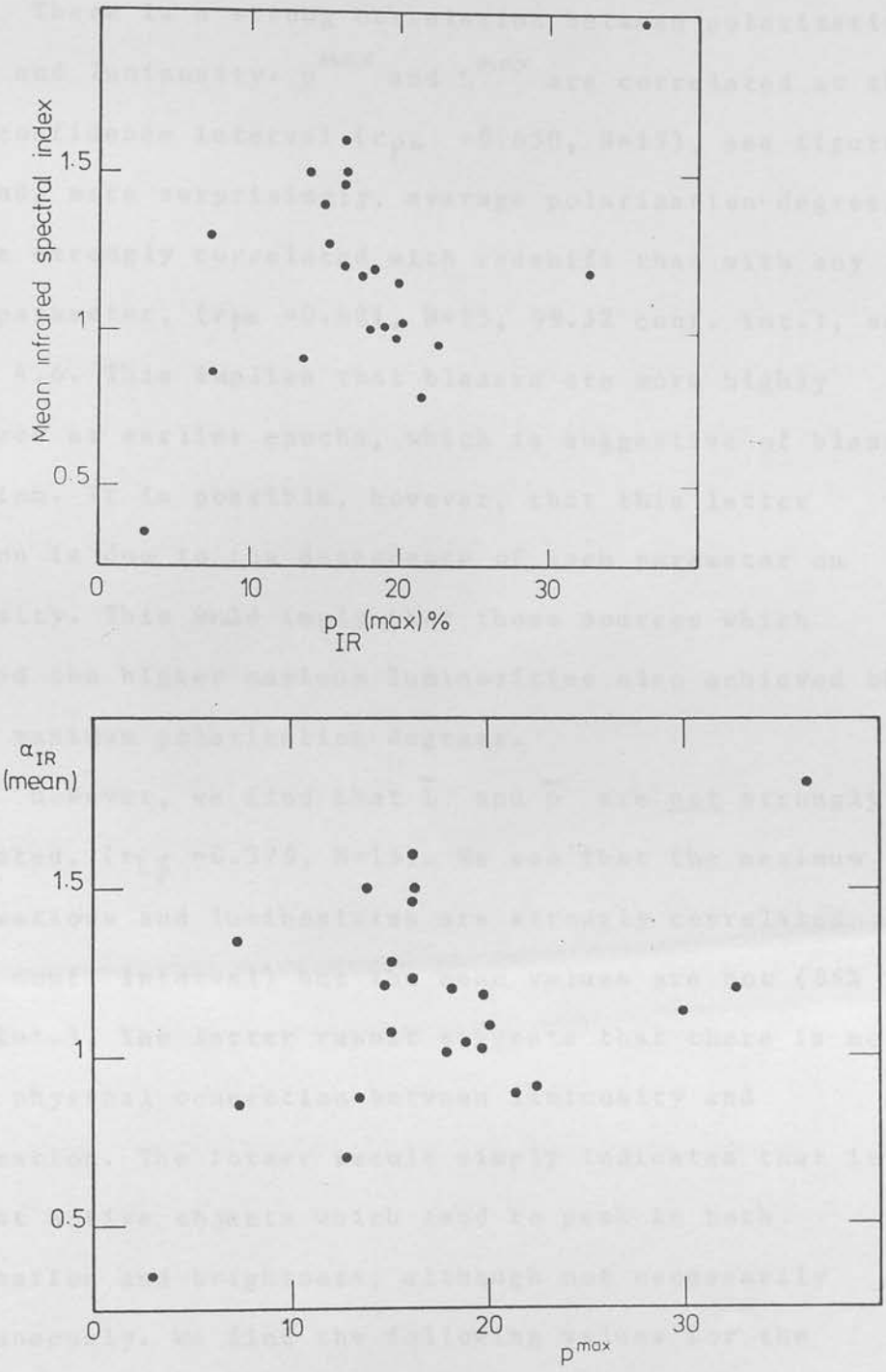

Figure 4.4 Mean infrared spectral index ($\bar{\alpha}_{IR}$) versus maximum polarization degree (p^{max}) a) shows the data from papers I,II and III only and b) shows the data from the whole programme, emphasising the dilution of the initial apparent correlation.

4.4.4 Polarization-Luminosity-Redshift.

There is a strong correlation between polarization degree and luminosity. p^{max} and L^{max} are correlated at the 99.8% confidence interval (r_{pL} =0.650, N=15), see figure 4.5, and, more surprisingly, average polarization degree, $\bar{p}$, is more strongly correlated with redshift than with any other parameter, (r_{pz} =0.621, N=15, 99.5% conf. int.), see figure 4.6. This implies that blazars are more highly polarized at earlier epochs, which is suggestive of blazar evolution. It is possible, however, that this latter relation is due to the dependence of each parameter on luminosity. This would imply that those sources which achieved the higher maximum luminosities also achieved the higher maximum polarization degrees.

However, we find that $\bar{L}$ and $\bar{p}$ are <u>not</u> strongly correlated, ($r_{\bar{L}\bar{p}}$ =0.379, N=15). We see that the maximum polarizations and luminosities are strongly correlated (99.8% conf. interval) but the mean values are not (86% conf. int.). The latter result suggests that there is no strong physical connection between luminosity and polarization. The former result simply indicates that it is the most active objects which tend to peak in both polarization and brightness, although not necessarily simultaneously. We find the following values for the correlation coefficients:-

correlation	r	conf. int.
$p^{max} - L^{max}$	0.650	99.8%
$p^{max} - \bar{L}$	0.575	98%
$\bar{p} - z$	0.621	99.5%
$\bar{p} - \bar{L}$	0.379	86%
$\bar{p} - L^{max}$	0.382	86%

The Spearman partial rank test for $\bar{p}$, L^{max} and z yields a value $D_{pz,L} = 2.3$ which strongly suggests (98% confidence interval) an intrinsic nature for the $\bar{p} - z$ relation. This correlation is clear of selection effects. There are no luminosity selection effects that could give rise to $r_{\bar{p}z} > r_{p^m L^m}$.

4.4.5. Polarization.

If the degree of polarization varies stochastically with time, we would expect a correlation between the number of observations of each object (N(p)) and both p^{max} (see figure 4.7a) and Δp and these are in fact observed at better than 99.99% confidence interval. We would not expect, however, to find a relation between N(p) and $\bar{p}$, whatever the distribution of polarizations amongst blazars. Our observations support this ($r_{N\bar{p}} = 0.001$), see figure 4.7b. Figure 4.8 shows the distribution of maximum versus mean polarizations.

Of the 26 shown, 19 lie in the region $12\% < p^{max} < 24\%$ and $8\% < \bar{p} < 18\%$, revealing only a small spread around the mean values $\langle\bar{p}\rangle = 11.5\%$ and $\langle p^{max} \rangle = 17.2\%$.

4.4.6 Luminosity.

If blazar luminosity varies stochastically with time, in a similar way to polarization, then we would expect

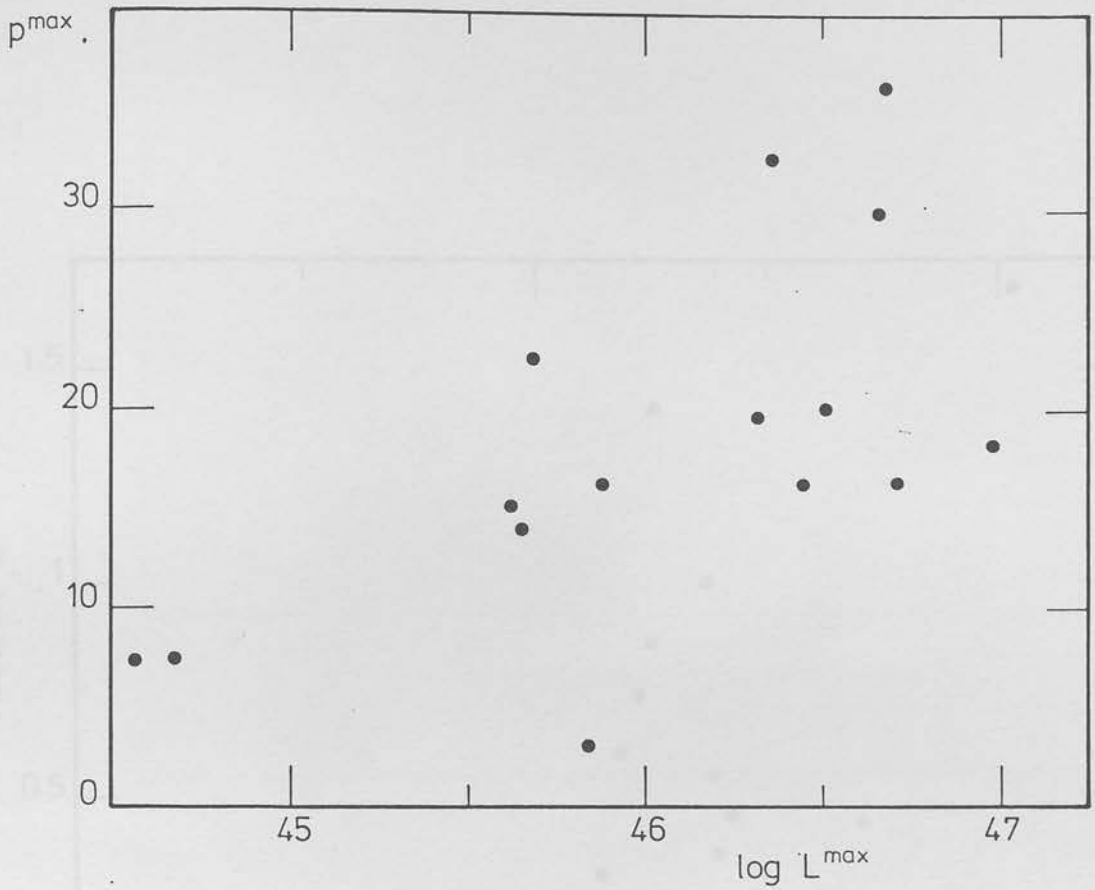

Figure 4.5 Maximum polarization degree plotted against maximum 1-2 micron luminosity.

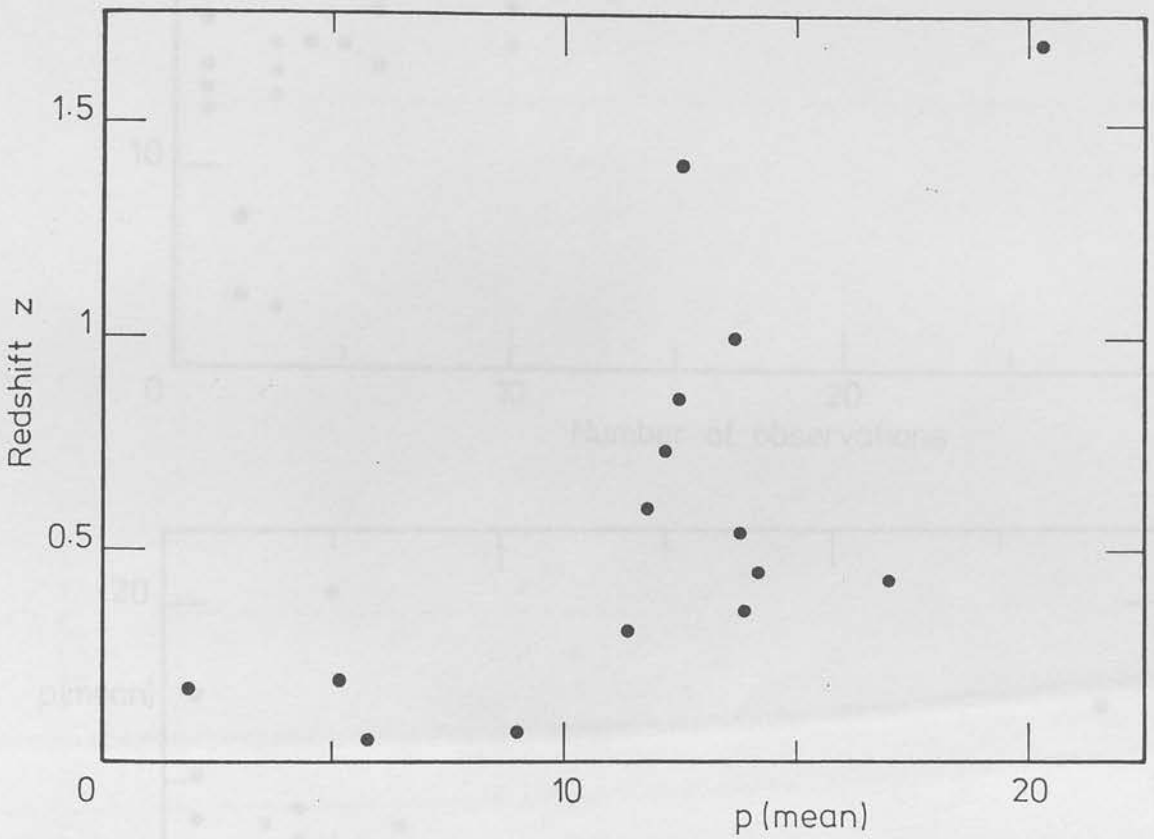

Figure 4.6 Redshift plotted against mean polarization degree.

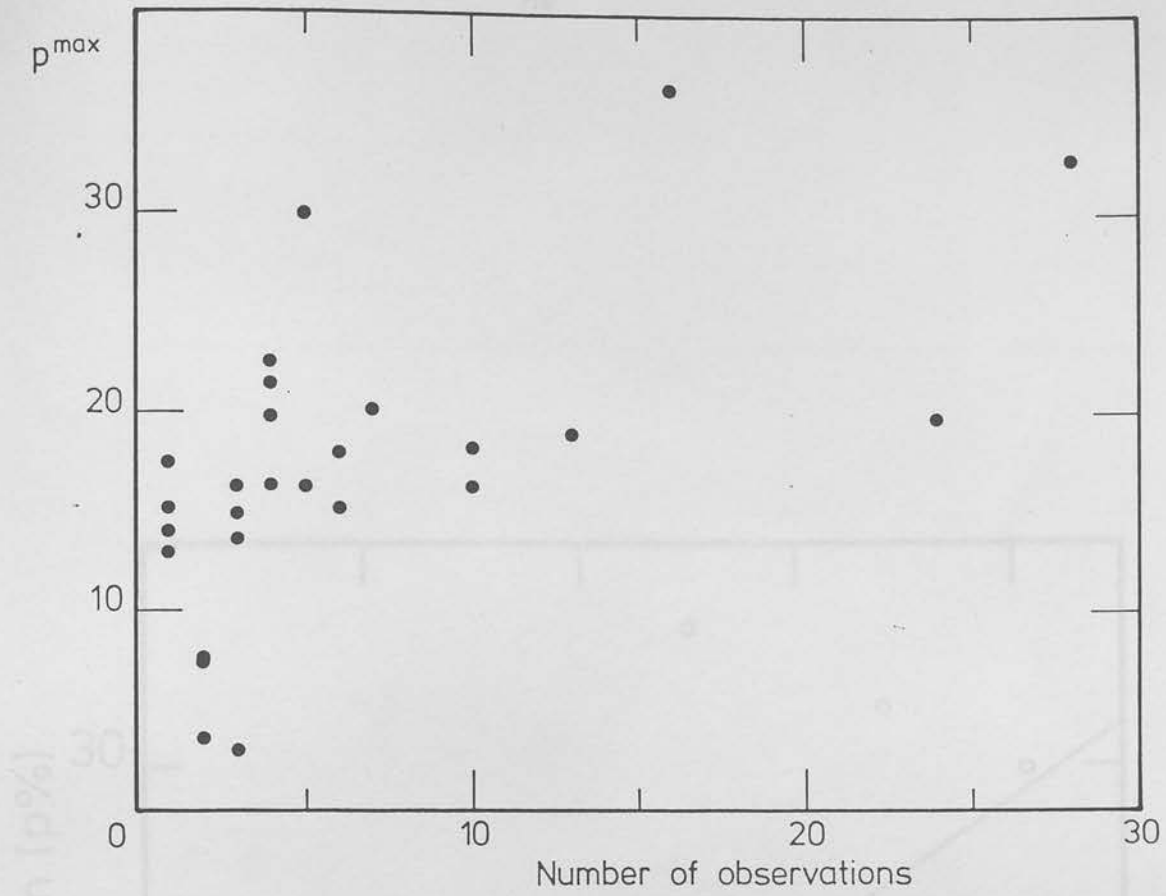

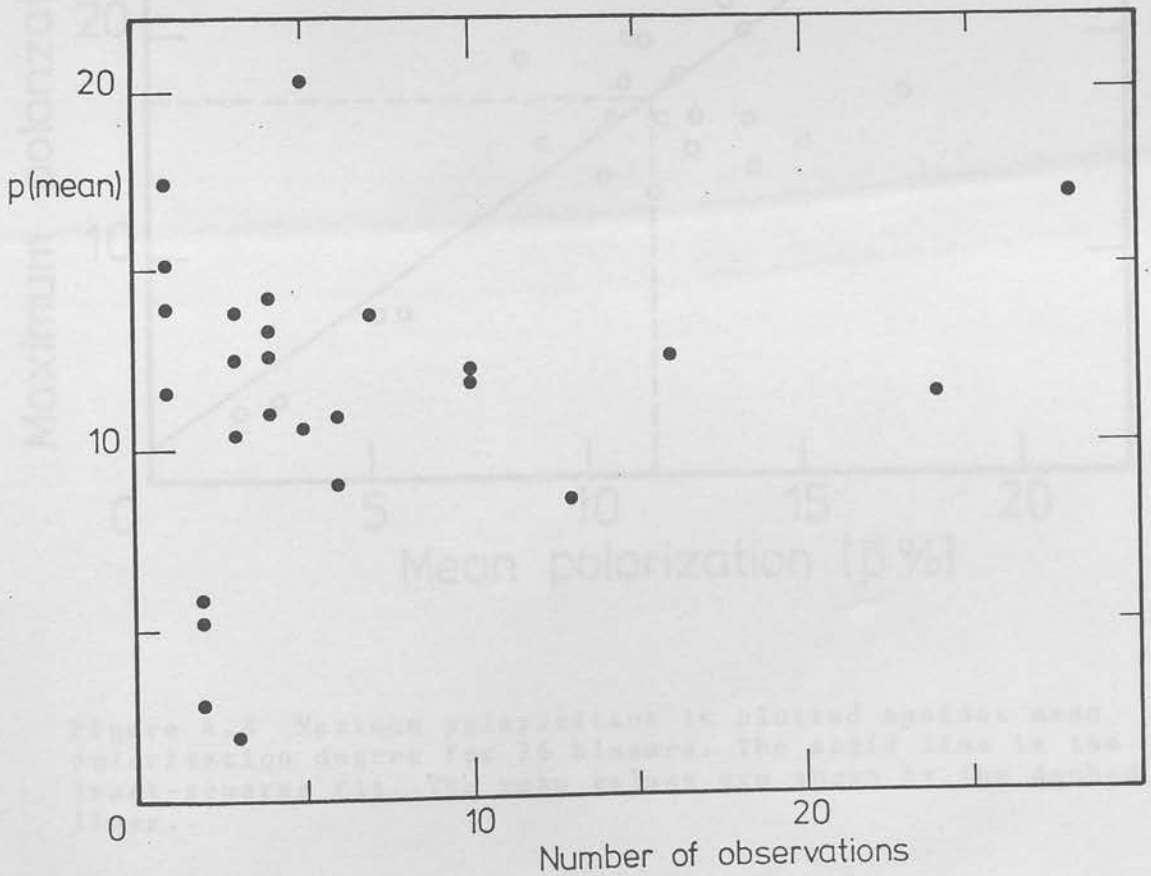

Figure 4.7 a) maximum polarization and b) mean polarization plotted against the number of observations, illustrating the stochastic nature of variations in the polarization degree.

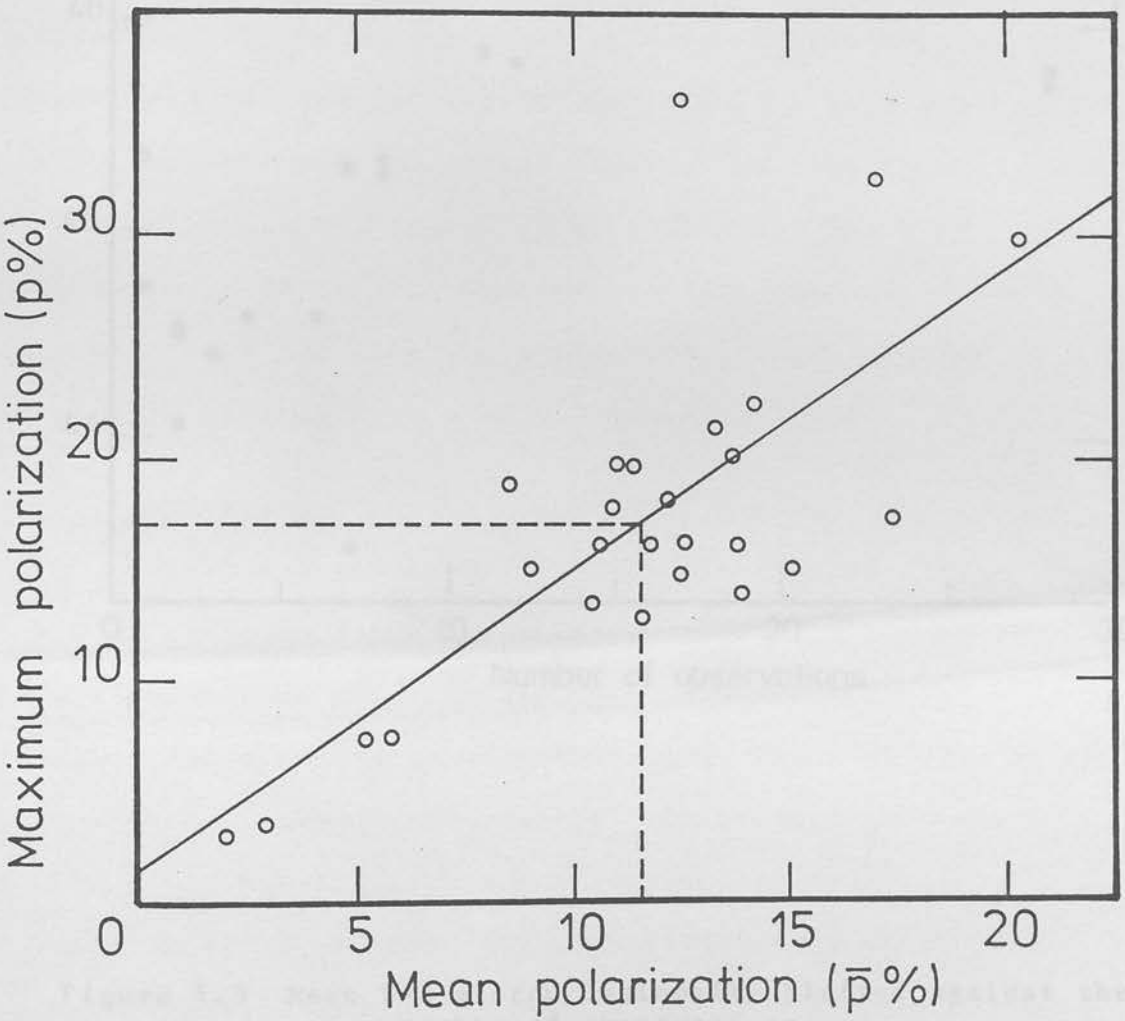

Figure 4.8 Maximum polarization is plotted against mean polarization degree for 26 blazars. The solid line is the least-squares fit. The mean values are shown by the dashed lines.

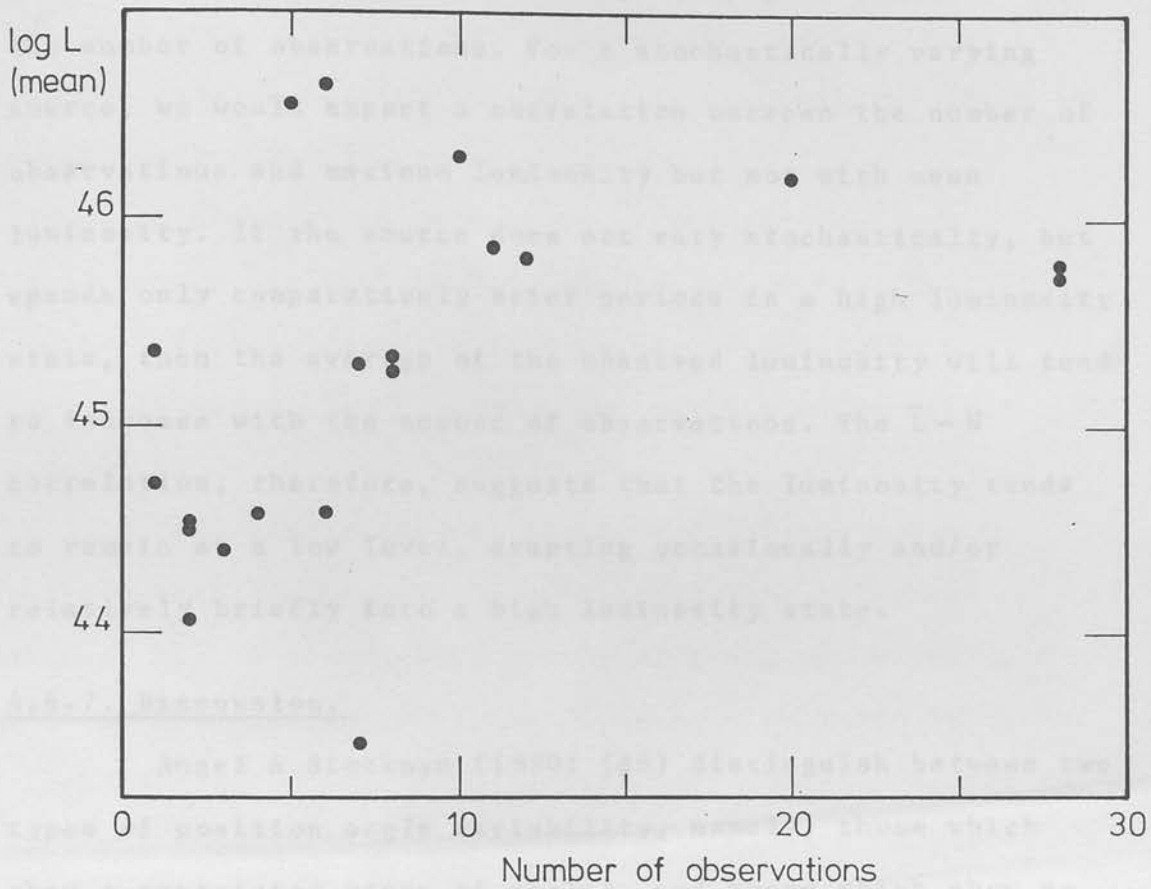

Figure 4.9 Mean 1-2 micron luminosity plotted against the number of observations.

no correlation between $\bar{L}$ and N(L), see figure 4.9. However, a rank coefficient of $r_s = 0.516$ (N=20, 98% conf. int.) reveals a significant correlation between these two parameters with average luminosity tending to increase with the number of observations. For a stochastically varying source, we would expect a correlation between the number of observations and maximum luminosity but not with mean luminosity. If the source does not vary stochastically, but spends only comparatively brief periods in a high luminosity state, then the average of the observed luminosity will tend to increase with the number of observations. The $\bar{L} - N$ correlation, therefore, suggests that the luminosity tends to remain at a low level, erupting occasionally and/or relatively briefly into a high luminosity state.

4.4.7. Discussion.

Angel & Stockman (1980) (AS) distinguish between two types of position angle variability, namely, those which show a restricted range of angles, and those which show no tendency for a preferred position angle. Those objects which display only a restricted range of angles tend to be less luminous, in agreement with our correlation noted in subsection 4.4.1. AS note the possibility that these two types of variability may be due to beaming effects (see section 8.5). Those blazars with jets pointing at a small angle to the line of sight will tend to exhibit larger and more rapid changes in position angle (e.g. Björnsson 1982) and also be flux boosted (Blandford & Königl 1979).

In 4.4.2, we find a marginally significant correlation between spectral index and redshift. The results

are not conclusive, although, since $D_{\alpha z, L} > D_{\alpha L, z}$, it seems that the $\alpha -$ z relation is more likely to be intrinsic. A given power-law spectrum maintains its spectral index irrespective of recessional velocity, therefore an $\alpha -$ z relation might indicate evolution of the blazar energy source. Another possibility is spectral curvature, which is briefly discussed in section 4.6.2

A correlation between spectral index and polarization was described in sub-section 4.4.3. The null result indicates that the members of the sample do not generally all achieve the same degree of magnetic field alignment.

From the results in sections 4.4.5 and 4.4.6 we believe that blazars vary stochastically in polarization degree, but vary in luminosity by erupting occasionally from a relatively quiescent state. If this is so, then section 4.4.4 also indicates that the most luminous sources are <u>not</u> more highly polarized (since $r_{\bar{p}\bar{L}} \sim r_{\bar{p}L^{max}} \simeq 0.38$) but <u>are</u> more variable (since $r_{p^{max}L^{max}} \simeq 0.65$ and $r_{p^{max}\bar{L}} \simeq 0.58$). The $L^{max} - \Delta\Theta$ correlation also supports the luminosity — variability relationship.

The following conclusions may be drawn from the data presented in table 4.3.

(i) The luminosity—position angle range relationship appears to be intrinsic, thus linking luminosity with a purely geometrical parameter.

(ii) As distinct from the results reported in papers I and II, polarization and spectral index are not correlated.

(iii) It is possible that our results show blazar evolution,

as evidenced by (a) the $\bar{p}$ – z relation (r_s=0.621, N=15, 99.5% conf. int.) and (b) the $\bar{\alpha}$ – z relation (r_s=0.444, N=20, 96% conf. int.).

(iv) polarization degree varies stochastically with time about some mean value ($p \sim 10\%$) while luminosity erupts occasionally from a relatively quiescent base level.

(v) The most luminous sources have the most variable polarization properties.

4.5 Rotation.

4.5.1. Polarized Sub-Units Model.

Blandford and Rees (1978) considered a model consisting of several highly-polarized sub-units. This assumes that variations in flux and polarization properties are caused by a sub-unit turning on/off. If these sub-units are randomly oriented to one another, then we may predict the resultant behaviour.

Consider n sub-units, each with a polarization degree $\tilde{p}$, and a luminosity L/n, where L is the total luminosity. The resultant polarization is $p \sim \tilde{p}\ n^{-1/2}$. If one sub-unit is added or subtracted, the luminosity and polarization degree will change by $|\Delta L| / L \sim 1/n$, and $|\Delta p| / p \sim 1/2n$ respectively and we expect a rotation of $\Delta\theta \sim n^{-1/2}$ radians. These predictions may be tested by our observations.

4.5.2. Results.

The only useful definition of the number of sub-units, for the purposes of rotation, is given by the relative polarized flux.

$$n \equiv I_{pol} / |\Delta I_{pol}| \qquad 4.14$$

where ΔI_{pol} is the change in the polarized flux from night to night, so that this change may be considered due to one of n sub-units turning on/off.

If, then, the variations in polarized flux are accompanied by rotations in position angle, as predicted above, we would expect to find a correlation between rotation and number of sub-units. The data from papers III and IV (i.e. all the data collected for this thesis) are plotted in figures 4.10(a,b,c). The polarimetric accuracy of the data in papers I and II are inadequate for this purpose.

The fractional change in polarized flux is plotted against rotation squared, since

$$\left|\frac{\Delta I_{pol}}{I_{pol}}\right| \equiv \frac{1}{n} \sim |\Delta\theta|^2 \qquad 4.15$$

For 66 data points, we find a Spearman coefficient of $r_S = 0.383$, i.e. correlated at the 99.9% confidence interval. Figure 4.10a shows a good comparison between the best fit line and the $|\Delta\theta| \sim n^{-1/2}$ line. Removal of one rogue point (due to the aforementioned unusual behaviour of 0J 287 in January 1983), however, destroys this comparison. Also, approximately 60% of the points are clustered about the origin ($\Delta\theta < 15$ and $n^{-1} < 0.4$). If these data are treated as two separate populations, we see (figures 4.10 b,c) that any apparent correlation has disappeared. The conclusion, therefore, is that variability in our sample of blazars is <u>inconsistent</u> with a <u>randomly-oriented</u> sub-units model.

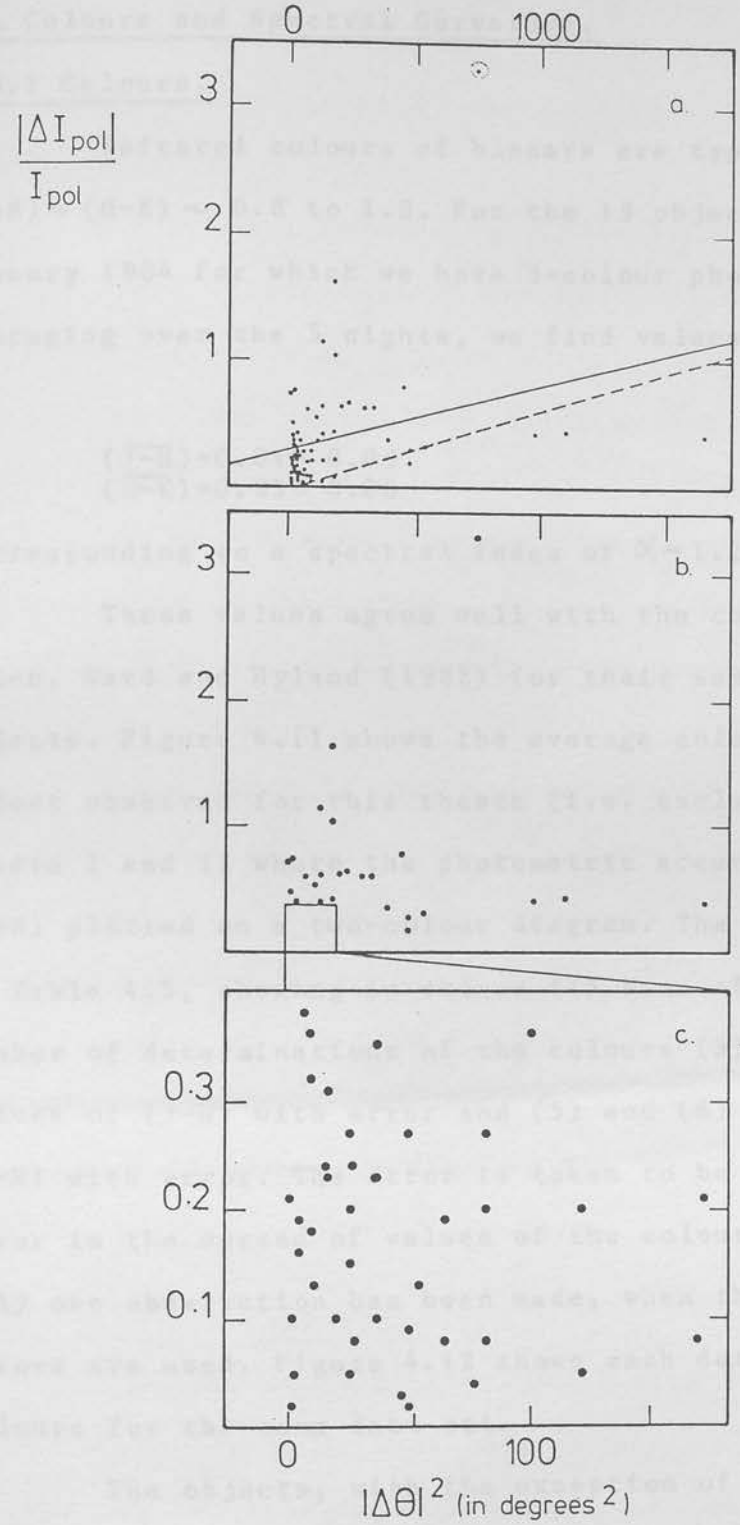

Figure 4.10 a) $|\Delta I_{pol}| / I_{pol}$ ($\equiv n^{-1}$) is plotted against $(\Delta\theta)^2$ for internight variations in polarized flux and position angle for all the data in this paper and paper III. The solid line shows the least-squares (Pearson) fit ($r_S = 0.31$, N=66) and the dashed line shows the $(\Delta\theta) = n^{-1/2}$ radian line. b) and c) show a similar plot, emphasising the true random scatter of the data points. The data plotted in b) have correlation parameters $r_P = 0.016$, $r_S = -0.304$, N=25 and the data in c) have correlation parameters $r_P = 0.12$, $r_S = -0.113$, N=41, showing no real correlation in the data.

4.6 Colours and Spectral Curvature.

4.6.1 Colours.

Infrared colours of blazars are typically $(J-H) \sim (H-K) \sim 0.8$ to 1.0. For the 19 objects observed in January 1984 for which we have 3-colour photometry, averaging over the 5 nights, we find values for the colours of

$$\overline{(J-H)} = 0.84 \pm 0.09$$
$$\overline{(H-K)} = 0.85 \pm 0.06$$

corresponding to a spectral index of $\alpha \sim 1.2$.

These values agree well with the colours found by Allen, Ward and Hyland (1982) for their sample of 53 BL Lac objects. Figure 4.11 shows the average colours for each object observed for this thesis (i.e. excluding the data of papers I and II where the photometric accuracy was not as good) plotted on a two-colour diagram. The data is presented in Table 4.5, showing in column (1) Name of object (2) number of determinations of the colours (3) and (4) mean values of (J-H) with error and (5) and (6) mean values of (H-K) with error. The error is taken to be the statistical error in the spread of values of the colour, except where only one observation has been made, when the photometric errors are used. Figure 4.12 shows each determination of the colours for the same data set.

The objects, with the exception of 1308+326 and BL Lac, are all consistent with a power-law slope of spectral index ~ 1.2, thus there is, in general, no need to invoke a thermal component (see also paper II; Bailey et al. 1981).

Figure 4.13 shows the mean values for the colours

for the 22 objects with error bars, the power-law and black body loci are superimposed, marked with spectral indices and temperatures respectively.

The unusual results for 1308+326 and BL Lac should be considered separately. BL Lac has a galaxian component easily identifiable on Schmidt plates. We, therefore expect some dilution due to the underlying galaxy. The result presented here (consistent with the colours for a T=2300 K black body) may be anomalous as there is only one determination of the colours. Typical values for BL Lac lie closer to the power-law region, with a typical spectral index of $\alpha \sim 1.0$ to 1.5.

There are only two observations of the colours of 1308+326. Puschell and Stein (1980) find colours consistent with a power-law of spectral index ~ 1.2. The unusual colours presented here cannot be due to a composite system of galaxy plus an embedded blazar, and we may only conclude that the behaviour is intrinsic to the blazar. 1308+326 has elongated VLBI structure (Weiler and Johnson 1980), possibly indicating the presence of a galaxy.

4.6.2. Spectral Curvature.

Spectral index is correlated with redshift at the 5% significance level. As discussed in section 4.4.7, one explanation for this is spectral curvature. There is strong evidence to suggest that spectral curvature may be a common property of blazars. Many multiwavelength observations have revealed spectra which steepen with increasing frequency in the infrared-optical-ultraviolet region (e.g. 0735+178, Bregman et al. (1983); 1156+295, Glassgold et al. (1983)).

Table 4.5 Mean infrared colours.

Object	N	J-H	Err	H-K	Err
0048	1	0.85	0.04	0.78	0.04
0215	5	0.82	0.06	0.85	0.04
0219	4	0.77	0.14	0.76	0.08
0235	8	0.98	0.11	0.90	0.05
0420	1	0.92	0.07	0.78	0.07
0422	4	0.86	0.04	0.83	0.02
0735	10	0.90	0.06	0.81	0.05
0736	2	0.85	0.02	0.94	0.04
0752	1	0.81	0.04	0.88	0.03
0754	4	0.84	0.04	0.83	0.02
0818	1	0.80	0.06	0.92	0.06
0829	6	0.88	0.03	0.85	0.04
0851	13	0.80	0.05	0.81	0.06
0912	2	0.71	0.02	0.71	0.01
1147	1	0.81	0.04	0.79	0.04
1156	1	0.88	0.05	0.84	0.04
1215	2	0.70	0.04	0.70	0.02
1219	1	0.83	0.05	0.86	0.03
1253	2	0.94	0.12	0.93	0.03
1308	2	0.69	0.07	1.07	0.04
1418	1	0.81	0.03	0.81	0.03
2200	1	0.94	0.05	0.62	0.04

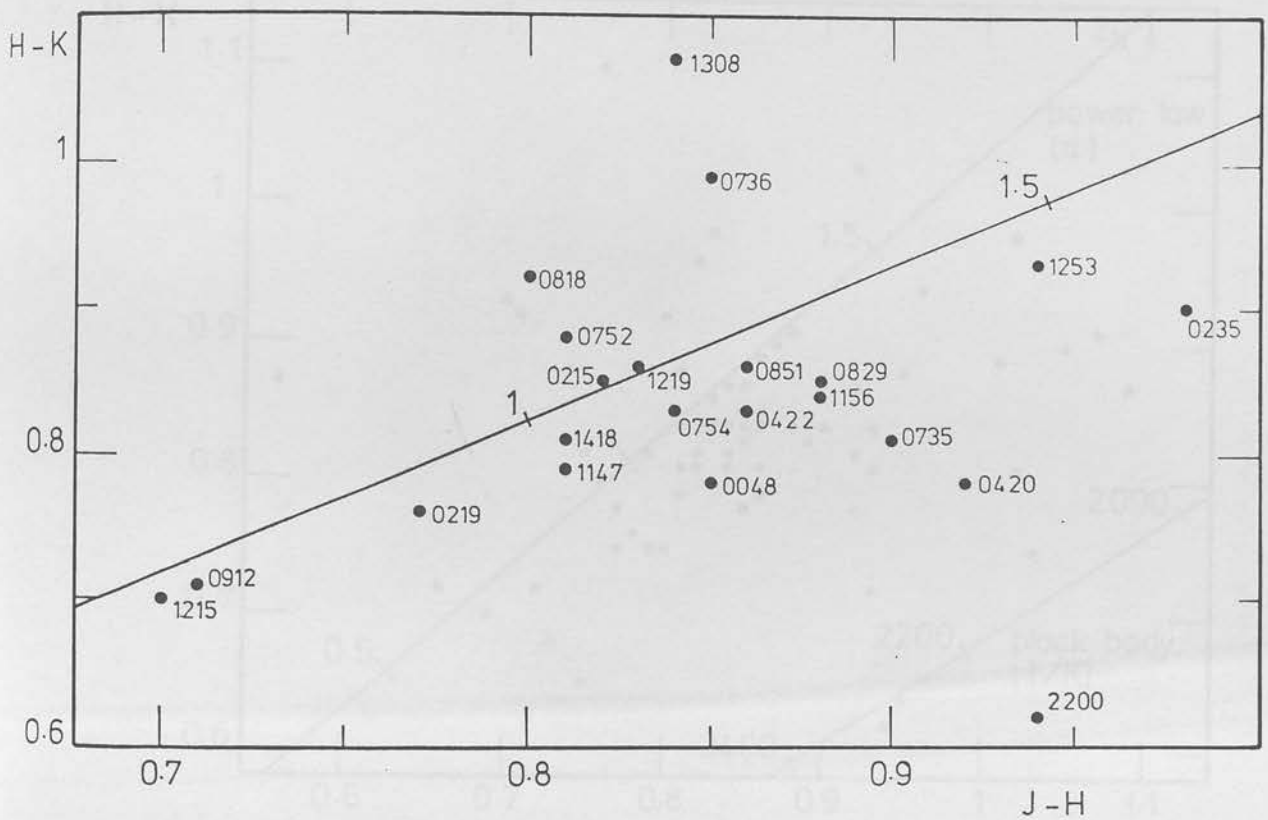

Figure 4.11 Two-colour diagram. $\overline{(H-K)}$ is plotted against $\overline{(J-H)}$ for all the objects observed for this thesis (i.e. papers III and IV). The R.A. of each object is given. The solid line is the locus of the power-law colours with α =1 and α=1.5 marked.

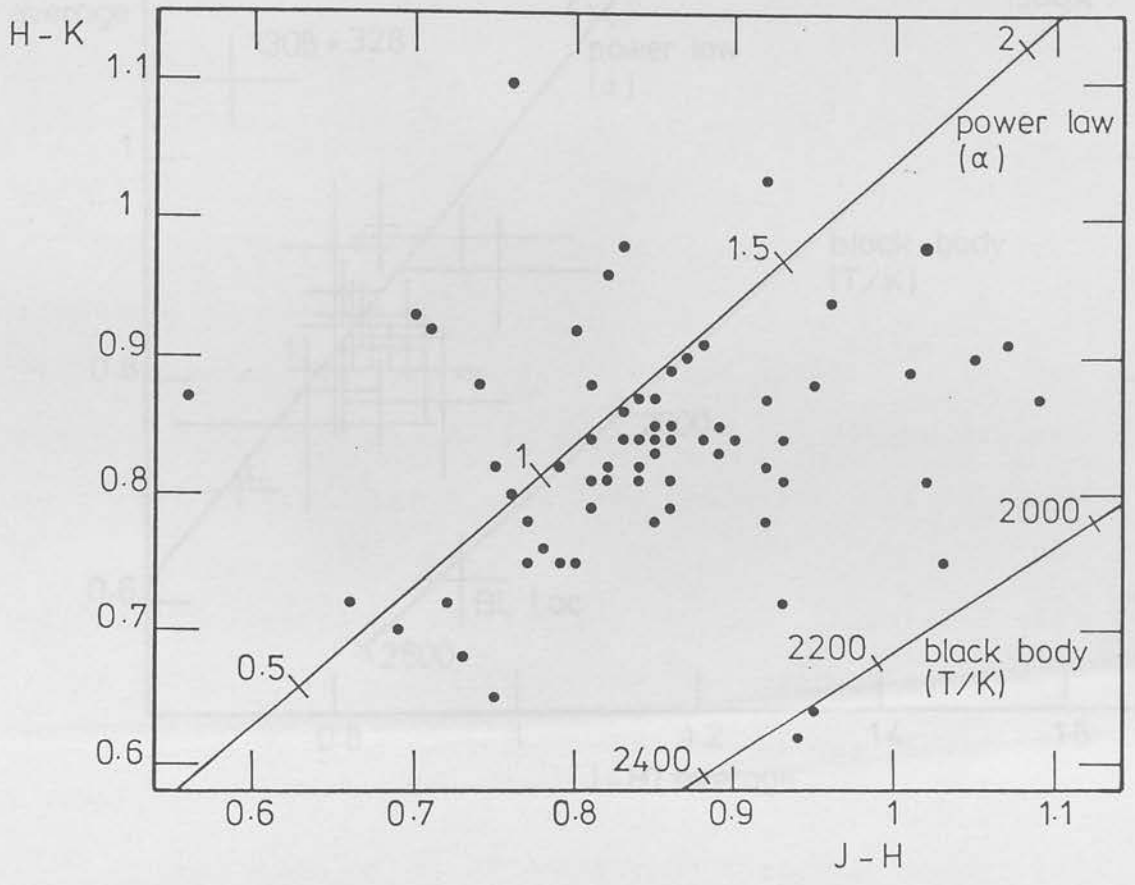

Figure 4.12 Two-colour diagram showing (H-K) plotted against (J-H) for each determination of these colours. The power-law and black-body loci are shown.

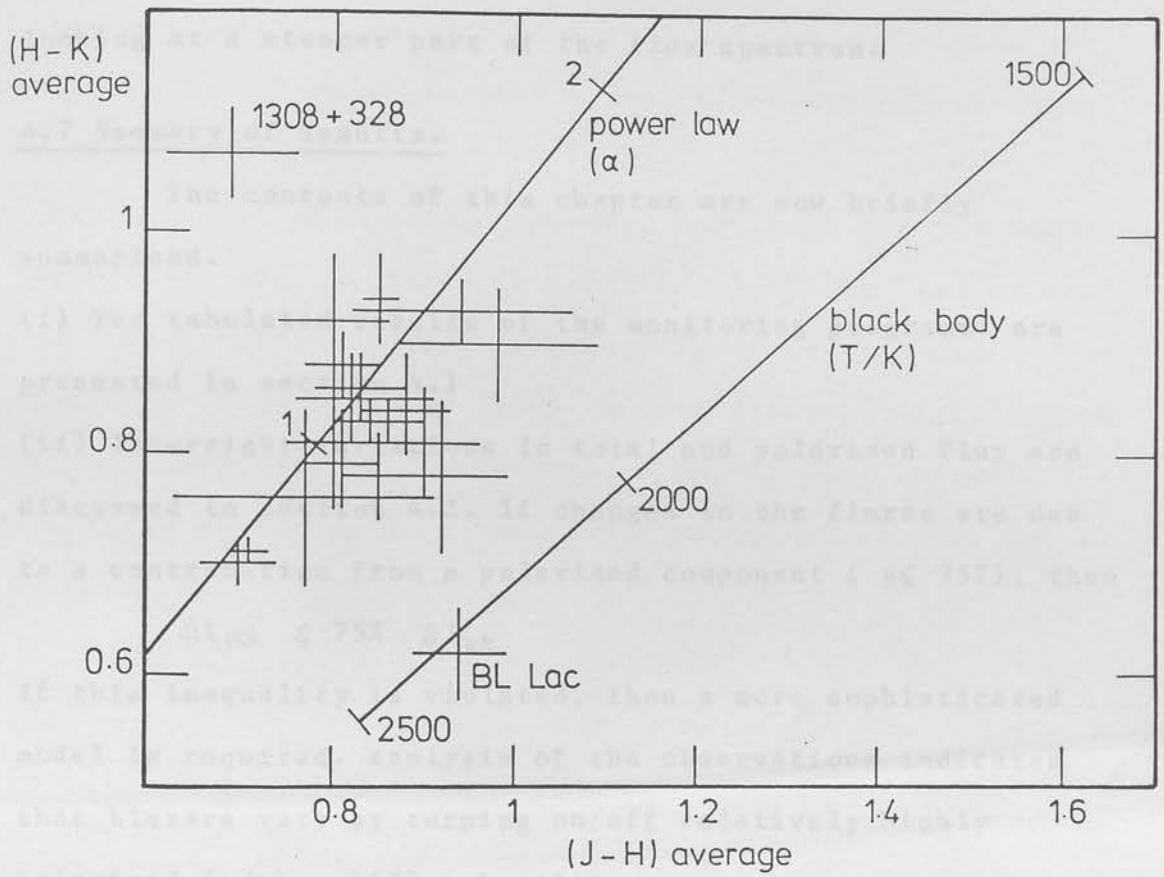

Figure 4.13 Two-colour diagram showing $(\overline{H-K})$ plotted against $(\overline{J-H})$ for each object with their associated error bars. The power-law and black-body loci are shown with several values of α and T(K) marked.

Also, non-simultaneous observations at optical and infrared wavelengths show a difference in mean spectral index ($\Delta\alpha = \alpha_{opt} - \alpha_{IR}$) of a typical value $\Delta\alpha \simeq 0.4$ for many blazars. If such positive curvature ($d\alpha / d \ln \nu > 0$) is general, then for higher redshift objects, we would be looking at a steeper part of the flux spectrum.

4.7 Summary of Results.

The contents of this chapter are now briefly summarised.

(i) The tabulated results of the monitoring programme are presented in section 4.1

(ii) Internight variations in total and polarized flux are discussed in section 4.2. If changes in the fluxes are due to a contribution from a polarized component ($p \lesssim 75\%$), then

$$\Delta I_{pol} \leqslant 75\% \ \Delta I_{tot}$$

If this inequality is violated, then a more sophisticated model is required. analysis of the observations indicates that blazars vary by turning on/off relatively highly polarized ($\langle p \rangle \sim 16\%$) sub-units.

Observations of 0829+046 show that the January 1983 variations may be understood in terms of a shallow-sloped synchrotron source ($p \sim 30\%$, $\theta \sim 109^{\circ}$) turning on.

(iii) Luminosity calculations and variability arguments are discussed in section 4.3. Five objects have now been observed to violate the Elliot & Shapiro criterion. The January 1983 variability of OJ 287, together with the Fabian & Rees criterion requires a mass to energy conversion efficiency of $\eta > 20\%$.

(iv) Correlations between various parameters have emerged

from the monitoring programme database, and these are described in section 4.4. The main results and conclusions are discussed in sub-section 4.4.7.

(v) Analysis of the fractional change in polarized flux and rotations of position angle is described in section 4.5. This analysis indicated that variability in our sample of blazars is inconsistent with a randomly-oriented sub-units model.

(vi) Infrared colours and spectral curvature for our sample of blazars are discussed in section 4.6. These colours are consistent with a power-law energy spectrum of typical spectral index $\alpha \sim 1.2$. The α -z correlation, together with non-simultaneous multiwavelength observations, indicate that spectral curvature over optical-infrared wavelengths may be general.

Chapter 5 OJ 287

5.1 Introduction.

OJ 287 (0851+202) is one of the best studied BL Lac objects. Its properties are described in section 2.3.12.

Multiwavelength observations of OJ 287 were made in January 1983. The infrared observations were carried out at UKIRT as part of the monitoring programme, and are described in chapter 2. Three-colour (J,H,K) photometry and polarimetry was collected on each of the 6 consecutive nights, and on 5 nights, L photometry was also collected. J,H,K photometry was performed twice on January 8th, revealing a 7% variation in flux in one hour (discussed in section 4.3.2.).

Optical observations were carried out on the UCSD/ Minnesota telescope. Five-colour (U,B,V,R,I) photometry and polarimetry was collected on 9 consecutive nights, from 2nd to 10th January inclusive. The filters and their effective wavelengths were U(0.36 micron), B(0.44 micron), V(0.55 micron), R(0.64 micron) and I(0.79 micron). Only the 4 nights where simultaneous optical-infrared photometry was collected are discussed in this chapter.

5.2 Results.

Table 5.1 shows the multiwavelength flux and polarization measurements for OJ 287 on four consecutive nights in January 1984. It shows in column (1) filter (2) & (3) flux density in mJy (with errors) (4) & (5) polarization degree in % (with errors) and (6) & (7) position angle in degrees (with errors).

TABLE 5.1

Flux and Polarization Measurements (with errors)

	w/b	F_ν(mJy)	$\sigma(F_\nu)$	p%	σ(p%)	θ^0	$\sigma(\theta^0)$
7 Jan 83	U	16.3	0.5	8.2	0.3	68.8	1.0
	B	21.7	0.8	7.4	0.2	70.3	0.7
	V	28.5	1.2	7.5	0.1	71.4	0.5
	R	31.7	0.6	7.8	0.1	71.9	0.5
	I	41.0	3.0	7.8	0.1	73.4	0.5
	J	60.0	2.2	8.3	0.9	71	3
	H	77.1	2.8	9.2	0.2	78	1
	K	88.8	0.8	9.4	0.3	99	1
8 Jan 83	U	19.0	0.6	2.5	0.3	21.6	3.1
	B	25.0	0.9	1.1	0.2	17.8	5.2
	V	32.7	1.3	0.8	0.2	22.3	5.6
	R	38.9	0.8	0.4	0.1	69.5	7.6
	I	52.0	3.7	0.7	0.1	99.3	5.5
	J	77.6	1.4	1.5	0.2	98	3
		74.8	1.4				
	H	103.6	1.9	2.6	0.2	91	2
		98.0	1.8				
	K	133.2	3.6	3.5	0.3	78	4
		123.7	3.4				
	L	183.3	5.5	-	-	-	-
9 Jan 83	U	16.7	0.5	4.7	0.2	142.8	1.4
	B	22.7	0.9	4.0	0.1	141.3	1.1
	V	30.1	1.2	3.9	0.1	133.2	1.0
	R	34.5	0.7	3.7	0.1	126.8	0.9
	I	45.9	3.3	3.8	0.1	124.0	1.1
	J	67.0	1.2	4.4	0.4	116	3
	H	85.4	3.1	4.6	0.1	114	1
	K	121.4	1.2	6.8	0.6	111	3
	L	168.7	3.4	-	-	-	-
10 Jan 83	U	14.8	0.4	5.7	0.3	154.2	1.3
	B	19.3	0.7	4.9	0.2	147.4	1.0
	V	26.1	1.1	4.0	0.2	141.6	1.1
	R	30.2	0.6	3.8	0.1	142.1	1.0
	I	40.2	2.9	3.9	0.2	134.2	1.1
	J	62.2	0.6	3.6	0.3	119	2
	H	80.8	0.8	4.4	0.1	120	1
	K	106.8	1.9	5.7	0.4	114	2
	L	159.6	4.8	-	-	-	-

5.3 Description.

The infrared flux of most blazars is well approximated by a power-law (e.g. Allen, Ward and Hyland, 1982). Our spectra, taken in January 1983, however, show significant curvature in the optical-infrared region (see figure 5.1) with local spectral index increasing with frequency. Typical values are $\alpha_{IR} \sim 0.87$, and $\alpha_{opt} \sim 1.25$ (where $\alpha = -d \ln S_\nu / d \ln \nu$). Similar curvature has also been seen in the optical-ultraviolet region of OJ 287 by Maraschi et al. (1983) and also in the BL Lac object 1156+295 by Glassgold et al. 1983. The spectral index-redshift relation (see section 4.4.2) indicates that spectral curvature over greater frequency ranges may be general.

The spectrum maintains its shape approximately from night to night, with the exception of the 2.2 micron flux on 7th January. It is, however, the unusual polarization data which give the best indication of the nature of the object. The polarization degree, p, shows a strong wavelength-dependence with p decreasing with frequency ($dp/d \ln \nu < 0$) in the infrared region, reaching a minimum in the near-infrared (I,R), and increasing with frequency ($dp/d \ln \nu > 0$) thereafter. See figure 5.2. Wavelength-dependence of the polarization position angle, $\Theta(\lambda)$, is also observed. On 8th January we see a huge and unprecedented rotation ($\Delta\Theta \sim 80^\circ$) between 0.5 and 0.8 micron. See figure 5.3. Coincident with this rotation was a pronounced dip in the polarized flux at 0.64 micron.

We can immediately reject a single synchrotron component model, as this could not yield the observed

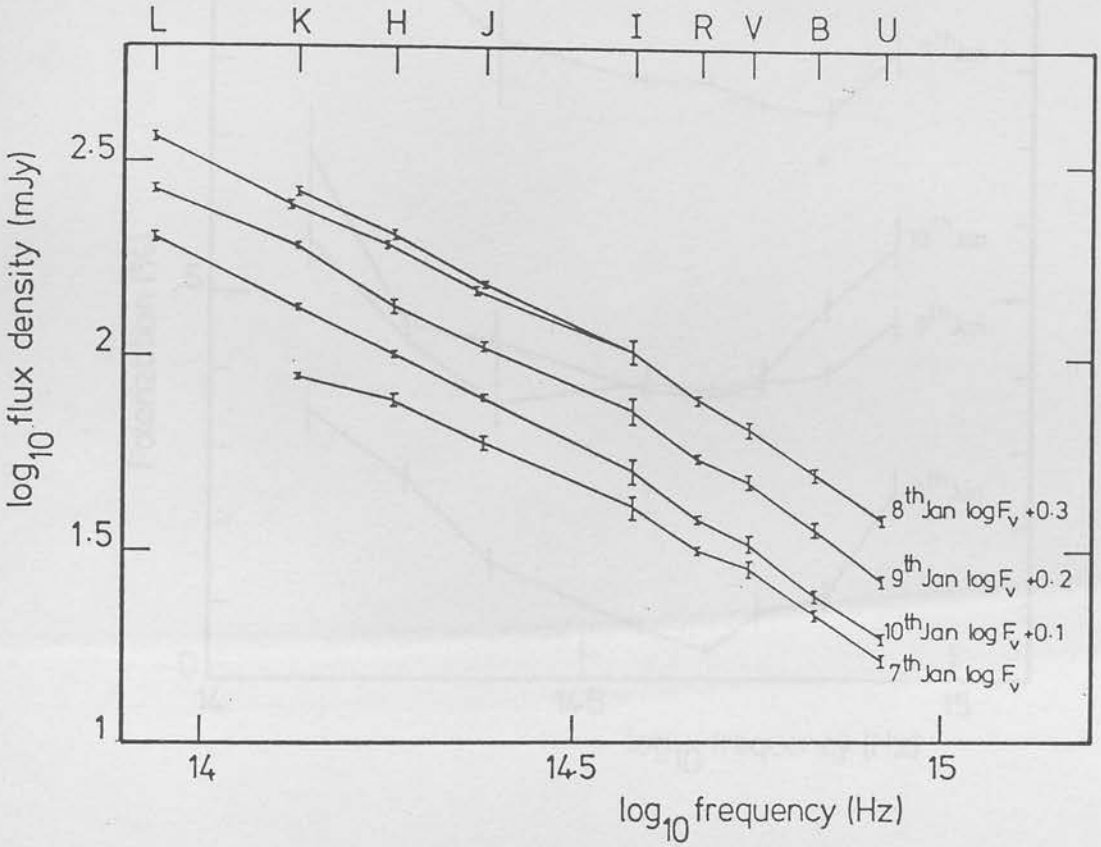

Figure 5.1 Flux Spectrum of OJ 287. Log flux density in mJy plotted against log frequency (in Hz).

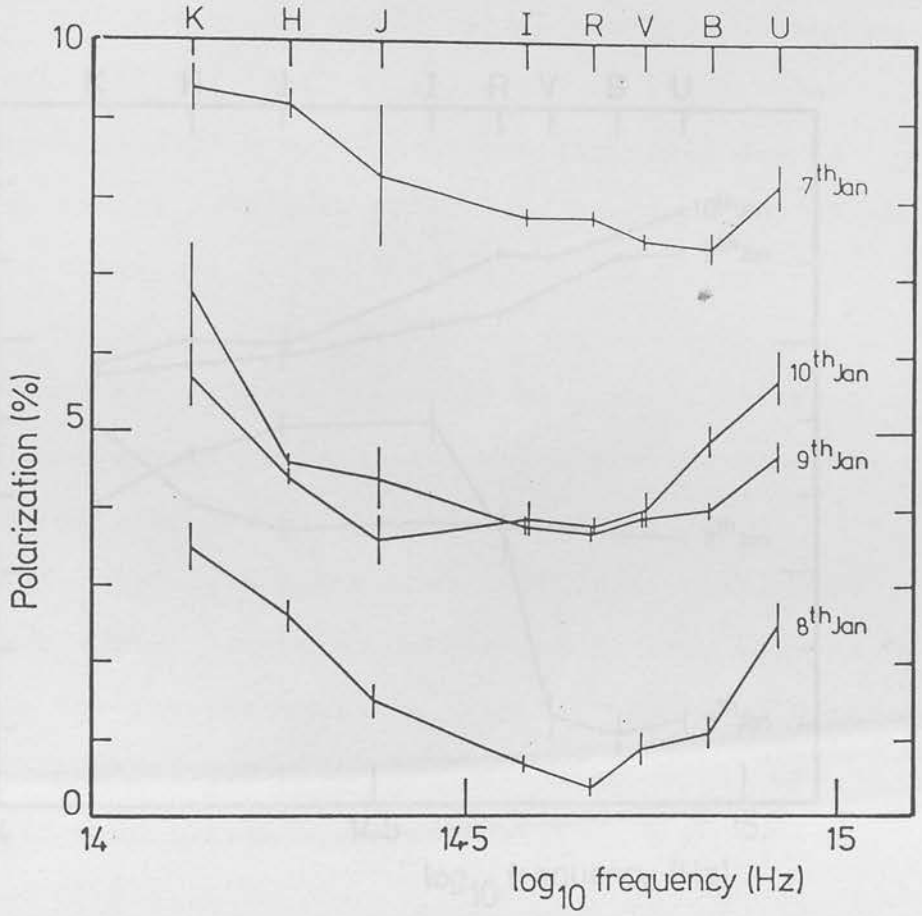

Figure 5.2 Spectral Polarization of OJ 287. Polarization percentage plotted against log frequency (in Hz)

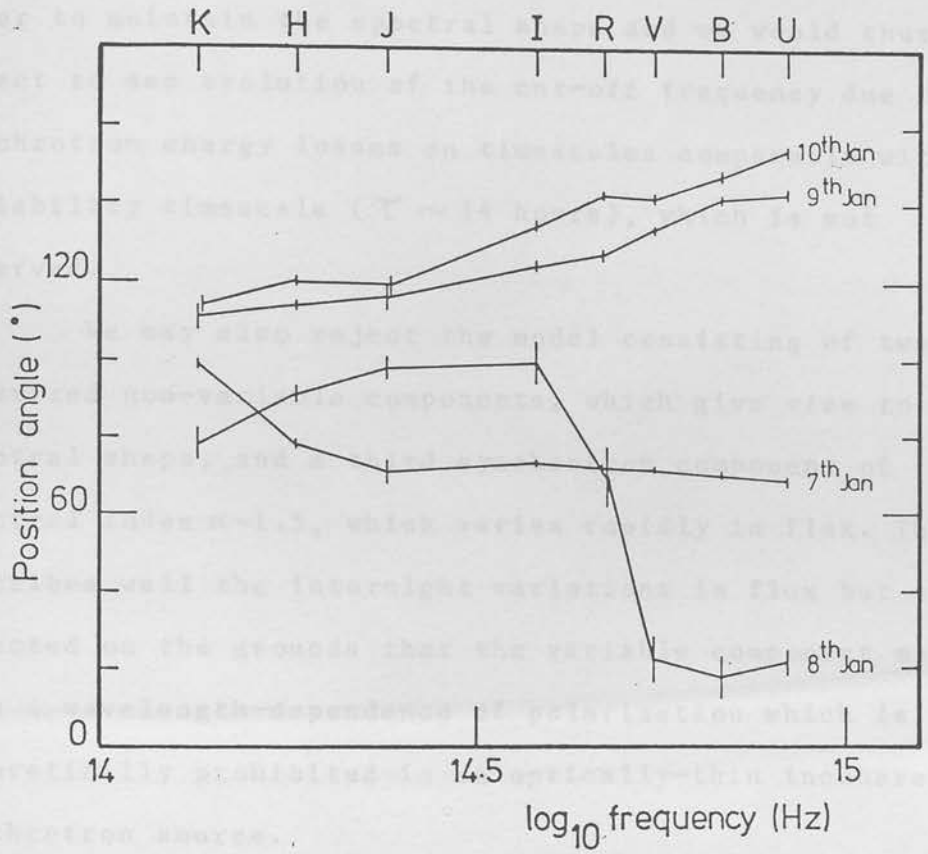

Figure 5.3 Spectral position angle of OJ 287. Position angle (θ) plotted against log frequency (in Hz).

wavelength-dependence. We can also reject the model consisting of two components with spectral cut-offs. This model would produce an abrupt change in p and θ at the cut-off frequency of this first component, when the second component begins to dominate completely. Such behaviour is not observed. Also, such components would need to vary in unison in order to maintain the spectral shape and we would thus expect to see evolution of the cut-off frequency due to synchrotron energy losses on timescales comparable with the variability timescale ($\tau \sim 14$ hours), which is not observed.

We may also reject the model consisting of two polarized non-variable components, which give rise to the spectral shape, and a third synchrotron component of spectral index $\alpha \sim 1.5$, which varies rapidly in flux. This describes well the internight variations in flux but can be rejected on the grounds that the variable component must have a wavelength-dependence of polarization which is theoretically prohibited in an optically-thin incoherent synchrotron source.

5.4 The Two-Component Model.

The model we propose seeks to explain the gross behaviour of the data in terms of two, optically thin, polarized components (p,θ independent of frequency). That such a superposition can produce p,θ curves similar to those observed can readily be seen. Consider two power-law components of spectral slope α_1, α_2 respectively.

If (S,p,θ), (S_1,p_1,θ_1) and (S_2,p_2,θ_2) are the flux, polarization degree and position angle for the

resultant radiation, and components 1 and 2 respectively, then we may write (see equation 3.19 in 3.3.3).

$$p^2 = \frac{p_1^2 + p_2^2 (S_2/S_1)^2 + 2 p_1 p_2 (S_2/S_1) \cos 2\xi}{(1 + S_2/S_1)^2} \qquad 5.1$$

where $\xi = \theta_2 - \theta_1$

and $$\tan 2\theta = \frac{p_1 \sin 2\theta_1 + p_2 S_2/S_1 \sin 2\theta_2}{p_1 \cos 2\theta_1 + p_2 S_2/S_1 \cos 2\theta_2} \qquad 5.2$$

and $$S_2/S_1 = (\nu/\nu_0)^{\alpha_1 - \alpha_2} \qquad 5.3$$

where ν_0 is the "cross-over" frequency, i.e. the frequency at which the fluxes of each component are equal (see equation 3.21 in 3.3.3).

The resultant spectral polarizations and position angles are then sensitive functions of ξ. The $p(\nu)$ and $\theta(\nu)$ are well approximated by taking the values $p_1 \simeq p_2 \simeq$ 11-20%, $\theta_1 \simeq 100^\circ$, $(\alpha_1 - \alpha_2) = 1/2$, where p_1, p_2, θ_1, θ_2 are all independent of frequency, and only θ_2 and ν_0 vary with time. The minimum degree of polarization on each night occurs at the frequency for which the polarized fluxes of each component are equal ($\forall |\xi| > 0$).

The $p(\nu)$, $\theta(\nu)$ curves are relatively insensitive to the exact values of the parameters $p_1, p_2, \theta_1, \theta_2, \nu_0$. The $p(\nu)$ curve is independent of θ_1 and θ_2, and the $\theta(\nu)$ curve is independent of the absolute values of p_1 and p_2, but is sensitive to the ratio p_1/p_2. Both curves are very sensitive to the value of ξ, especially for $\xi \geq 80^\circ$. This is well illustrated by the resultant curves shown in figures 5.4 a,b,c.

Such a double power-law component model is only a first approximation. Although it reproduces the p and θ curves remarkably well, the resulting spectrum must nec-

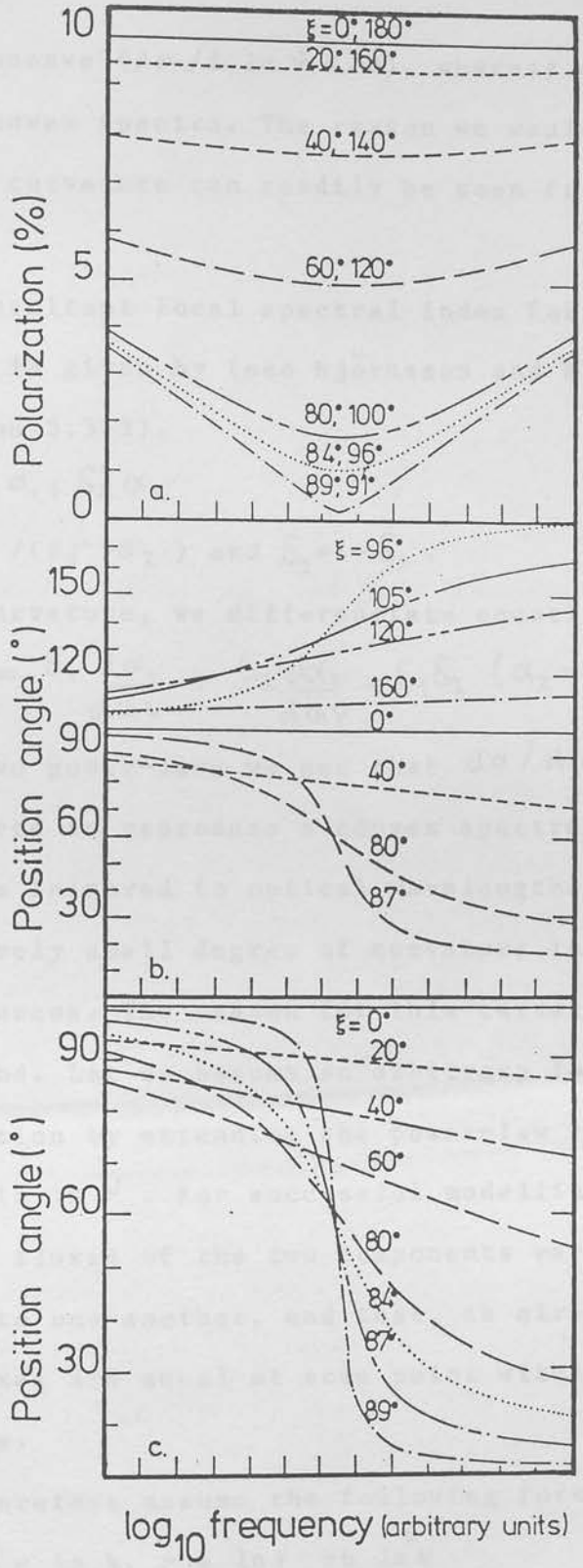

Figure 5.4 a) Polarizations and b) Position angles plotted against log frequency for several values of ξ . b) shows rotations for $0^\circ \leqslant \xi \leqslant 180^\circ$ while c) shows, in more detail, rotations for $0^\circ \leqslant \xi < 90^\circ$, emphasisng the rapid rotations with frequency for $\xi > 80$. Parameter values used:

$$p_1 = p_2 = 10\%, \quad \theta_1 = 100^\circ, \quad \alpha_2 - \alpha_1 = 1/2.$$

essarily be concave ($d\alpha / d \ln \nu < 0$), whereas our observations show convex spectra. The reason we would find concave (or negative) curvature can readily be seen from equation 5.6.

The resultant local spectral index for two superposed sources is given by (see Björnsson and Blumenthal 1982 and sub-section 3.3.3).

$$\alpha = \delta_1 \alpha_1 + \delta_2 \alpha_2 \qquad 5.4$$

where $\delta_1 = S_1 / (S_1 + S_2)$ and $\delta_2 = 1 - \delta_1$. 5.5

To find the curvature, we differentiate equation 5.4 to give

$$\frac{d\alpha}{d \ln \nu} = \delta_1 \frac{d\alpha_1}{d \ln \nu} + \delta_2 \frac{d\alpha_2}{d \ln \nu} - \delta_1 \delta_2 (\alpha_2 - \alpha_1)^2 \qquad 5.6$$

For two power-laws we see that $d\alpha / d \ln \nu < 0$. However, we need to reproduce a convex spectrum, with $\Delta\alpha \sim 0.4$ from infrared to optical wavelengths. This requires a relatively small degree of curvature in the spectra of the two sources. The reason for this curvature is not well understood. Let us assume an arbitrary form for the flux distribution by extending the power-law relation to second order in $\ln \nu$. For successful modelling, we require only that the fluxes of the two components vary smoothly with respect to one another, and that, as already noted, the polarized fluxes are equal at some point within the observed spectral range.

We therefore assume the following forms

$$\begin{aligned} \ln S_1 &= \ln k_1 - a \ln \nu - b \ln^2 \nu \\ \ln S_2 &= \ln k_2 - a \ln (\nu + \nu') - b \ln^2 (\nu + \nu') \end{aligned} \qquad 5.7$$

where $(k_1 - k_2)$ and ν' represent a relative shift in the spectra on both axes. We would emphasise that these forms are arbitrary, their sole purpose being to reproduce the

observed curvature, thus enabling us to calculate the expected polarization properties accurately. There is no loss of generality in adopting these forms in preference to any other.

We then allow the polarizations to be functions of the local spectral index, such that,

$$p_{1,2} = \Pi_{1,2} (\alpha_{1,2} + 1)/(\alpha_{1,2} + 5/3) \qquad 5.8$$

where Π is the "alignment parameter" of the magnetic field ($\Pi = 1$ for perfect alignment, and $\Pi = 0$ for a tangled field) which results in

$$p^2 = (p_1 \delta_1)^2 + (p_2 \delta_2)^2 - 2(p_1 \delta_1)(p_2 \delta_2) \cos 2\Xi \qquad 5.9$$

and $$\tan 2\theta = \frac{(p_1 \delta_1) \sin 2\theta_1 + (p_2 \delta_2) \sin 2\theta_2}{(p_1 \delta_1) \cos 2\theta_1 + (p_2 \delta_2) \cos 2\theta_2} \qquad 5.10$$

The spectra may be well approximated by taking $a = 0.8 - 0.95$, $b = 0.12 - 0.15$ and $\nu' = 3$, and where ν, ν' are in units of 10^{14} Hz. The flux constants k_1, k_2 need not be specified, but are defined implicitly by the values of and the cross-over frequency ν_0.

Parameter values which give a reasonable fit to the observational p, θ curves for each night, and also closely describe the spectral curvature are

	7th	8th	9th	10th
Π_1	26	17	20	22
Π_2	21	18	20	22
θ_1	99	104	91	96
Ξ	64	89	104	103
ν_0	3.9	4.8	3.9	3.1

These values are by no means unique, and the observational data are insensitive particularly to ν_0 over a small range. We have arbitrarily chosen $a = 0.8$ $b = 0.15$ and $\nu' = 3$

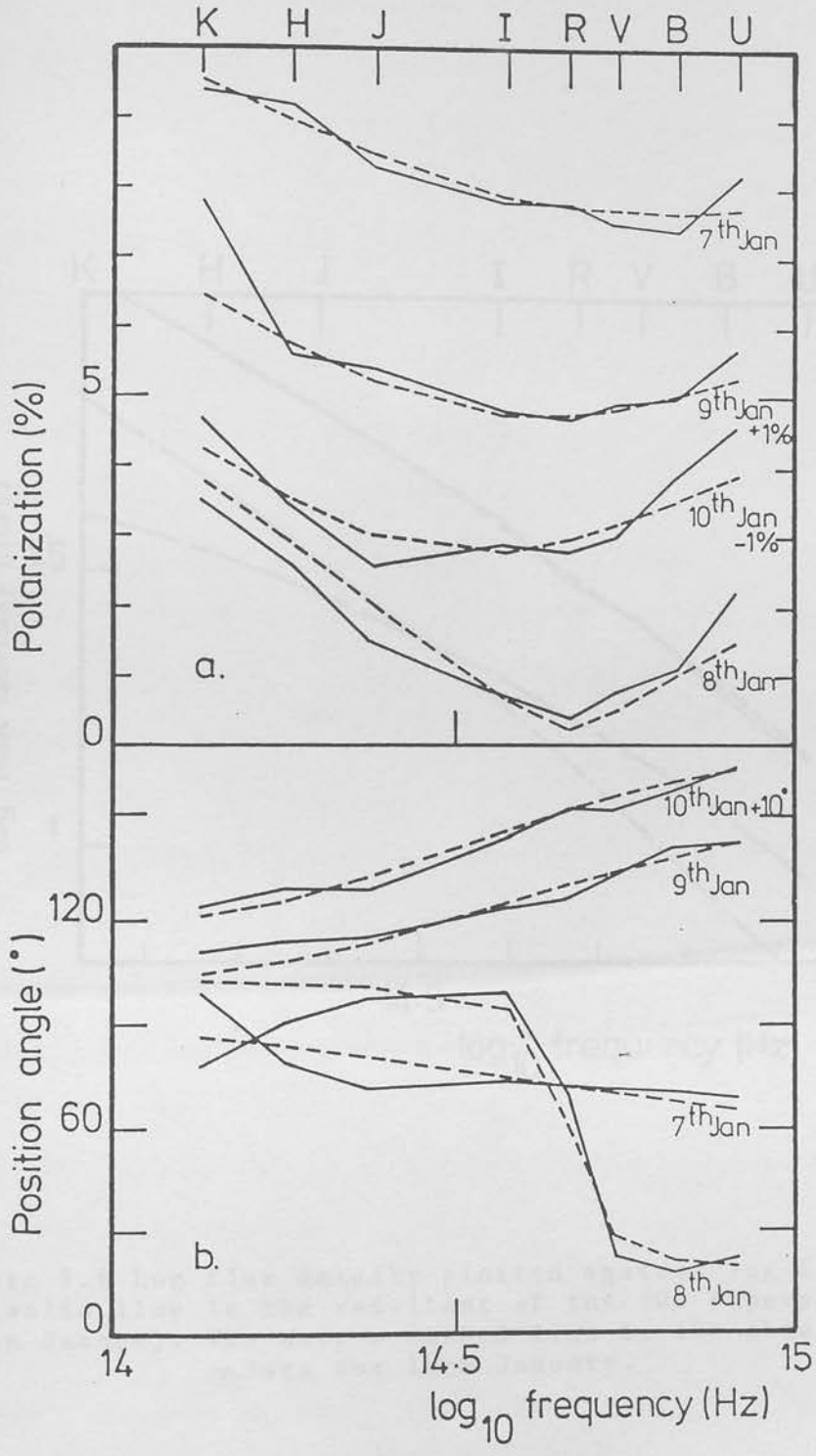

Figure 5.5 a) and b) Theoretical fits to the $p(\nu)$ and $\theta(\nu)$ curves respectively.

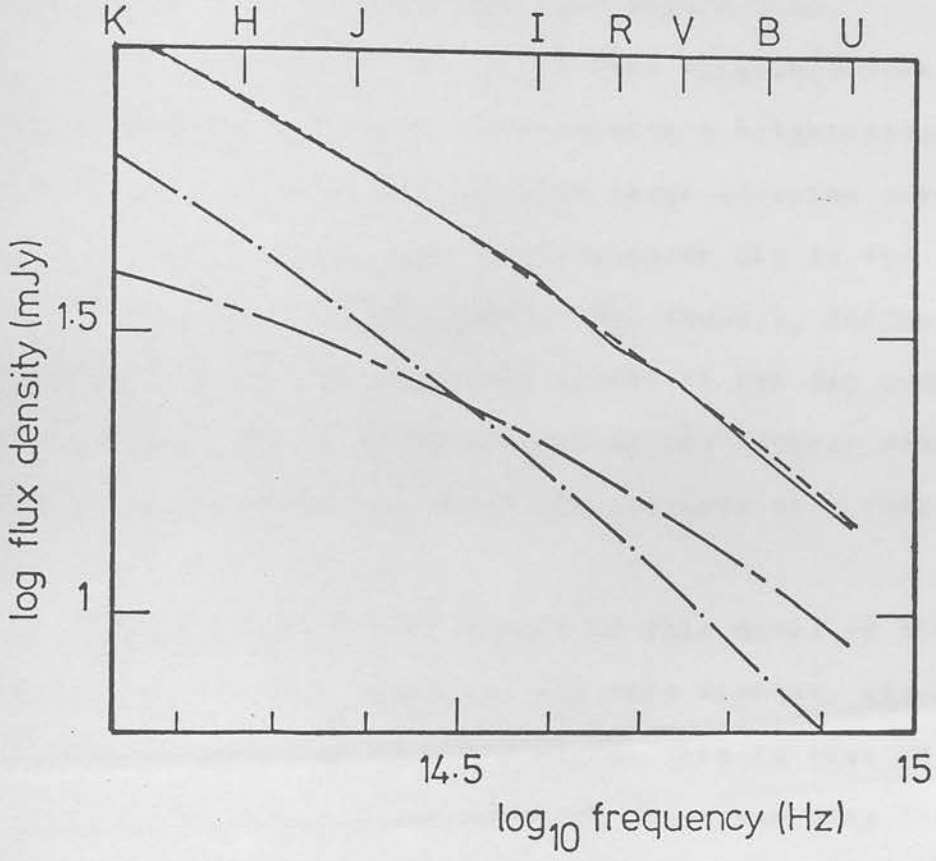

Figure 5.6 Log flux density plotted against log frequency. The solid line is the resultant of the two superposed spectra (wide dashes). The narrow dashed line is the observational data for 10th January.

for each night to generate the theoretical curves (figures 5.5 a,b). However a range of values of a and b is required to fit the spectral curvatures more accurately (as explained above). For example, the spectrum of 10th January is reproduced using a = 0.95 and b = 0.15, together with the polarization values tabulated above. (See figure 5.6).

It is clear that the cross-over frequency does change from night to night, representing a brightening of one source relative to another. The large rotation over a small wavelength renge, and the pronounced dip in the polarization curve, which occur on 8th January, define the frequency at which the polarized fluxes of the two components are equal. It is possible that at the longest wavelengths, the θ curve indicates the presence of a third component.

The most noticeable aspect of this model is that the polarizations of each component are very similar, and tend to vary in unison from night to night. This is true of the flux distribution also, for although the cross-over frequency varies from night to night, it does so only over a narrow range considering the relatively large internight variations in total flux. This strongly suggests that the two components are physically connected. The first component has a stable position angle ($\theta_1 = 100^\circ$) while the second component shows a gradual rotation from East through North. This behaviour may be understood in terms of a physical rotation of the magnetic field.

5.5 Discussion.

We have described the complex polarization behaviour

of OJ 287 during the January 1983 outburst in terms of two "simple" synchrotron emitters, i.e. regions where a (presumably partially tangled) magnetic field gives rise to a wavelength-independent polarization and position angle of the emitted radiation. The emitted flux densities from the two postulated sources need not be power-laws in frequency but their ratios must vary slowly and smoothly with frequency, as expressed by the index difference $\alpha_2 - \alpha_1$, which we take to be 1/2. This value was chosen to represent the steepening of the flux spectrum in the presence of a constant injections of electrons and energy losses by synchrotron radiation (Kardashev 1962). Although the slight variation of ν_0 suggests that the flux densities of these two sources do not vary quite in unison, the differences are slight, certainly much less than if the sources were independent.

We stress that a minimum of two components are required to dominate the emission in the optical-infrared region only. This is further supported by the results of the monitoring programme (papers III and IV and section 4.2 and chapter 8). This by no means excludes the possibility that there are other components dominating at other wavelengths such as far-infrared and radio.

It should be emphasised here that the model used to describe OJ 287 is not generally applicable to other blazars. Arguments put forward in sections 4.5 and 7.3 indicate that the components of blazars tend to be aligned, probably by the same magnetic field. The observations of OJ 287 are unique in that they require non-aligned components to explain the huge rotations with wavelength. Furthermore,

while one component remains constant in position angle, the second rotates with time. Coincident with this rotation was a peak in the flux and a minimum in the polarization degree. It might be unusual behaviour such as this that provides the strongest clues as to what is going on in a blazar.

The flux variability of $\sim$ 7% in one hour observed on 8th January 1983, shows that the infrared luminosity is near the Eddington limit for accretion onto a massive black hole (paper III and section 4.3.2) which strongly suggests the presence of a jet (Rees 1978). The observed radiation may then be modelled in terms of a cloud of emitting electrons being accelerated in the jet (e.g. Blandford and Königl 1979, Marscher 1980). We have seen, however, that the fluxes for each component vary approximately in unison while the curvature remains fairly constant. This leads naturally to a picture of a single independent source of electrons impinging upon two magnetic field regions. The two fields have differing magnetic field vectors but similar degrees of alignment. The energy spectrum must be "imprinted" upon the electron distribution before encountering the two magnetic field regions.

Several possibilities have been considered in the OJ 287 paper (H+13), including a core/halo magnetic field structure, and two clouds of electrons being accelerated in a jet. Such speculation is beyond the scope of this chapter.

Chapter 6. Wavelength-dependence--Theoretical.

6.1 Introduction.

This chapter deals with the spectral polarization properties expected from various distributions of electron energy and magnetic field.The initial purpose of this was to attempt to reproduce the observed frequency dependence of the infrared polarization seen in OJ 287 (see chapter 5) by pure synchrotron radiation, without resorting to either a) more than one component or b) more complex geometries and emission processes.

The theory is described in some detail, together with a brief description of the computer model and results. The formalism of Björnsson and Blumenthal (1982) (hereafter BB) is followed closely throughout. The remainder of this section is adapted mainly from BB and Nordsieck.

The polarization properties of synchrotron radiation from a perfectly aligned magnetic field are well understood. (e.g. Korchakov & Syrovatskii 1962; Nordsieck 1976; Westfold 1959). The degree of polarization is, to an excellent approximation, given by

$$\Pi_\nu = (\alpha_\nu + 1)/(\alpha_\nu + 5/3) \qquad 6.1$$

where $\alpha \equiv -d \ln S_\nu / d \ln \nu$ is the local spectral index. For an electron energy distribution of the form $N(\gamma) \propto \gamma^{-2.5}$, for example, the expected degree of polarization from a perfectly aligned field is $\Pi \sim 72.5\%$. Although high degrees of polarization have been observed for many blazars (e.g. 0235+164, $p \sim 44\%$, Impey, Brand and Tapia 1982), typical vaues for optical-infrared wavelengths are $\langle p \rangle \sim 11\%$. (See section 4.5). This implies at least some degree of

"tangling" of the magnetic field (or a superposition of several non-aligned components).

For synchrotron radiation from an ensemble of ultra-relativistic electrons, we may write the Stokes parameters (to first order in γ^{-1}) as

$$S_\nu = C \int b^2 H(b,\chi,\gamma) F(x)\, db\, d\chi\, d\gamma$$

$$\begin{matrix} Q_\nu \\ U_\nu \end{matrix} = C \int b^2 H(b,\chi,\gamma) \begin{matrix} \cos 2\chi \\ \sin 2\chi \end{matrix} G(x)\, db\, d\chi\, d\gamma \qquad 6.2$$

$$V = 0 \text{ (i.e. no circular polarization)}$$

where C is a constant, γ is the Lorentz factor of the radiating electron, and $\underline{b}$ is the transverse component of the magnetic field.

χ is the angle between some fixed direction (celestial North, say) and a direction perpendicular to $\underline{b}$, (see figure 6.1). $H(b,\chi,\gamma)$ is the trivariate probability density of finding an electron with Lorentz factor γ radiating in a magnetic field specified by b and χ .

The quantity x is defined by $x \equiv \nu/\nu_c$, ν_c is the characteristic frequency of an electron and is given by

$$\nu_c = 3eB\gamma^2 \sin\psi / 4\pi m \simeq 3eb\gamma^2/4\pi m \qquad 6.3$$

since $B \sin\psi \simeq b$ when $\gamma >> 1$, when ψ is the electron pitch angle (see fig 6.1). Spectral properties are given by the functions

$$F(x) \equiv x \int_x^\infty K_{5/3}(y)\, dy$$

$$G(x) \equiv x K_{2/3}(x) \qquad 6.4$$

where $K_{2/3}$ and $K_{5/3}$ are modified Bessel functions of fractional order (Abramowitz and Stegun 1970).

The trivariate probability density may be divided

into 3 permutations of bivariate and single probability densities which exhibit qualitatively different behaviour, namely

$$H(b,\chi,\gamma)= \begin{matrix} h(b,\gamma)\,\theta(\chi) \\ h(b)\;N(\chi,\gamma) \\ h(b,\chi)\;N(\gamma) \end{matrix} \qquad 6.5$$

Case a). When χ does not correlate with b or γ. The polarization degree and position angle, Π_ν , Ξ_ν , respectively, are given by

$$\begin{aligned} \Pi_\nu &= (Q_\nu^2 + U_\nu^2)\,/S \\ &= \eta\,(\gamma)\,(\alpha_\nu+1)/(\alpha_\nu+5/3) \end{aligned} \qquad 6.6$$

since

$$\frac{(\alpha_\nu+1)}{(\alpha_\nu+5/3)} \quad \frac{b^2 h(b,\gamma)\;G(x)\;db\;d\gamma}{b^2 h(b,\gamma)\;F(x)\;db\;d\gamma} \qquad 6.7$$

is the polarization degree from an aligned magnetic field, and when

$$\eta(x) \equiv \frac{\left\{\left[\int\theta(\chi)\cos 2\chi\;d\chi\right] + \left[\int\theta(\chi)\sin 2\chi\;d\chi\right]\right\}^{1/2}}{\int\theta(\chi)\;d\chi} \qquad 6.8$$

is the "alignment parameter".

$$\tan 2\Xi = \frac{U_\nu}{Q_\nu} = \frac{\int\theta(\chi)\;\sin 2\chi\;d\chi}{\int\theta(\chi)\;\cos 2\chi\;d\chi} \neq \mathrm{fn}(\nu) \qquad 6.9$$

We see that the position angle Ξ is independent of frequency and that the polarization degree is only weakly dependent upon frequency.

Case b). When the magnetic field strength varies independently of χ and γ. This results in a frequency-dependence $(\Pi(\nu), \Xi(\nu))$ because the electron energy distribution changes with position, i.e. χ & γ are interdependent. This can be regarded as a superposition of <u>many</u> sources with differing

electron energy distributions.

Case c). When the electron energy distribution is independent of the magnetic field distribution. The resulting frequency-dependence is due to the coupling of b & χ.

Nordsieck (1976) investigated this case for 3 forms of the bivariate probability $h(b,\chi)$. These forms included probability contours described by a)concentric ellipses and b) concentric circles offset from the origin, produced by a spatial squash of the isotropic field and by a vectorially superposed field, respectively. The third form was $h(b,\chi) = H(b)\Theta(\chi)$, i.e. separable field strength and alignment distributions. He finds that, except in "rather special situations", a polarization-spectral index correlation would be predicted, i.e. $\Pi' > 0$ when $\alpha' > 0$. There are two "rather special situations": (i) where the magnetic field distribution is exponential and (ii) the special case where the bivariate form is separable into two single probability densities, i.e. $h(b,\chi)=H(b)\Theta(\chi)$.

6.2 The Computer Model.

The program evaluates the integrals

$$S_\nu = \int_{\gamma_{lower}}^{\gamma_{upper}} d\gamma \int_{b_{lower}}^{b_{upper}} b^2 \, db \; F(x) \int_{\chi_{lower}}^{\chi_{upper}} H(b,\chi,\gamma) \, d\chi$$

and

$$\begin{matrix} Q \\ U \end{matrix} = \int d\gamma \int b^2 \, db \; G(x) \int H(b,\chi,\gamma) \begin{matrix} \cos 2\chi \\ \sin 2\chi \end{matrix} d\chi \qquad 6.10$$

(with similar integral limits for Q_ν and U_ν), by calling the NAG Fortran Library Routines D01AHF (single integral) and D01DAF (double integral).

The Stokes parameters are evaluated by performing the single integral in χ once for every different value of γ

and b in the double integral, for successive values of ν. They are separated into single and double integrals in this way because of the frequency dependence of the modified Bessel functions. Since $x \equiv \nu/\nu_c \propto \nu/\gamma^2 b$, we see that only the χ integral is separable from frequency. The values of the functions F(x) and G(x) are calculated for each value of ν, performing a spline fit to the data tabulated in Westfold (1959). See figures 6.2.

To test the accuracy of the program, several checks were made.

(i). Letting $H(b,\chi,\gamma) = \gamma^{-1}$ in an aligned magnetic uniform field should yield $\Pi = 60\%$ ($\neq \Pi(\nu)$) and also frequency independent flux, S_ν, and position angle, Ξ_ν. This result was accurately reproduced. Weak frequency dependence could be effected by altering the limits of integration of the 3 variables, as would be expected. The limiting factor was found to be the upper limit in γ.

(ii). Letting $H(b,\chi,\gamma) = \gamma^{-2}, \gamma^{-3}, \gamma^{-4}$ accurately reproduced the results expected from $\Pi = (x+1)/(x+7/3)$, where $N(\gamma) \propto \gamma^{-x}$. On occasion it was found necessary to improve the accuracy parameters for the smaller values of ν. The value of Π_ν decreased as a range in χ was introduced. This corresponds to a decrease in the value of the alignment parameter $\eta(x)$. See equation 6.8.

(iii). The spectral polarization from a monoenergetic distribution of electrons radiating in an aligned uniform field was faithfully reproduced (see figure 6.3).

Many different forms for the trivariate probability density were used. Table 6.1 summarises the results of the computer

simulations. Firstly the notation is defined and secondly the results tabulated. It shows in column (1) the form of the trivariate probability distribution, (2) the range of values used to describe electron energy and field distributions (3) a qualitative description of the results, and in column (4) comments.

An attempt was made to reproduce the infrared polarization behaviour of OJ 287 by superposing three simple synchrotron sources with similar position angles. These sources had electron energy distributions of the form $N(\gamma) \propto \gamma^{-3}, \gamma^{-2}, \gamma^{-1}$, respectively, thus producing, in the power-law region, polarizations of Π_ν= 75%, 69.2%, 60%. The Stokes parameters were added together in varying ratios, and the resultant polarizations and intensities show that even in the most extreme cases, the degree of polarization decreases only by $\Delta p/p \sim$ few percent over a large frequency range.

6.3 Conclusions.

It is unlikely that any physically simple distributions of magnetic field and electron energies can reproduce the behaviour observed in the infrared data for OJ 287, namely $\Pi' < 0$, $\alpha > 0$, and $\Xi' \neq 0$. More generally, any single synchrotron source is unlikely to produce $\Pi' < 0$ except in the case of a convex spectrum ($\alpha' < 0$), which is a rare, if not unknown, phenomenon in blazars.

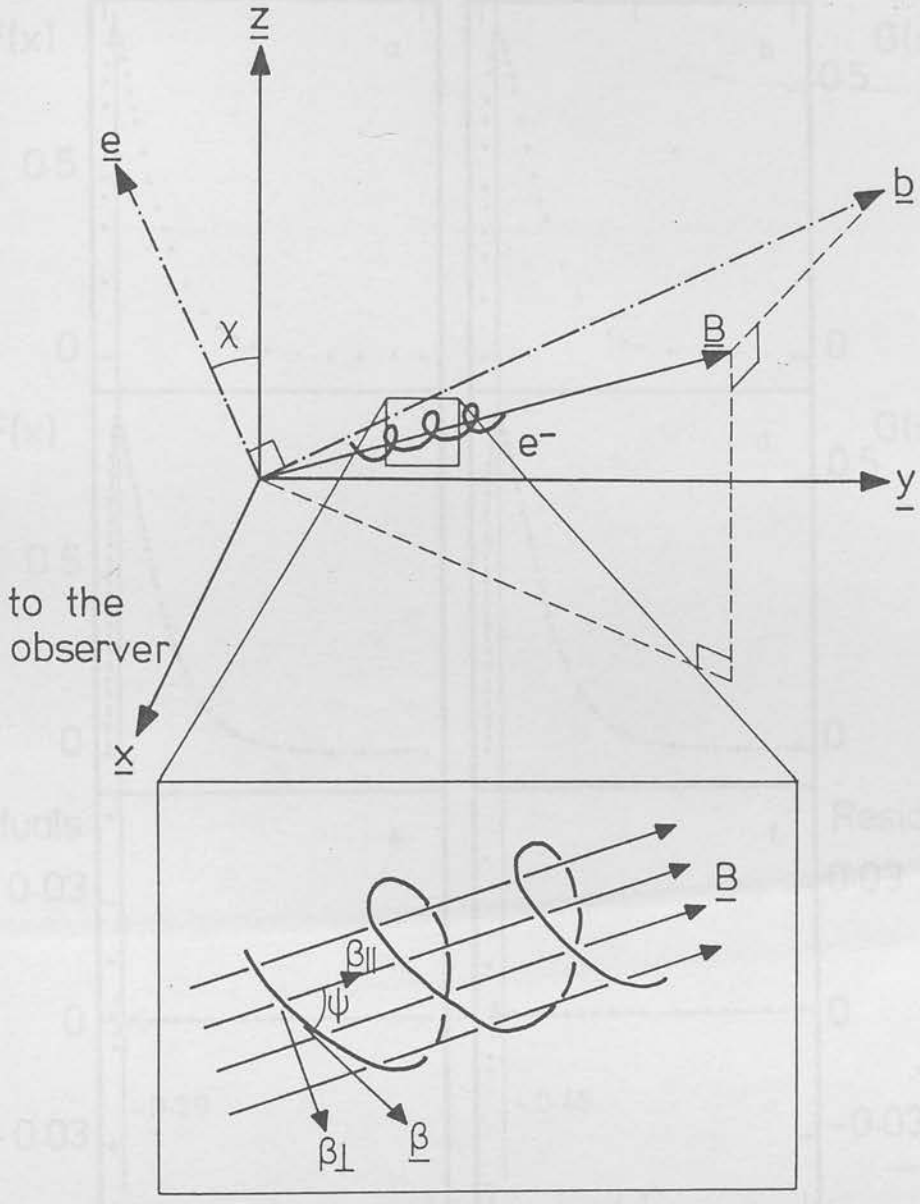

Figure 6.1 Magnetic Field Geometry. An electron with Lorentz factor γ ($\equiv [1-\beta^2]^{-1/2}$) spirals around a magnetic field $\underline{B}$. $\underline{b}$ is the component of the magnetic field projected onto the plane of the sky (the y-z plane). The angle χ is the angle between some reference direction and the direction perpendicular to $\underline{b}$. The angle ψ between the electrons velocity vector $\underline{\beta}$ and its component parallel to the magnetic field ($\beta_{\parallel}$) defines the pitch angle.

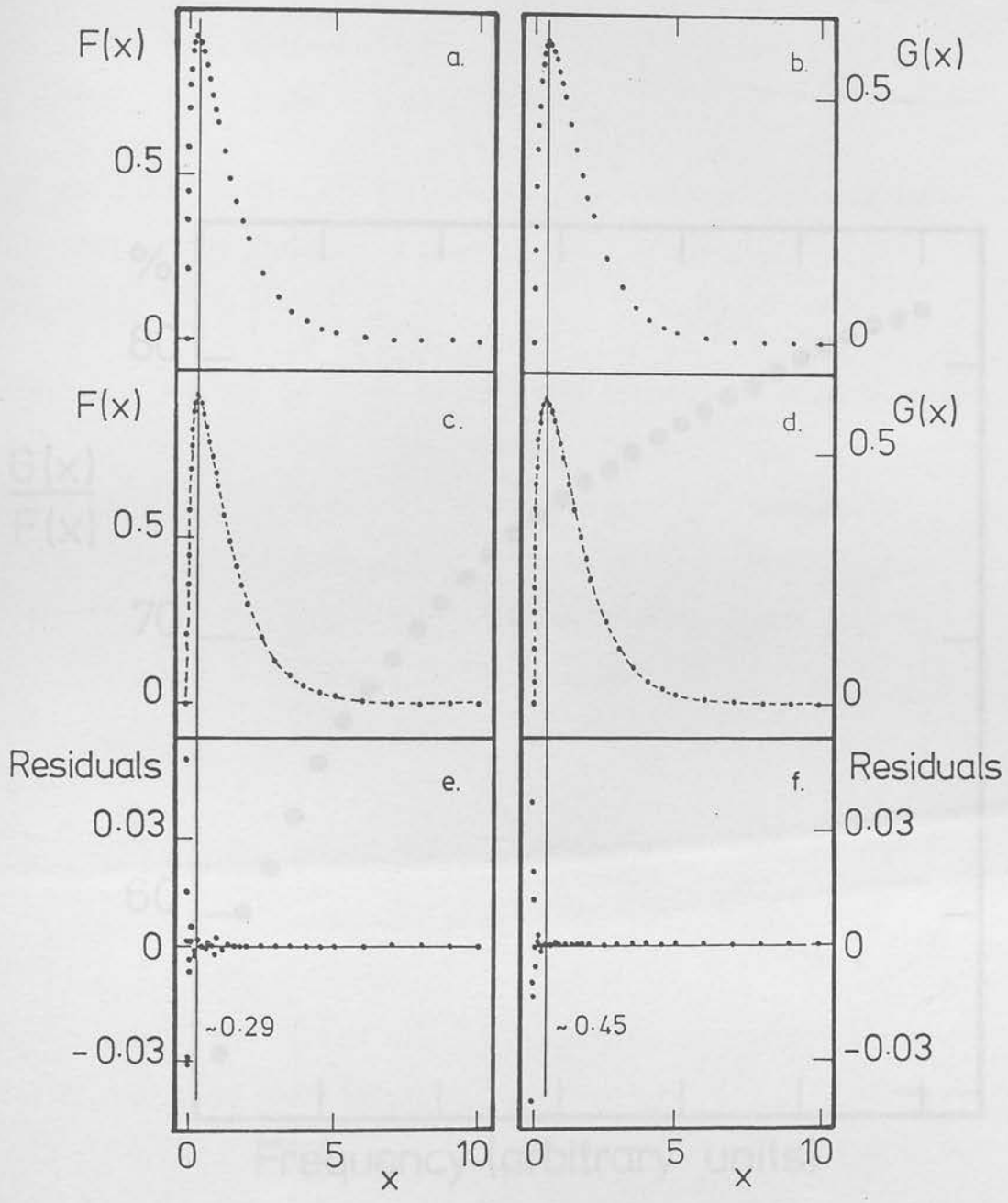

Figure 6.2 a) and b) show the tabulated values of F(x) and G(x) respectively, plotted against x. The maxima are marked. Data are taken from Westfold (1959). c) and d) Show the spline interploations of the above functions. e) and f) Show the residuals of the spline fits. These show accuracies of better than 1% for all values of $x \geqslant 0.2$ and better than 0.1% for $x \geqslant 1.0$.

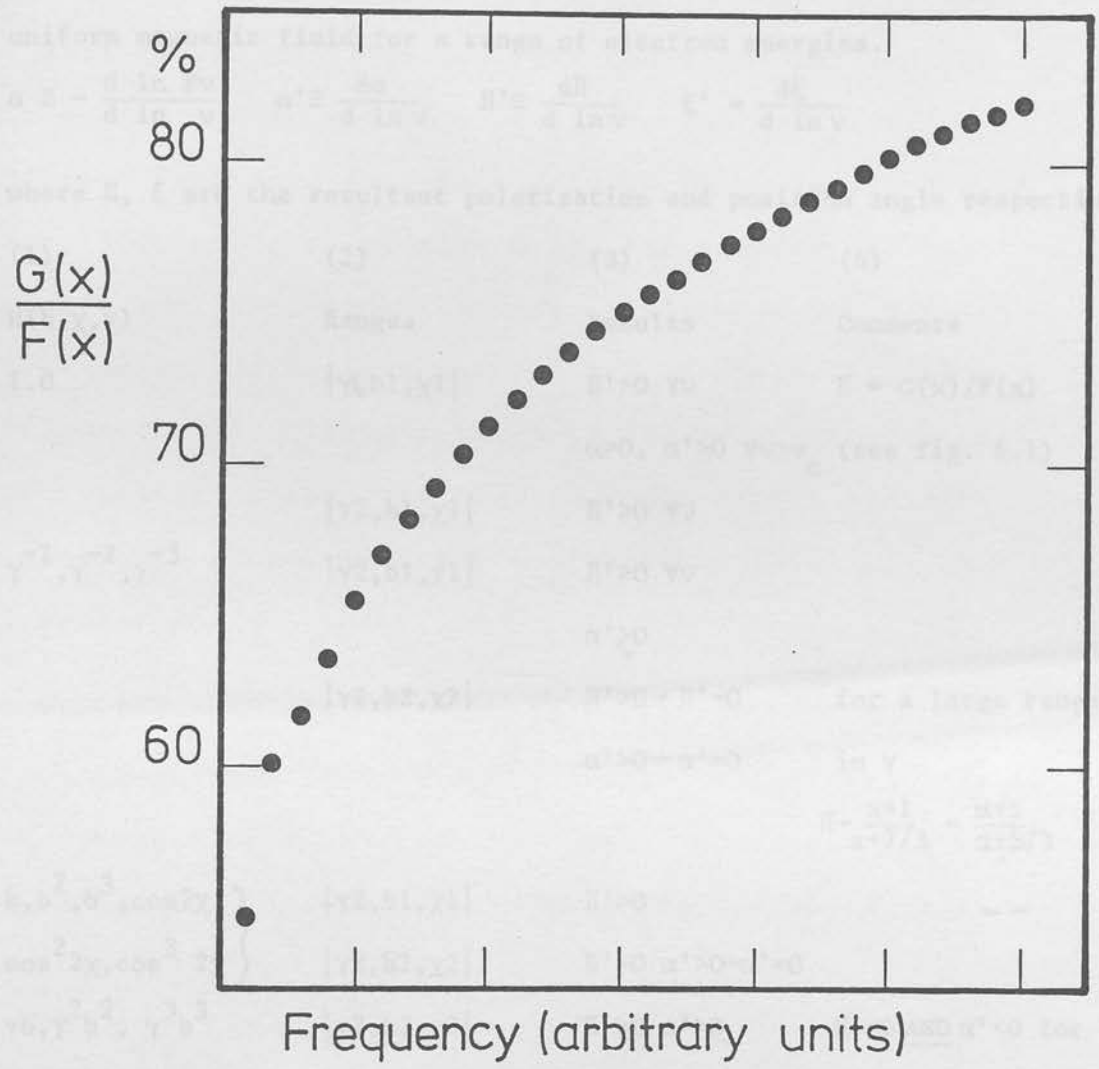

Figure 6.3 Degree of linear polarization plotted against frequency (or x) in arbitrary units. Polarizations are given by $\Pi_y = G(x)/F(x)$.

TABLE 6.1 Results of the Computer Model

Notation: $|\gamma 1|$ monoenergetic electrons

$|b1|$ uniform field strength

$|\chi 1|$ aligned field

$|\gamma 2|$, $|b2|$, $|\chi 2|$ range of values

So, for example, $|\gamma 2, b1, \chi 1|$ refers to the emission from an aligned uniform magnetic field for a range of electron energies.

$\alpha \equiv -\frac{d \ln F\nu}{d \ln \nu}$ $\alpha' \equiv \frac{d\alpha}{d \ln \nu}$ $\Pi' \equiv \frac{d\Pi}{d \ln \nu}$ $\xi' = \frac{d\xi}{d \ln \nu}$

where Π, ξ are the resultant polarization and position angle respectively.

(1)	(2)	(3)	(4)
$H(b,\chi,\gamma)$	Ranges	Results	Comments
1.0	$\|\gamma 1, b1, \chi 1\|$	$\Pi'>0$ $\forall\nu$	$\Pi = G(x)/F(x)$
		$\alpha>0$, $\alpha'>0$ $\forall\nu>\nu_c$	(see fig. 6.1)
	$\|\gamma 2, b1, \chi 1\|$	$\Pi'>0$ $\forall\nu$	
$\gamma^{-1}, \gamma^{-2}, \gamma^{-3}$	$\|\gamma 2, b1, \chi 1\|$	$\Pi'>0$ $\forall\nu$	
		$\alpha' \gtrsim 0$	
	$\|\gamma 2, b2, \chi 2\|$	$\Pi'>0 \rightarrow \Pi'=0$	for a large range
		$\alpha'>0 \rightarrow \alpha'=0$	in γ
			$\Pi \rightarrow \frac{x+1}{x+7/3} = \frac{\alpha+1}{\alpha+5/3}$
$b, b^2, b^3, \cos 2\chi$	$\|\gamma 2, b1, \chi 1\|$	$\Pi'>0$	
$\cos^2 2\chi, \cos^3 2\chi$	$\|\gamma 2, b2, \chi 2\|$	$\Pi'>0$ $\alpha'>0 \rightarrow \alpha'=0$	
$\gamma b, \gamma^2 b^2, \gamma^3 b^3$	$\|\gamma 2, b2, \chi 2\|$	$\Pi'>0$ $\alpha'>0$	$\Pi'<0$ AND $\alpha'<0$ for a small frequency range
$b \sin 2\chi, b^2 \sin 2\chi, b^3 \sin 2\chi, b \cos 2\chi, b^2 \cos 2\chi, b^3 \cos 2\chi$	$\|\gamma 2, b2, \chi 2\|$	$\Pi'>0$	
$\gamma^{-1} \cos 2\chi, \gamma^{-2} \cos 2\chi$	$\|\gamma 2, b2, \chi 2\|$	$\Pi'>0$	$\Pi'<0$ AND $\alpha'<0$
$\gamma^{-3} \cos 2\chi$		$\alpha > 0$	for brief frequency range
Various			
$H(b,\chi,\gamma) = h(b)N(\chi,\gamma)$	$\|\gamma 2, b2, \chi 2\|$	$\Pi'>0$ $\alpha'>0$	

Chapter 7. Wavelength-dependence--Observational.

7.1 Introduction.

In this chapter we adopt the notation $p(\lambda)$ and $\theta(\lambda)$ to represent wavelength-dependence of polarization degree and position angle respectively. One of the defining characteristics of blazars as a class is their high and variable linear polarization. The canonical explanation for this phenomenon is emission of incoherent synchrotron radiation from relativistic electrons (e.g. Jones, O'Dell & Stein 1974; see also section 8.2). For a power-law spectrum, a single undiluted synchrotron source yields wavelength-independent polarization properties. Furthermore, the continuity in flux from optical to infrared suggests the same emitting region, and thus we would expect similar polarimetric properties. For most blazars this is a good approximation.

7.2 Wavelength-dependent Polarization.

Nordsieck(1976) has shown that polarization degree is a function of local spectral index. Björnsson and Blumenthal (1982) demonstrated that the maximum deviation from the relation

$$p \propto (\alpha+1)/(\alpha+5/3) \qquad 7.1$$

is approximately 7.5% for concave downward spectra ($d\alpha/d\ln\nu>0$). This variation with spectral index is too small to account for the observed $p(\lambda)$ of some of the objects and we are forced to resort to several-component models for an explanation.

Although dilution by an underlying galaxy of a pure synchrotron source would result in wavelength-dependent polarization, it has never been convincingly demonstrated to be the cause of the observed wavelength-dependence of polarization for any object. The effect of dilution will be weak, since the non-thermal flux usually completely dominates any galaxian component. Also, variation arguments and the transience of $p(\lambda)$ eliminate the possibility that galaxian dilution is entirely responsible.

Several objects have now exhibited wavelength-dependent polarization in our monitoring programme. Impey et al. (paper I) reported wavelength-dependence in AO 0235+164 and also PKS 0735+178, with polarization increasing at shorter wavelengths in both cases. In November 1982, 0235+164 again showed a strong $p(\lambda)$, with polarization increasing into the blue, but no such dependence in January 1983, when the polarization degree was down to normal. The unusual wavelength-dependence of OJ 287 seen in January 1983 is described in chapter 5. When the polarization degree returned to normal again in January 1984, we found only marginal evidence for $p(\lambda)$. See figures 7.3.

0215+015 and 0735+178 both exhibited $p(\lambda)$ in January 1984, again with polarization increasing into the blue (see figures 7.1 and 7.2).

7.3 Wavelength-dependence of Position Angle.

Rotations of position angle with wavelength are seldom observed. This is noticeable in our data and in the data of Bailey, Hough and Axon (1983) (hereafter BHA) when we might have expected rotations with wavelength to accom-

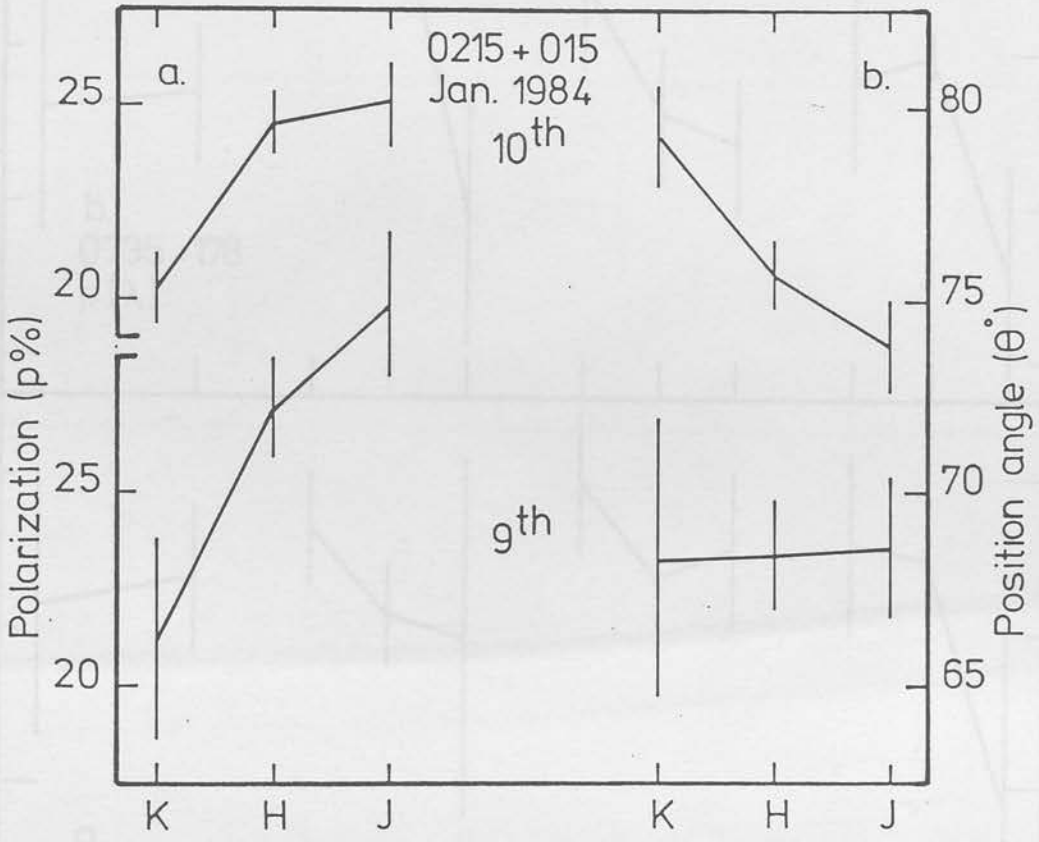

Figure 7.1 a) Polarization degrees and b) Position angles plotted against log frequency for 0215+015 for 2 consecutive nights. Pronounced wavelength-dependence of polarization is seen on both nights. The position angle shows significant rotation and a wavelength-dependence on the second night.

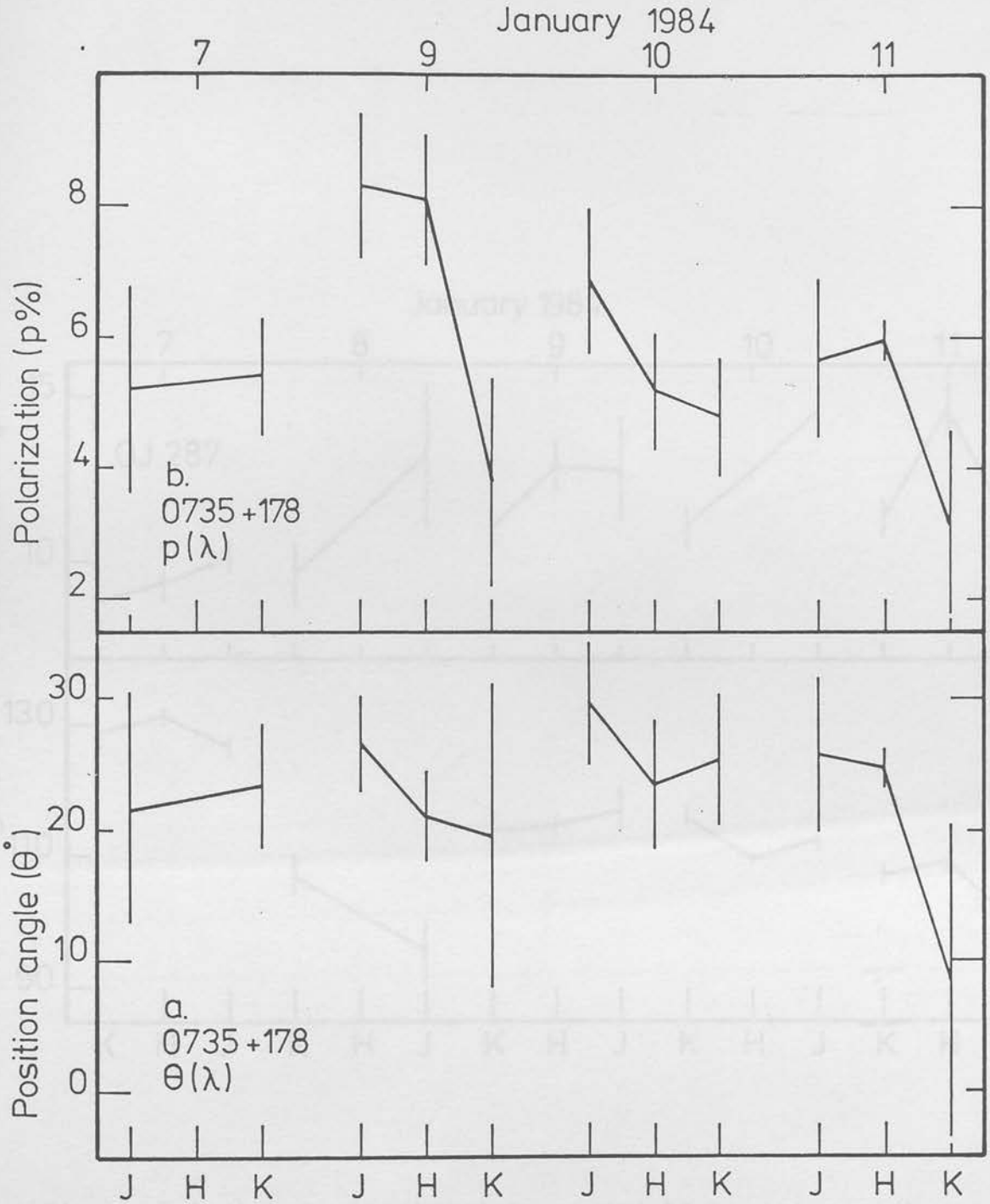

Figure 7.2 a) Polarization degrees and b) position angles plotted against log frequency for 0735+178 for 4 nights in January 1984. Again we see stochastic changes in polarization and wavelength-dependence (especially on the 9th) combined with a relative stability and wavelength-independence of position angle.

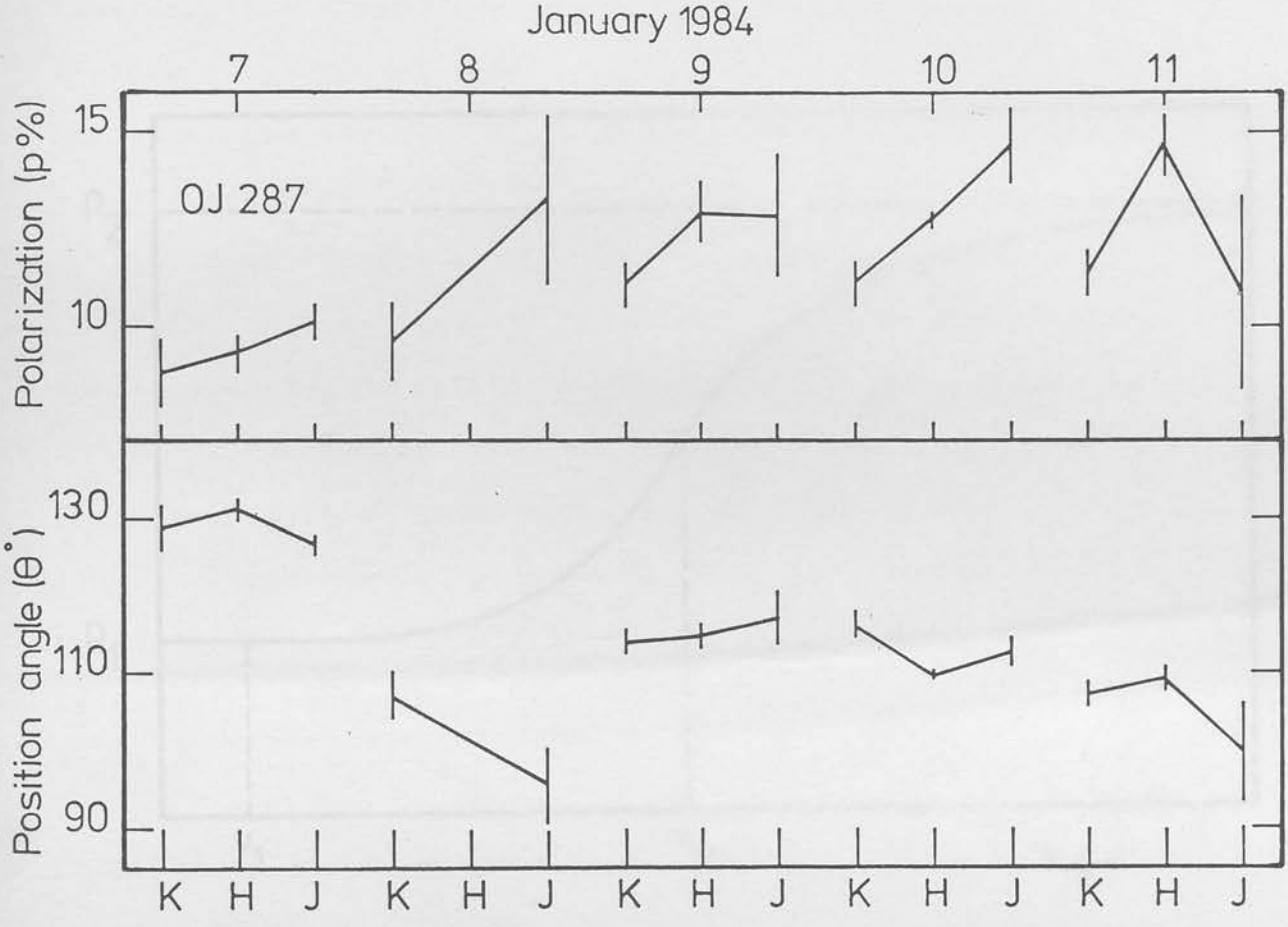

Figure 7.3 a) Polarization degrees and b) position angles plotted against log frequency for OJ 287 for the 5 consecutive nights in January 1984. Marginal wavelength-dependence of polarization is evident, although the position angle remains relatively stable throughout.

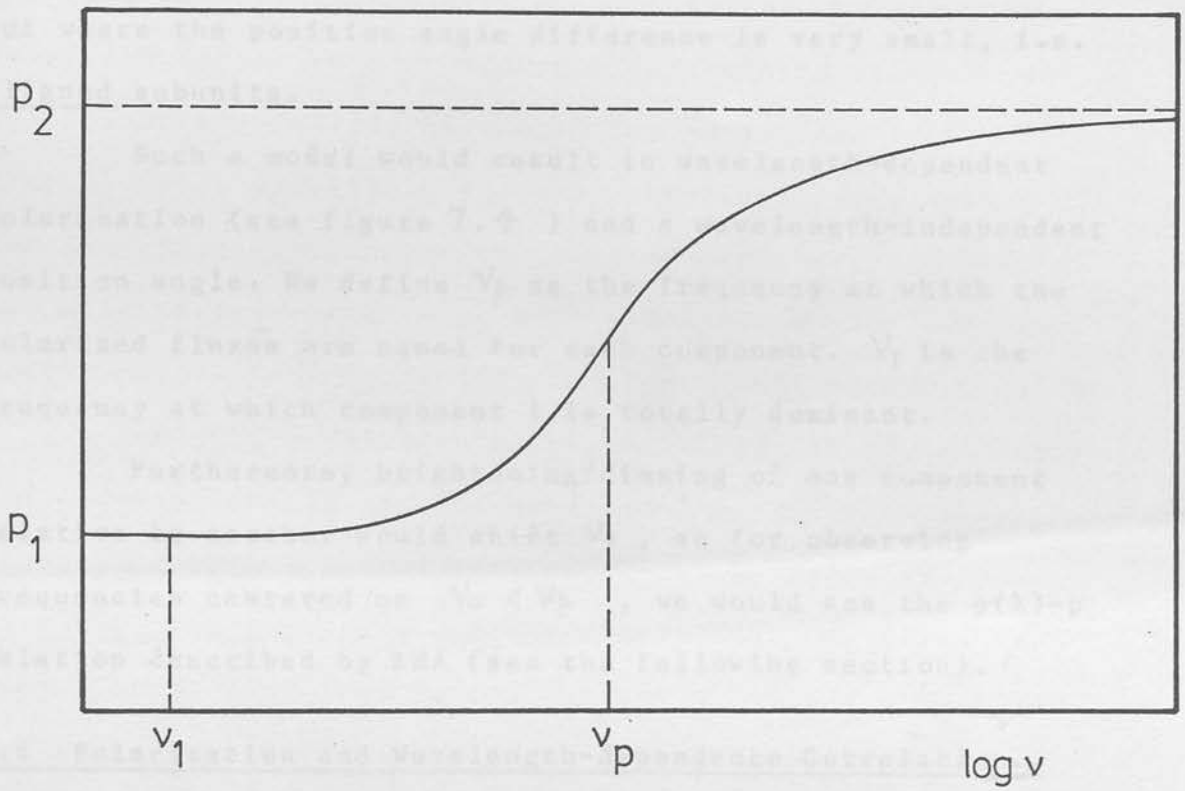

Figure 7.4 Polarization curve for two components (p_1 and p_2) with similar position angles but differing spectral indices. ν_p is the frequency at which the polarized fluxes are equal.

pany the observed wavelength-dependence of polarization.

The model used to describe the remarkable behaviour of OJ 287 invokes two components with differing spectral indices and position angles. A general property of such a model however, is the occurrence of $\Theta(\lambda)$, which is not usually observed. One way to circumvent this problem, while retaining the simplicity of the model, is to consider a similar two-component model, where the polarizations differ, but where the position angle difference is very small, i.e. aligned subunits.

Such a model would result in wavelength-dependent polarization (see figure 7.4) and a wavelength-independent position angle. We define ν_p as the frequency at which the polarized fluxes are equal for each component. ν_1 is the frequency at which component 1 is totally dominant.

Furthermore, brightening/dimming of one component relative to another would shift ν_p , so for observing frequencies centered on $\nu_o < \nu_p$, we would see the p(λ)-p relation described by BHA (see the following section).

7.4 Polarization and Wavelength-dependence Correlation.

BHA first noticed the trend of increasing wavelength-dependence with increasing polarization [hereafter p(λ)-p]. From observations of 7 blazars (6 BL Lac objects and 1 highly polarized quasar), they find that the ratio of optical to infrared polarizations increases with optical polarization for $p_{opt} > 10\%$, and is not significantly different from unity for $p_{opt} < 10\%$. Their 25 data points yield a Spearman coefficient of $r_s = 0.765$, revealing a correlation at >> 99.9% confidence interval. Their data are clearly incon-

sistent with wavelength-independent polarization, although a large χ^2 value ($\chi^2/N=2.1$) reveals genuine scatter about the best fit line, not due to measurement error. (See sub-section 3.3.2).

It should be noted here that two unrelated variables (x,y) would produce a weak correlation when plotted as x/y vs y. This "stretching effect" is small and is not the cause of the observed correlation. This can be easily seen by considering how a square lattice of points on an x-y plot transforms onto an x-x/y plot. The "stretching effect" was also tested numerically by scattering points about (i) a $p_J = p_K$ plot and (ii) a $p_J = p_K$ xconstant plot, with Gaussian errors comparable to those of our observations, also with Gaussian errors up to 5 times the typical observational error. In no case did a $p(\lambda)$-p result emerge.

The $p(\lambda)$-p relationship is also seen in our narrower band observations in the infrared. At the time when observations in papers I and II were made, the polarimetric accuracy was poor and yet a correlation is still evident. For paper I data, a plot of p_H/p_K versus p_H yields a Spearman coefficient $r_s=0.663$ (correlated at >> 99% confidence interval). The small χ^2 value ($\chi^2/N=0.6$) results from the poor accuracy and prevents us inferring intrinsic "cosmic" scatter. A similar result is found by plotting p_J/p_K against p_J for paper II data.

The most marked confirmation of the $p(\lambda)$-p phenomenon came with the data presented in this thesis (papers III and IV). We choose the longest wavelength range from J(1.25 μm) to K(2.2 μm). For the data in paper III, the

best-fit line yields a Chi-square value χ^2 =29.5 for 28 data points, compared with the value for the Null Hypothesis (m=0, c=1, i.e. wavelength-independent polarization) of χ^2_o =169. The Spearman coefficient r_S=0.81 reveals a correlation at >> 99.9% confidence interval (see figure 7.5 a). Unlike BHA we find that polarizations at two wavelengths are not equal within errors for values below p=10%. If we omit the OJ 287 data (for which we already have a model), however, we find that $p_J \sim p_K$ for $p_{J,K} < 10\%$, in agreement with BHA's result, for which we offer a possible explanation in the following section. We also draw attention to the $p(\lambda)$-p relationship, not only for the sample, but for the individual members of the sample. All 6 objects for which there are 3 or more points exhibit a $p(\lambda)$-p relation.

When the data of paper IV (January 1984) is added to that of paper III, the correlation is still highly significant although considerably diluted. This is due to the extreme behaviour of 0735+178 (see figures 7.2 and section 7.2). When these 4 data points are excluded, we find a Spearman coefficient of r_s=0.793 for 37 data points, i.e. correlated at >>99.9% confidence interval (see figure 7.5 b).

7.5 Transience.

Wavelength-dependence of either polarization degree or position angle are transient phenomena. Wavelength-independence is general at optical and infrared wavelengths, and for those few objects that have exhibited $p(\lambda)$ or, more rarely, $\theta(\lambda)$, this dependence has either changed or vanished on other occasions. Such transience is consistent

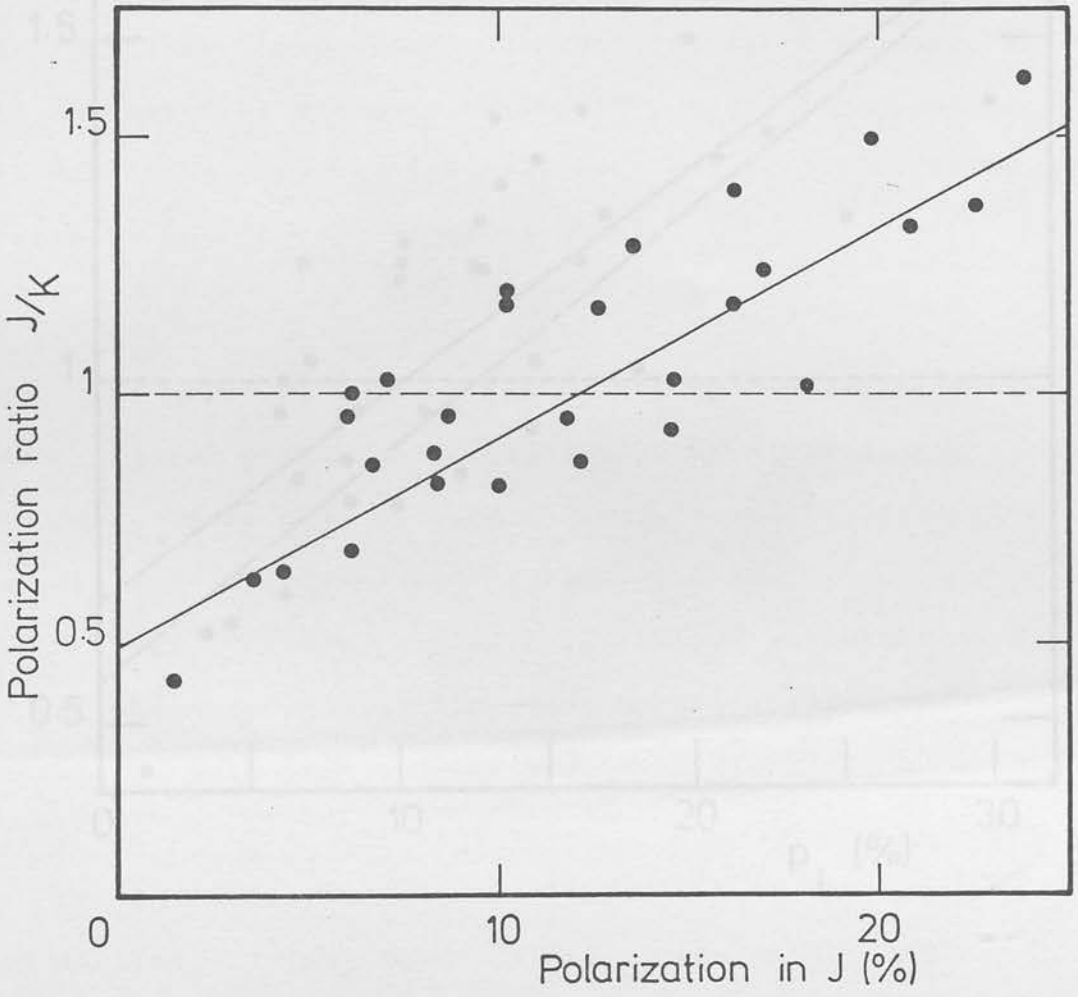

Figures 7.5. The $p(\lambda)$-p graphs. The ratio of p_J / p_K is plotted against p_J to reveal a strong correlation between the strength of wavelength-dependence and the polarization degree.

a) shows the data presented in paper III, which is clearly inconsistent with the canonical assumption of wavelength-independence: $r_p = 0.849$, $r_s = 0.811$, and $\chi^2_{min} = 29.5$ for N=28, c.f. χ^2_0 ($p \neq p(\lambda)$)=169. The solid line is the best fit line defined by the minimum χ^2.

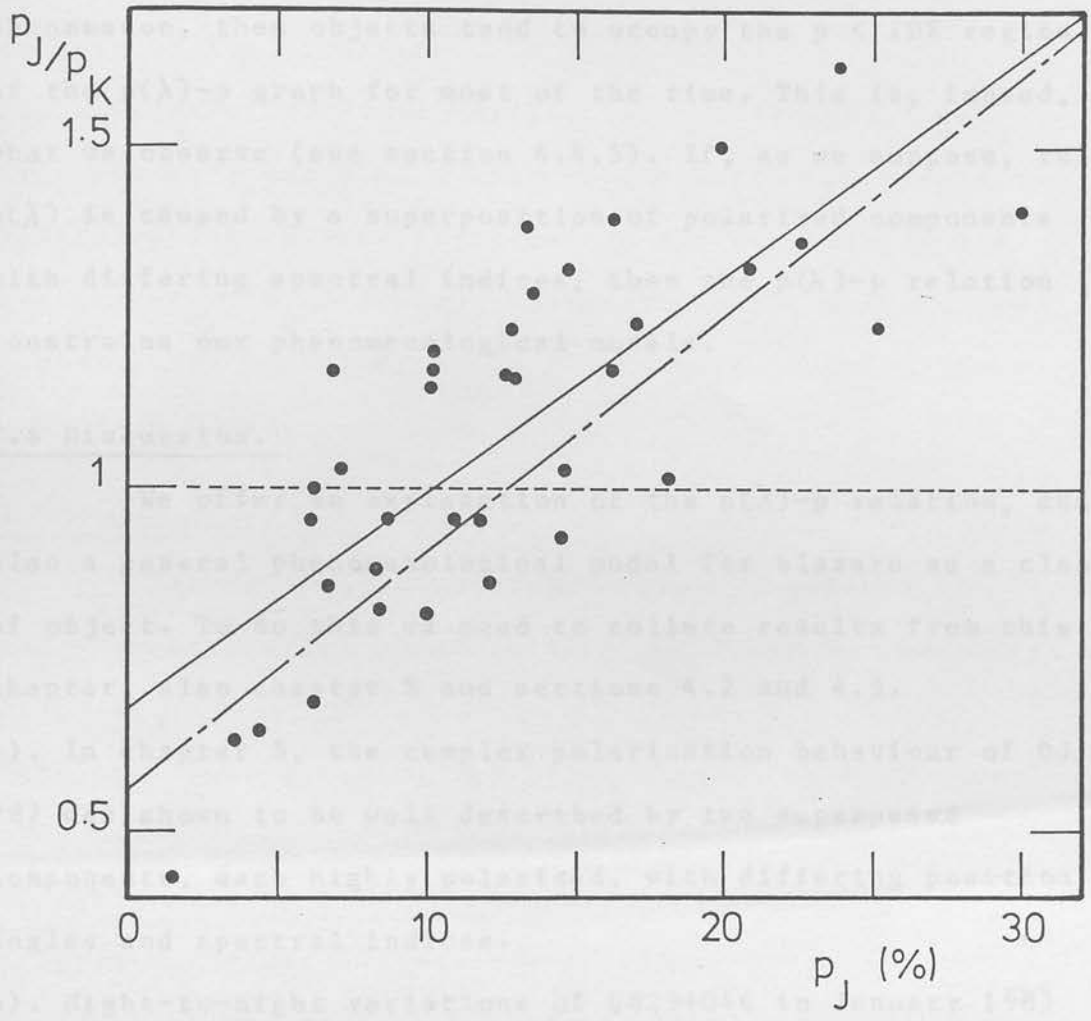

b) shows the data presented in paper IV. The solid line shows the least-squares fit (r_p =0.772, N=37, m=0.03, c=0.68) and the dash-dot line shows the minimum-χ^2 fit, taking account of the errors in both axes (χ^2_{min} =51, N=37, m=0.035, c=0.56). The dashed line represents wavelength-independent polarization.

with the large and rapid variations in both flux and polarization properties that are common properties of blazars.

Since wavelength-independence is only a transient phenomenon, then objects tend to occupy the $p < 10\%$ region of the $p(\lambda)$-p graph for most of the time. This is, indeed, what we observe (see section 4.4.5). If, as we suppose, this $p(\lambda)$ is caused by a superposition of polarized components with differing spectral indices, then the $p(\lambda)$-p relation constrains our phenomenological models.

7.6 Discussion.

We offer an explanation of the $p(\lambda)$-p relation, and also a general phenomenological model for blazars as a class of object. To do this we need to collate results from this chapter, also chapter 5 and sections 4.2 and 4.5.

a). In chapter 5, the complex polarization behaviour of OJ 287 was shown to be well described by two superposed components, each highly polarized, with differing position angles and spectral indices.

b). Night-to-night variations of 0829+046 in January 1983 (see section 4.2) may be described by an "underlying" component ($p \sim 7\%$, $\Theta \sim 125^{\circ}$) with a superposed variable component "turning-on". This variable component is (i) relatively highly polarized (ii) wavelength-independent ($p \sim 30\%, \Theta \sim 109^{\circ}$) and (iii) relatively shallow-sloped. A similar result is found for the January 1984 observations of OJ 287.

c). Analysis of internight variability (section 4.2) for all the observations of the monitoring programme show that

night-to-night variations may be understood in terms of the "turning on/off" of relatively highly polarized sub-units, with $p \sim 16\%$. This value is significantly higher than the typical value for polarization observed in these objects throughout the programme.

d). Absence of observed rotation (i) with wavelength (section 7.3) and with number of sub-units (section 4.5) indicates that blazar polarization and variability are consistent with an aligned sub-units model, whereas the January 1983 behaviour of OJ 287 requires a non-aligned sub-units model.

7.7 Conclusions.

Taking these 4 results together, we conclude that the characteristics of our blazar model may be summarized as follows:

(i)Blazars, in general, may be considered as a superposition of a small number of aligned, polarized sub-units.

(ii)They vary by turning on/off a relatively highly polarized, relatively shallow-sloped component.

(iii)When these components have comparable polarized fluxes, significant wavelength-dependence may result.

It is now clear how such a model produces the observed $p(\lambda)$-p correlation. Typical blazar polarization is p=11% (see section 4.4.5). If a second, relatively shallow component turns on, its polarization properties become more dominant at shorter wavelengths. If it is also highly polarized, then $p_J > p_K$ for $p_J > 11\%$. The $p(\lambda)$-p relation, therefore, is consistent with, and provides further evidence for, the model characteristics described above.

The variability of blazars and the transience of wavelength-dependence may then be understood in terms of components which vary independently of one another. Their alignment, however, suggests that they are embedded in the same magnetic field.

Chapter 8. Models and Discussion.

Various types of models have been proposed to explain the observed phenomena. These are briefly discussed in this chapter.

8.1 The Power Source.

Huge luminosities ($L_{IR} \sim 10^{48}$ erg s^{-1}) and rapid variability ($\Delta t <$ 1 day) inevitably lead to a picture of the central power source being massive and compact. These considerations alone severely restrict possible models, and further consideations of high and variable polarization and rapid rotations of position angle present even more stringent limits. In this section we briefly consider possible models for the energy generation.

8.1.1. Dense Star Clusters.

Spitzer (1971) has shown that if the core of a galaxy contains a dense cluster of stars (10^{11} pc^{-3}) moving at an average of $\sim 10^4$ km s^{-1}, then each stellar collision could release $\sim 10^{51}$ erg. This, however, is a very short lived process, lasting only 10^2 -10^3 years, and is inconsistent with the surface density of quasars.

8.1.2. Multiple Supernovae.

In the dense star cluster model, if inelastic collisions lead to the formation of massive stars ($\sim$ 50 $M_\odot$), these may evolve into supernovae with an energy release of $\sim 10^{52}$ ergs each. Such a model would predict a rate of flux increase during a burst that is faster then the rate of decrease. Gilmore (1980) has shown, by extensive monitoring of southern quasars, that the rates of flux

variation are inconsistent with simple multiple supernovae models.

8.1.3. Supermassive stars.

Gravitational contraction of supermassive stars may lead to copious energy production. Such a star may form at the centre of a star cluster, and masses of up to 10^9 $M_\odot$ can be stabilised by differential rotation. However, these stars have periods of fundamental pulsation,

$$t_p \sim 10^{-7} \; M/M_\odot \quad \text{days} \qquad 8.1$$

and in no blazar has any regular period been convincingly demonstrated to exist. A further problem with such a model is that the energy release during stable evolution only has the efficiency of thermonuclear burning.

8.1.4. Spinars.

A spinar is a rotation-supported superstar formed by the collapse of a magnetised gas cloud. Energy and angular momentum are radiated away by the presence of magnetised fields, and an enormous amount of energy can be liberated in this fashion. A massive, highly magnetised spinar can store energy for $\sim 10^6$ years and can radiate very efficiently. The spinar model, however, also suffers from the same problems as the supermassive star model. Periodicity would be expected from a coherent, rotating object, and this has not been observed. Similarly, the spinar model predicts more rapid increases than decreases in flux, which is inconsistent with quasar variability.

8.1.5. Black Holes.

The black hole model for the power source of blazars and quasars is the current favoured model. There are several

reasons for this. a) For an accretion disc co-rotating around a maximally rotating Kerr black hole, mass to energy conversion efficiencies of up to $\eta \sim 42\%$ can be obtained. b) Extremely short timescales of variation are possible at the inner edge of the accretion disc. c) Black holes with accretion discs provide an explanation to the erratic variability observed in blazars, rather than the periodic variability predicted by other models.

Black holes with accretion discs will be further discussed later on in this chapter.

8.2 Polarization.

Any model which attempts to describe blazars as a class must explain a high and variable degree of linear polarization with little or no circular polarization. Polarization has been seen in a variety of extragalactic objects. In normal galaxies and Seyferts, polarization is predominantly due to dust scattering, whereas, in blazars, it is attributed to incoherent synchrotron emission. Other possibilities have been considered by various authors. Light transmitted through grains aligned by a magnetic field becomes linearly polarized. This is the effect responsible for the interstellar polarization of reddened stars in our Galaxy. A similar effect could be produced in the host galaxy, although this would not produce variable polarization properties.

Jones, O'Dell & Stein (1974) examined alternative radiation processes and concluded that coherent synchrotron emission and proton synchrotron emission were unrealistic. They state "High brightness temperature could be indicative

of coherence..; however, since it is generally difficult to obtain coherence over a broad frequncy range, only rather narrow peaks can be explained in this manner. At high frequencies, even narrow peaks are difficult to explain in terms of coherence, because extremely large densities are required" They also reject proton synchrotron emission. "The major difficulty in constructing a model in which this is the dominant emission process lies in hiding the electrons so that their contribution to the radiative transfer is negligible at observed frequencies."

We conclude that the only viable explanation for occasionally high (p% up to 44%) and rapidly variable linear polarization degree seen in blazars is incoherent synchrotron radiation.

8.3 Energy Spectrum and Source Evolution.

The principal requirement of any emission mechanism that is proposed to explain the blazar phenomenon is that it must reproduce a power-law energy spectrum. The dissipation of turbulent energy behind a shock front can naturally lead to a power-law spectrum. There is a problem, however, with turbulent acceleration and synchrotron emission occuring in the same volume. For turbulent acceleration we require that the turbulent energy dominates the magnetic energy, whereas a high degree of polarization requires that the magnetic field energy dominates the stochastic particle motions. The implication is that the electrons must be accelerated to a power-law energy spectrum before being injected into the magnetic field in a time less than the synchrotron lifetime.

A relativistic blast wave or rapid magnetic reconn-

ection would impulsively accelerate particles which would then radiatively cool. Alternatively, stochastic acceleration mechanisms such as turbulence and ion collisions could gradually accelerate the electrons. Bulk outflow from the nucleus is turned into turbulent energy across a shock. The electrons are accelerated from this region into a magnetic field region. A steady state may then be reached where the energy gained from the turbulent region is balanced by the synchrotron emission.

One of the most noticeable aspects of the spectra of blazars in the infrared region is the ubiquitous nature of the power-law with a spectral index $\alpha \sim 1.0$ to 1.2. As discussed in section 4.6 (and refernces therein) most blazars are well approximated by power-laws in the infrared with a small amount of spectral curvature towards higher frequencies. OJ 287 in particular maintains a constant spectral shape while varying in flux. In the January 1983 observations (see chapter 5) we see spectral curvature ($\Delta\alpha \sim 0.4$) on each of the four consecutive nights. Yet a 50% increase in flux from 7th to 8th January leaves the spectral shape unaltered. Similar behaviour is seen in our January 1984 observations, when the infrared colours remain remarkably constant despite fluctuations in flux (Δ m $\sim$ 0.3 mag). If this variation in flux was due to variations in the injected energy spectrum, we would expect to see evolution of the spectral shape. In his paper on the spectra of young, non-thermal sources, Kardashev (1971) states " The absence of any constant injection of new electrons must lead in the course of time to a cutoff in the high energy region of the

spectrum, while the presence of a constant injection would eventually lead to a change of 1/2 in the spectrum of emission"

It is at first tempting to attribute the spectral curvature to the above-mentioned effect of a constant injection together with synchrotron emission. However, if the 50% increase in flux was due to a sudden increase in injected energy, any spectral curvature would be masked, and a subsequent evolution of the spectrum would be seen at the higher frequencies. In the case of OJ 287, at least, these phenomena are not observed suggesting that it is not merely the injected spectrum that is responsible for the variation in flux. An alternative is a variation in the magnetic field strength.

8.4 Jets and Beaming.

Jets and/or beaming have now been observed in several types of astrophysical phenomena, e.g. jets emanating from M87 and quasars, bipolar outflows, pulsar beaming. Jets have been seen at high resolution in Hercules A (twin jets), NGC 1265 (twin jets swept back by intergalactic ram pressure) and NGC 6251 (jets with knots), and are believed to be physical conduits which transport mass, momentum, energy and magnetic flux (Begelman, Blandford and Rees, hereafter BBR). Beams were introduced by Rees (1971) to explain the energy transport to the lobes of double-lobed radio sources.

The reasons for invoking the presence of jets and/or relativistic beaming in blazars include

(a) Occasional super-Eddington luminosities imply that

relativistic beaming is important.

(b) Beaming towards the observer reduces the energy requirements and also the apparent timescale of variations.

(c) Superluminal expansions have been observed or inferred in some blazars, e.g. BL Lac, 1641+399, and 1253-055.

(d) Rapid rotations of postion angle may result from accelerating a cloud of synchrotron emitting electrons along a jet at a small angle to the line of sight to the observer. (Blandford & Königl, 1979; Björnsson 1982).

Any model decribing the production of astrophysical jets must have two ingredients. First, there must be a source of material with enough energy to escape the central object, and secondly, there must be a method of directing the flow.

Blandford & Rees (1974) postulated a twin-exhaust model. In this model, relativistic plasma is generated near the central object which is then squirted out in opposite directions. The plasma is collimated by a de Laval nozzle, created by the interaction of the beam with the external medium. Two-dimensional hydrodynamic calculations by Norman et al. (1981) show the formation of a de Laval nozzle when hot gas is injected at the centre of a flattened gas cloud. Such calculations show, however, that a twin-exhaust pattern is only stable for a limited range of energy fluxes.

As Blandford & Rees (1974) pointed out, if the nozzle occurs close to a massive black hole, the confining cloud lies in a potential well of the form r^{-1}, and this makes it harder to establish a stable twin-exhaust geometry.

Funnels are slightly different to nozzles, in that nozzles are formed by the interaction of the gas cloud with a stream whereas funnels are pre-existing channels. One method of creating such a funnel is by a thick-disc accretion (see later discussion in section 8.5).(A second type of funnel occurs in the innermost regions of thick accretion discs. It is relativistic in nature and we shall not discuss it further). Once the electron stream has escaped the funnel, there may be a problem with collimation (Sikora & Wilson 1981) depending upon the shape and stability of the funnel, and the velocity of the escaping material.

Jets may be formed by a variety of other means, including winds, plasmoids, hydromagnetic and electron-positron jets. There are also several ways to collimate the jets, including collimation by gas pressure, cooling effects, and magnetic collimation, but further detailed discussion is beyond the scope of this thesis.

8.5 Specific Models.

There are several types of models that have been proposed to explain the unusual behaviour of blazars. We will briefly discuss three types, namely (i) Rotation (ii) Relativistic effects and (iii) Geometrically thick accretion discs.

8.5.1 Rotation.

The main thrust of this type of model is that position angle rotations, observed in several blazars, are due to a physical rotation of the source.

Altschuler (1980) provides convincing evidence for

rotation for 5 blazars during well-defined outburts (ΔF_ν (3.7cm) = 50%). Plotting position angles against time gave good evidence for a linear rotation with time, after allowing for the 180n (n=1,2,..) ambiguity. Rotation during outbursts is not always present. He notes that a linear rotation could be masked if successive outbursts are superposed in time, or if there is more than one component. His observations suggest that rotation starts immediately prior to the the beginning of the outburst and continues until the outburst has died away. In the 5 objects which exhibited this behavour, the polarization degree remains fairly stable at a few percent throughout. Such behaviour would be consistent with relativistic effects, i.e. apparent rotation coincident with flux boosting, as discussed in 8.5.2, except that for relativistic effects, the apparent rotation is limited to 180 degrees only. Thus, these observations show perhaps the clearest evidence for physical rotation in blazars.

Ledden & Aller (1979) find similar evidence for rotation in AO 0235+164, also at radio wavelengths ($\lambda\lambda$ 8.0, 14.5cms). In 1975, 0235+164 underwent one of the largest outbursts ever seen in an extragalactic object. The main feature of the data is the change with time of the position angle at both frequencies. Faraday rotation could not have been responsible, the simplest explanation being a rotation of the magnetic field structure. Similarly to Altschuler's data, the rotation begins near the beginning of the outburst. There is an approximately linear rotation during the peak of the outburst and the rotation begins to

stabilise when the outburst tails off in early 1976. Several alternative explanations of the rotation can be ruled out by the close agreement at the two frequencies. For example, all frequency-dependent effects, such as Faraday rotation, can be eliminated. Evolution of the emission region from optically thin to thick could cause a 90 degree rotation. However, the rotation is greater than 90 degrees and the time of transition should be frequency-dependent. The most straightforward explanation of the observations is a physical rotation of the magnetic field structure.

8.5.2. Relativistic Effects.

Relativistic effects may be invoked to explain a variety of phenomena in blazars, such as very high brightness temperatures, huge luminosities together with very rapid variability, and apparent rotations of positon angle. As discussed in section 4.3.2, super-Eddington lumionosities strongly suggest that relativistic beaming is important, although this is not the only explanation possible. Apparent super-luminal expansion has been measured in some sources (see section 8.4) and relativistic effects are required to explain this. In their classic paper on Relativistic Jets as Compact Radio Sources, Blandford and Königl (1979) describe the observational consequences of accelerating a cloud of synchrotron emitting electrons to relativistic velocities in a jet oriented at a small angle to the line of sight. The polarization properties of such a source are further described by Bjornsson (1982) and the geometry of the model is shown in figure 8.1

For a source moving with a Lorentz factor γ, The

observed flux density ($S_{ob}(\nu)$) in the object's rest frame is given by

$$S_{ob}(\nu) = S(\nu)\, \vartheta^{3+\alpha} \qquad 8.2$$

where α is the spectral index ($= -d\ln S\nu / d\ln \nu$) and ϑ is the Doppler factor ($\equiv \gamma^{-1}(1-\underline{\beta}.\underline{n})^{-1}$) and where $S(\nu)$ is the flux emitted in the comoving frame.

Scheuer & Readhead (1979) point out that in the case of a continuous jet, the exponent becomes $(2+\alpha)$ instead of $(3+\alpha)$. This is because we may consider a jet as a succession of ejected components so that the apparent lifetime of each component is shorter than the proper lifetime by a Doppler factor. The total observed flux from all the components in a jet is then boosted by a factor of $\vartheta^{2+\alpha}$.

For a small angle to the line of sight, the observed flux is boosted by a factor $\vartheta^{3+\alpha}$, which can satisfactorily explain the high brightness temperatures of $T \sim 10^{15}$ K that have been observed for relatively modest Lorentz factors of $\gamma \sim 5$ or 10.

A further important consequence of accelerating a source of radiation is that the position angle of the polarization is seen to rotate. This is because the total electric field is weakened by a contribution (proportional to the velocity) from the magnetic field (i.e. the induced electric component). In this case of collinear acceleration, we see, from figure 8.1, that the field and velocity components are

$$B_{ob},_x = B_{cb}\cos\eta\sin\psi \qquad e_{cb},_x = -e_{cb}\cos\xi\sin\theta$$
$$B_{cb},_y = -B_{cb}\sin\eta \qquad e_{cb},_y = e_{cb}\sin\xi \qquad 8.3$$
$$B_{cb},_z = B_{cb}\cos\eta\cos\psi \qquad e_{cb},_z = e_{cb}\cos\xi\cos\theta$$
$$n_x = n\cos\theta \qquad n = n_z\sin\theta \qquad \beta_x = \beta$$

The total fields (including contributions from the radiation field and the static (in the comoving frame) magnetic field) are given by

$$\underline{E}_{ob},_{total} = \underline{e}_{cb} - \underline{\beta}\,X\underline{B}_{cb}$$
$$\underline{B}_{ob},_{total} = \underline{B}_{ob} + \underline{n}X\underline{e}_{ob} \qquad 8.4$$

Making use of the Lorentz invariant $\underline{E}.\underline{B}=0$ for the total fields gives

$$\tan\xi = \frac{\cos\psi\,[\beta - \cos\theta\,(1-\tan\psi\,\tan\theta\,)]}{\tan\eta\,(\beta\cos\theta - 1)} \qquad 8.5$$

As $\beta \to 1$ (for $\psi, \theta << 1$), then ξ will swing from $\xi \sim (\pi/2 - \eta)$ to a constant value $\xi \sim (\eta - \pi/2)$. The maximum observable amplitude of the swing is 180°. Similar results for uniform circular motion, with a fixed or convected magnetic field, may be derived. In no case would a rotation of > 180 result. If Altschuler's observations of rotation are correct, then relativistic effects alone are inadequate.

Björnsson (1982) assumes that the change in polarization degree is due to a change in velocity of the source, i.e. a change in the viewing angle of the magnetic field distribution. There are two qualitatively different polarization properties. a) When the magnetic field distribution has a high degree of rotational symmetry around some direction, it can be characterised by its average direction (the single vector model) otherwise b) it is very similar to a two component model, when a change in polariz-

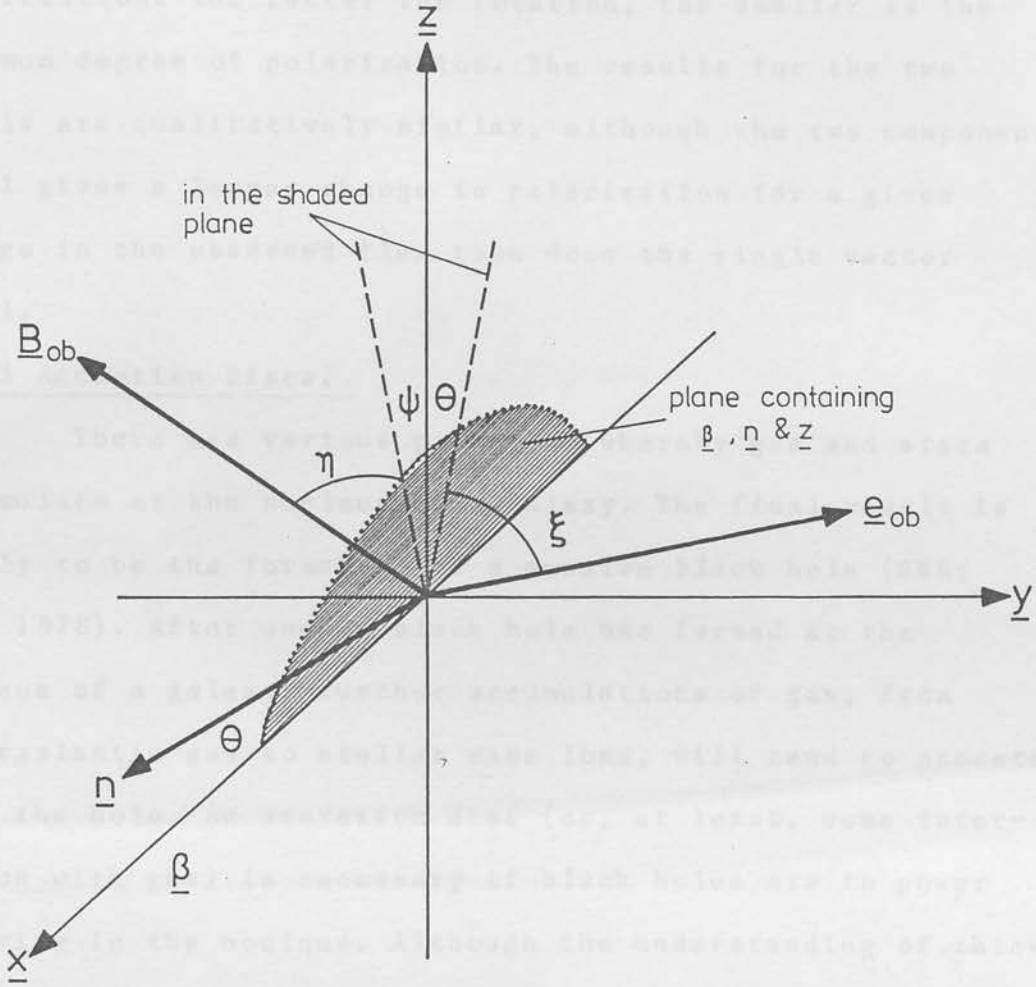

Figure 8.1 (adapted from Blandford & Konigl, 1979) shows the field geometry discussed in 8.5.2. The emitting region moves with velocity $\underline{\beta}$ (relative to the stationary frame) and at an angle θ to the line of sight ($\underline{n}$). Synchrotron radiation (with electric vector $\underline{e}_{ob}$) is emitted by electrons spiralling in a static magnetic field $\underline{B}_{ob}$. The shaded plane is defined by $\underline{n}$ and $\underline{\beta}$. The radiation has an observed position angle Ξ, being the angle in the plane of the sky between $\underline{e}_{ob}$ and some fixed direction (usually North). The observed magnetic field makes an angle η with the shaded plane, and its projection makes an angle ψ with the z-axis.

ation is due to changes in the relative fluxes of the components.

A general property of both models is that rapid changes in position angle occur close to a minimum in the polarization. The faster the rotation, the smaller is the minimum degree of polarization. The results for the two models are qualitatively similar, although the two component model gives a larger change in polarization for a given change in the observed flux than does the single vector model.

8.5.3 Accretion Discs.

There are various processes whereby gas and stars accumulate at the nucleus of a galaxy. The final result is likely to be the formation of a massive black hole (BBR; Rees 1978). After such a black hole has formed at the nucleus of a galaxy, further accumulations of gas, from intergalactic gas to stellar mass loss, will tend to accrete onto the hole. An accretion disc (or, at least, some interaction with gas) is necessary if black holes are to power activity in the nucleus. Although the understanding of thick accretion discs has barely emerged from its infancy, the physics of black holes is well understood, due to some fortunate simplifications.

After gravitational collapse, a black hole may be characterised by just two parameters (for a Kerr hole), spin and mass (also charge for a Kerr-Newman hole). Also, very close to the hole, differential Lense-Thirring precession and viscous torques will cause the gas flow to be axisymmetric. These are important simplifications of the problem.

Accretion discs are less well understood, and the current state of understaning is now briefly discussed. The two types of accretion discs are (i) thin discs (optically thick but geometrically thin) and (ii) Tori or thick discs.
(i) Thin discs. These are assumed to be (nearly) Keplerian discs (Lynen-Bell & Pringle 1974). Viscosity causes a slow radial infall, with a gradual transport of angular momentum away from the hole. The energy dissipated by the viscous stresses is assumed to be radiated locally). Thin discs are, perhaps, more relevent to the study of cataclysmic binaries than to blazars. In the case of the former, the disc is responsible for a large fraction of the radiation, whereas for blazars, any thermal emission from the disc must be completely dominated by the non-thermal emission.

Malkan (1983) presents evidence for an intermediate case, where thermal emission from a thin accretion disc and non-thermal emission combine to reproduce the spectrum of the quasar PKS 0405-123. The main problem with thin discs for explaining the observed spectra of blazars, is how to produce a power-law spectrum which is sufficiently strong to totally dominate the thermal emission from the disc. If there is sufficient ambient pressure, then a jet can emerge from a de Laval nozzle (as discussed in section 8.4). There are a number of instabilities which affect thin discs. These will not be discussed in detail. The general effect of viscous instabilities is to cause a disc to break up into rings. Convective instabilities could lead to formation of a hot corona surrounding the disc, and this is believed to occur in cataclysmic variables, and may well have observ-

ational consequences for X-ray emission from blazars when they are in relatively stable quiescent states.

(ii) Thick Discs. When the accretion rate of gas onto the hole increase until it is unable to cool in an inflow time, then internal pressure will build up and the disc will become geometrically thick. There has been considerable controversy over whether thich discs can exist, or whether, once created, they are stable. We will concern ourselves here only with a description of geometrically thick discs, on the assumption that they exist.

Detailed study of the behaviour of geometrically thick discs took a new step forward with the work of Abramowicz, Calvani & Nobili (1980) (ACN), Paczynski & Wiita (1980), and Jaroszynski, Abramowicz & Paczynski (1980) (JAP). The new approach to the problem avoided the lack of knowledge of the physics of the inside of the disc, by specifying two structure functions: the surface distributions of the angular momentum and of the flux of radiation. Having specified these two functions, one can compute the total luminosity (L), the accretion rate and other disc characteristics, with no reference to the interior of the disc at all.

One advantage of thick rather than thin discs as an explanation for the blazar phenomenon, is that thick discs may exceed the Eddington luminosity (L_{Edd}) by factors of up to 100 (for a 10^8 $M_\odot$ black hole) whereas the maximum luminosity from a geometrically thin disc is approximately the Eddington one. ACN show that only rotating objects can have $L > L_{Edd}$. Figure 8.2 shows a schematic depiction of

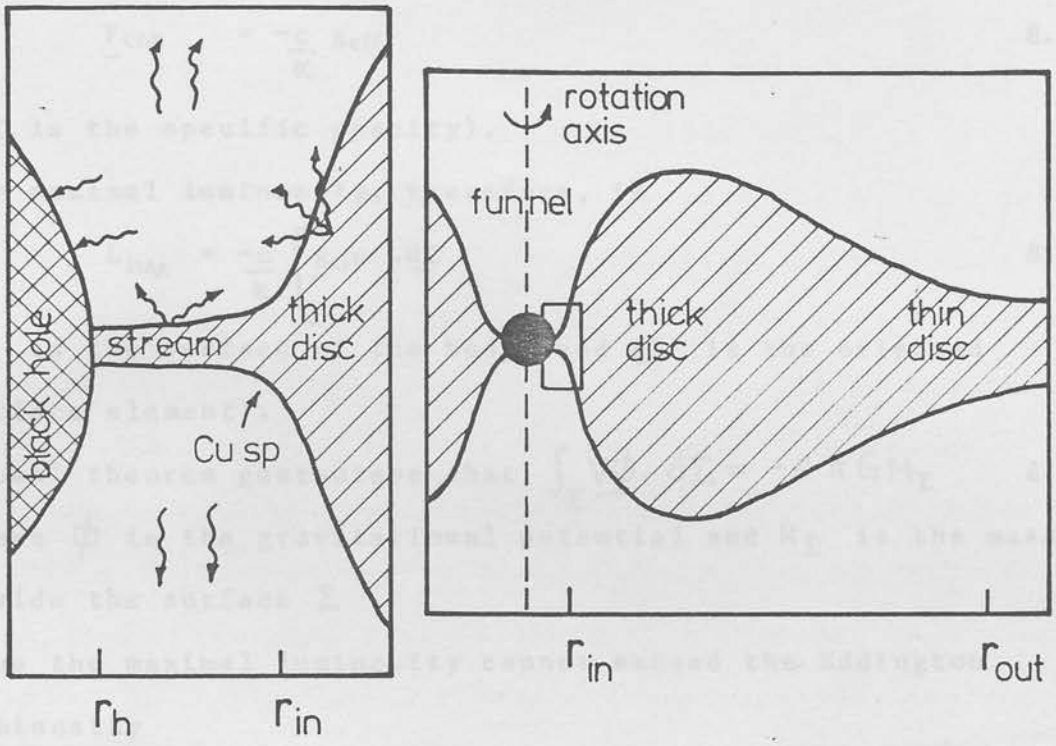

Figure 8.2 (adapted from ACN). The main properties of a thick accretion disc are shown (not to scale). Between r_h (radius of the hole) and r_{in}, the gas streams onto the equator of the hole, regardless of the orientation of the rotation axes of hole and disc (here depicted to be the same) Between r_{in} and r_{out}, the disc is thick and non-Keplerian. Beyond r_{out}, the disc is thin and assumed to be Keplerian. Radiation emitted from the disc may be (i) absorbed and re-emitted, (ii) swallowed by the hole, or (iii) emerge from the funnel. The result is a strong collimation of the radiation in the direction of the disc's rotation axis.

the main properties of a thick disc.

The radiation flux (F) of a stationary, neutral body reaches its critical value when the effective gravitational force ($\underline{g}_{eff}$) is balanced by the radiation pressure-gradient force.

$$\underline{F}_{crit} = \frac{-c}{\kappa} \underline{g}_{eff} \qquad 8.6$$

(κ is the specific opacity).

The maximal luminosity, therefore, is

$$L_{Max} = \frac{-c}{\kappa} \int_{\Sigma} \underline{g}_{eff} \cdot d\underline{\Sigma} \qquad 8.7$$

(Σ is the surface of the body, and $d\underline{\Sigma}$ is the oriented surface element).

Gauss' theorem guarantees that $\int_{\Sigma} \nabla\underline{\phi} \cdot d\Sigma = -4\pi G M_{\Sigma}$ 8.8

where ϕ is the gravitational potential and M_{Σ} is the mass inside the surface Σ .

Thus the maximal luminosity cannot exceed the Eddington luminosity

$$L = 4\pi GMc / \kappa \qquad (M \geqslant M_{\Sigma}) \qquad 8.9$$

In the case of a rotating object, we have

$$\underline{\nabla} \cdot \underline{g}_{eff} = -4\pi G \epsilon - 1/2 \ (\sigma^2 - \omega^2) \qquad 8.10$$

where ϵ =mass density, σ =shear, and ω =vorticity.

Thus for objects with small vorticity and density, and large shear (e.g. thick accretion discs) then $\omega^2/\sigma^2 << 1$ and $2\pi G \epsilon / \sigma^2 << 1$ lead to $L / L_{Edd} >> 1$.

It must again be pointed out that it is not yet known whether such discs are stable. Papaloizou and Pringle (1984) have shown that a toroidal configuration known to be marginally stable to axisymmetric disturbances possesses global non-axisymmetric dynamical instabilities. It will

apparently destroy itself in a few orbital periods unless non-linear terms can saturate the instability at a low amplitude. It is not known whether thick discs have this property.

8.6 Conclusions.

In section 8.1 the possible mechanisms for energy generation were discussed. The only viable mechanism which can produce the huge luminosities and rapid variability seen in blazars is a massive black hole releasing gravitational energy from an accretion disc. The physics of accretion discs is not sufficiently well known to be able to choose between thin discs or tori as the most likely mechanism. Both are subject to instabilities. Intrinsic instabilities in thin accretion discs can cause the eruptive activity of cataclysmic binaries, similar to the flaring seen in blazars. Thick discs (see figure 8.2) can provide super-Eddington luminosities without recourse to beaming, although it is not known whether such discs may exist. We may only conclude that a disc (thick or thin) of gas is accreting onto a massive black hole, thus liberating huge amounts of gravitational energy.

Incoherent synchrotron radiation is believed to be the emission process producing such a high degree of linear polarization, as discussed in section 8.2. However, it seems likely that the electrons must have their power-law energy distribution before encountering the magnetic field. Only in this way is it possible to avoid the competition between turbulent and magnetic energies.

Relativistic effects undoubtedly occur when beaming is important, although relativistic effects alone cannot account for the rotations described in 8.5.1. So we are left with a picture of a massive black hole ($M \geqslant 10^8 M_\odot$) surrounded by an accretion disc which is subject to instabilities. The occasional eruptive activity seen in blazars may be due to these instabilities, inhomogeneities (or hot spots) in the disc, or possibly knots in the emergent jet. Electrons are "boiled off" the inner edge of the disc, and are accelerated to relativistic energies by turbulence, or a relativistic blast wave (for example) before impingeing upon a region of strong, aligned magnetic field. The rapid variability of polarization degree and position angle may be caused by variations in the magnetic field, possibly due to field line reconnection. The two-components model described in chapters 5 & 7 may be readily understood in terms of two separate clouds of electrons impingeing upon two regions with differing magnetic field distributions.

Chapter 9. Conclusions.

9.1 Summary.

The data for the three observing runs (papers III and IV) and results for the whole monitoring programme are presented. For this thesis, 24 objects were observed. 20 objects were observed photometrically, and 9 were observed with quasi-simultaneous three-colour photometry and polarimetry. In the monitoring programme, 35 objects were observed photometrically, and most of these polarimetrically also. Almost half of all known blazars have now been studied.

The results and conclusions of this thesis may be summarised as follows:

(i) Study of the internight variations for the total and polarized flux shows that blazar variability may be understood in terms of the "turning on/off" of a relatively highly polarized component. Detailed internight polarization behaviour of 0829+046 supports this (see section 4.2). The variability of this object may be understood in terms of an "underlying" component with a superposed "variable" component. This variable component is highly polarized and shallow-sloped relative to the underlying component.

(ii) Five objects in the programme have been seen to violate the Elliot and Shapiro luminosity-variability criterion, namely BL Lac, 0235+164, 1308+326, 3C 446, and OJ 287. This strongly suggests that beaming is an important mechanism in blazars (see section 4.3)

(iii) Examination of a table of various parameters reveals some interesting correlations (see sub-section 4.4.7)

a) The position angle - luminosity relationship appears to be intrinsic, thus linking luminosity with a purely geometrical parameter. The correlation is not strong enough to be conclusive, although it is highly suggestive and should be the subject of further observation and investigation.

b) It is possible that our results are indicative of blazar evolution. The highly significant correlation between mean polarization and redshift and the marginally significant correlation between spectral index and redshift support this view. The observations indicate that blazars tended to have higher polarizations and steeper spectral indices at earlier epochs.

c) The most luminous sources have the most variable polarization properties. This result is indicated by the correlations discussed in 4.4.7. It is evident that luminosity (either $\overline{L}$ or L^{max}) is not strongly correlated with mean polarizaton, but that correlations exist with both position angle range and maximum polarization, indicating that it is the most variable sources which are the most luminous.

(iv) Analysis of internight rotations and flux variations reveals that blazar variability is inconsistent with a randomly-oriented sub-units model (see section 4.5). The lack of observed wavelength-dependence of position angle indicates that sub-units are generally aligned.

(v) Most blazars have spectra that are consistent with a power-law slope of infrared spectral index $\alpha \simeq 1.2$. There is, in general, no need to invoke a thermal component. There

is evidence to suggest that spectral curvature may be a common property of blazars (see section 4.6).

(vi) The January 1983 outburst of OJ 287 was observed with multi-colour photometry and polarimetry. The unusual behaviour is described by two superposed synchrotron spectra with differing spectral indices (see chapter 5). The huge rotations with wavelength require that the two dominant components have polarization vectors which are oriented at an angle to one another. The constancy of spectral slope combined with the variability of flux are explained in terms of a jet of electrons impinging upon two magnetic field regions.

(vii) It is unlikely that any reasonable distributions of magnetic field and electron energies can reproduce the behaviour observed in the infrared data for OJ 287. More generally, any single synchrotron source is unlikely to produce $dp/d \ln \nu < 0$ except for a convex spectrum, which is a rare, if not unknown, phenomenon in blazars (see section 6.3).

(viii) The unexpected $p(\lambda)$-p correlation is described in section 7.4. Together with results collated in section 7.6, we are able to summarise a phenomenological blazar model as follows:

a) Blazars, in general, may be considered as a superposition of a small number of aligned polarized sub-units.

b) They vary by turning on/off a relatively highly polarized, relatively shallow-sloped component.

c) When these components have comparable polarized

fluxes, significant wavelength-dependence may result (see section 7.7)

(ix) Theoretical considerations indicate that blazars are the result of the release of gravitational energy from an accretion disc surrounding a massive black hole. Electrons are accelerated by, for example, turbulence or a relativistic blast wave before impinging upon a strong magnetic field. The relativistic electrons then emit incoherent synchrotron radiation, which we assume to totally dominate any thermal emission from the accretion disc.

9.2 Future Work.

The ultimate aim of future work in the field of AGN in general and blazars in particular is to understand the physical processes which occur in these objects, and how blazars relate to all other extragalactic objects. To this end, a complete sample is required. Such a sample of so heterogeneous a class of object can only be the result of years of painstaking work. This would include optical polarization search techniques, optical identifications of radio sources, polarimetric monitoring of known quasars, etc.

A complete sample is vital for a number of reasons. Firtsly, it would allow a detailed statistical analysis of the polarimetric, variability and spectral properties of blazars. This would allow a meaningful comparison of all their properties with those of quasars. Secondly, it would enable us to calculate the local space density and the luminosity function. Knowledge of the luminosity function is critical to the "beaming statistics" discussed in section 1.2.

Long-term, multi-wavelength monitoring can be a very valuable technique. In our monitoring programme, multi-wavelength observations of just two objects, 0235+164 and OJ 287, have provided some of the most important insights into the workings of blazars. Such observations, however, require efficient organisation to overcome the inevitable problem of inertia which tends to beset such collaborations.

A very recently-developed technique, which will undoubtedly be of great value in the future, is that of Very Long Baseline Polarimetry (VLBP) (Roberts et al. 1984; Wardle et al 1984). This technique will provide direct evidence of several components and allow astronomers to probe the emitting regions of blazars in great detail (i.e. milliarcsecond).

It seems very likely that black holes with accretion discs are an important ingredient in any blazar model (see discussion in 8.5.3). There is much scope for further theoretical work in the field of black hole models for AGN; in particular, it would be of immediate interest to know whether geometrically thick accretion discs are stable. New observational techniques and multiwavelength monitoring programmes are probably the most promising areas of future research that will help to bridge the yawning gap between theory and observation in the field.

References.

Abramowicz, M.A., Calvani, M. & Nobili, L., 1980. Ap.J. 242, 772

Abramowicz, M.A. & Nobili, L., 1982. Nature 300, 506

Abramowitz, M. & Stegun, I.A. 1970 Handbook of Mathematical Functions (Dover)

Allen, D.A., Ward, M.J. & Hyland, A.R. 1982 Mon. Not. R. astr. Soc. 199, 969

Altschuler, D.R., 1980 A.J. 85, 1559

Andrew, B.H., Macleod, J.M., Locke, J.L., Medd, W.J., & Purton, C.R., 1969. Nature 223, 598

Angel, J.P.R., Boronson, T.A., Adams, M.T., Duerr, R.E. Giampapa, M.S., Gresham, M.S., Gural, P.S., Hubbard, E.N., Kopriva, D.A., Moore, R.L., Peterson, B.M., Schmidt, G.D., Turnshek, D.A., Wilkerson, M.S., Zotov, N.V., Maza, J. & Kinman, T.D., 1978. Pittsburgh Conference on BL Lac Objects, p.117, ed. Wolfe, A.M., Univ. of Pittsburgh.

Angel, J.P.R. & Stockman, H.S., 1980. Ann. Rev. Astr. Astrophys. 18, 321

Bailey, J., Cunningham, E.C., Hough, J.H. & Axon, D.J., 1981. Mon. Not. R. astr. Soc. 197, 627

Bailey, J., Hough, J.H. & Axon, D.J., 1983. Mon. Not. R. astr. Soc., 203, 339

Balonek, T.J. & Dent, W.A., 1980. Ap.J. 240,L3

Begelman, M.C., Blandford, R.D. & Rees, M.J. 1984. Rev. Mod. Phys. Vol 56, 255

Bjornsson, C-I., 1982. Ap.J. 260, 855

Bjornsson,C-I. & Blumenthal, G.R., 1982. Ap.J. 259, 805

Blades, J.C., Hunstead, R.W., Murdoch, H.S. & Pettini, M., 1982. Mon. Not. R. astr. Soc., 200, 1091

Blandford, R.D. & Konigl, A., 1979. Ap.J. 232, 34

Blandford, R.D. & Rees, M.J., 1974. Mon. Not. R. astr. Soc. 176, 443

Blandford, R.D. & Rees, M.J., 1978. Pittsburgh Conference on BL Lac Objects, p.328, ed. Wolfe, A.M., Univ. of Pittsburgh.

Bolton, J.G. & Wall, J.V. 1970. Aust J. Phys. 23, 789

Bregman, J.N., Glassgold, A.E., Huggins, P.J., Aller, H.D., Aller, M.F., Hodge, P.E., Rieke, G.H., Lebofsky, M.J., Pollock, J.T., Pica, A.J., Leacock, R.J., Smith, A.G., Webb, J., Balonek, T.J., Dent, W.A., O'Dea, C.P., Ku, W.H-M., Schwartz, D.A., Miller, J.S., Rudy, R.J., & Levan, P.D., 1984. Ap. J. 276, 454

Browne, I.W.A. & McEwan, N.J. 1972 Nat. Phys. Sci. 239, 101

Burbidge, G.R., Crowne, A.H. & Smith, H.E., 1977. Ap. J. Supp. 33, 113

Burstein, D. & Heiles, C., 1982 A.J. 87, 1165

Carswell, R.F., Strittmatter, P.A., Disney, M.J. Hoskins, D.G., Murdoch, H.S., 1973. Nat. Phys. Sci. 246, 89

Carswell, R.F., Strittmatter, P.A., Williams, R.E., Kinman, T.D. & Serkowski, K., 1974. Ap.J. 190, L101

Clarke, D. & Grainger, J.F., 1971. Polarized Light and Optical Measurement. (Pergammon).

Conover, W.J., 1971. Practical Non-Parametric Statistics (John Wiley & Sons).

Craine, E.R., Duerr, R. & Tapia, S., 1978. Pittsburgh Conference on BL Lac Objects, p.99, ed. Wolfe, A.M. Univ. of Pittsburgh.

Elliot, J.L. & Shapiro, S.L., 1974 Ap.J. Lett. 192, L3

Fabian, A.C. & Rees, M.J., 1978 IAU/COSPAR Symposium on X-ray Astronomy, eds. Baity, W.A. & Peterson, L.E., Pergammon Press, Oxford.

Gaskell, C.M., 1982. Ap.J. 252, 447

Gardner, F.F., Whiteoak, J.B. & Morris, D., 1975. Aust. J. Phys. Supp. 35

Gilmore, G., 1980. Mon. Not. R. astr.Soc. 190, 649

Glass, I.S., 1981. Mon. Not. R. astr.Soc. 194, 795

Glassgold, A.E. Bregman, J.N., Huggins, P.J., Kinney, A.L., Pica, A.J., Pollock, J.T., Leacock, R.J., Smith, A.G., Webb, J.R., Wisniewski, W.Z., Jeske, N., Spinrad, H., Henry, R.B.C., Miller, J.S., Impey, C.D.., Neugebauer, G., Aller, M.F., Aller, H.D., Hodge, P.E., Balonek, T.J. Dent, W.A., & O'Dea, C.P., 1983 Ap. J. 274, 101

Hewitt, A. & Burbidge, G. 1980. Ap. J. Supp. 43.

Hogbom, J.A., 1979. Astr. Astrophys. Supp. 36. 36, 173

Holmes, P.A., Brand, P.W.J.L., Impey, C.D. & Williams, P.M. 1984a Mon. Not. R. astr.Soc. (in press) (Paper III)

Holmes, P.A., Brand, P.W.J.L., Impey, C.D. & Williams, P.M. 1984b Mon. Not. R. astr.Soc. (in press) (Paper IV)

Holmes, P.A., Brand, P.W.J.L., Impey, C.D. & Williams, P.M. Smith, P., Elston, R., Balonek, T., Zeilik, M., Burns, J., Heckert, P., Barvainis, R., Kenney, J., Schmidt, G. & Puschell, J., 1984c. Mon. Not. R. astr.Soc. (in press) (H+13)

Impey, C.D. 1981. University of Edinburgh Thesis.

Impey, C.D., Brand, P.W.J.L., Wolstencroft, R.D. & Williams, P.M.,1982 Mon. Not. R. astr. Soc., 198, 1.

Impey, C.D., Brand, P.W.J.L. & Tapia, S., 1982. Mon. Not. R. astr. Soc. 200, 19 (Paper I)

Impey, C.D., Brand, P.W.J.L., Wolstencroft, R.D. & Williams, P.M.,1983. Mon. Not. R. astr. Soc. 209, 245 (Paper II)

Jones, T.W., O'Dell, S.L. & Stein, W.A. 1974. Ap.J. 192, 261

Kardashev, N.S., 1962. Soviet Astronomy-A.J. Vol.6 No.3, 317

Kikuchi, S., Mikami, V., Konno, M. & Inoue, M., 1976. Publs. astr. Soc. Japan., 28, 117

Kinman, T.D., 1976. Ap.J. 205, 1

Korchakov, A.A. & Syrovatskii, S.I. 1962. Soviet Astr-A.J. 5, 678

Knacke, R.F., Capps, R.W. & Johns, M., 1976. Ap. J. Lett., 219, L69

Laing, R.A., 1980. Mon. Not. R. astr. Soc. 193, 439

Ledden, J.E. & Aller, H.D. 1979. Ap.J. 229, L1

Ledden, J.E., Aller, H.D. & Dent, W.A., 1976. Nature. 260, 752

Lynden-Bell, D., 1978. Phys. Scr. 17, 185

Macklin, J.T., 1982. Mon. Not. R. astr. Soc. 199, 1119

Macleod, J.M. & Andrew, B.H., 1968. Ap. Lett. 1, 243

Malkan, M.A.. 1983. Ap.J. 268, 582

Maraschi, L., Tanzi, E.G., Treves, A. and Falomo, R. 1983. Astron. Astrophys. 127, L17

Marscher, A.P., 1980. Ap.J. 239, 296

Mattig, W., 1958. Astr. Nachr., 184, 109

Miller, J.S. & French, H.B., 1978. Pittsburgh Confernce on BL Lac Objects, p.228, ed. Wolfe, A.M. University of Pittsburgh

Miller, J.S., French, H.B. & Hawley, S.W., 1978. Pittsburgh Conference on BL Lac Objects, p.176, ed. Wolfe, A.M., Univ. of Pittsburgh.

Miller, J.S., 1978. Comm. Astrophys. 7, 175

Moore, R.L. & Stockman, H.S., 1983. Ap. J. (in press)

Norman, M.L. Smarr, L.L., Wilson, J.R. & Smith, M.D. 1981 Ap. J. 247, 52

Norsieck, K.H., 1976. Ap. J. 209, 653

O'Dell, S.L., Puschell, J.J., Stein, W.A., Owen, F., Porcas, R.W., Mufson, S., Moffett, T.J. & Ulrich, M-H. 1978. Ap.J. 224, 22

Oke, J.B., Neugebauer, G. & Becklin, E.E., 1969. Ap. J. 156, L41

Pettini, M., Hunstead, R.W., Murdoch, H.S. & Blades, J.C., 1983. Ap. J. 273, 436

Puschell, J.J. & Stein, W.A., 1980. Ap. J, 237, 331

Rees, M.J. 1971. Nature 229

Rees, M.J. 1978. Phys. Scripta. 17, 193

Rieke, G.H., Grasdalen, G.L., Kinman, T.D., Hintzen, P., Wills, B.J. & Wills, D., 1976. Nature, 260, 154

Roberts, D.H., Wardle, J.F.C., Potash, R.I., & Rodgers, A.E.E., 1984. Bull. Am. Astr. Soc. Vol.16 No.2 35.02

Savage, B.D. & Mathis, J.S., 1979. Ann. Rev. Astr. Astrophys. 17, 73

Schmidt, M. 1974. Ap. J., 193, 605

Schmitt, J.L. 1968. Nature 218, 663

Sikora, M. & Wilson, D.B. 1981. Mon. Not. R. astr. Soc. 197, 529

Smith, M.G. 1984. Preprint of the Royal Observatory Edinburgh.

Spinrad, H. & Smith, H.E., 1975. Ap. J. 201, 275

Spitzer, L., 1971. Active Galactic Nuclei, ed. O'Connell (North-Holland), 443

Sramek, R.A. & Weedman, D.W., 1980. Ap. J. 238, 435

Stein, W.A., O'Dell, S.L. & Strittmatter, P.A., 1976. Ann. Rev. Astr. Astrophys. 14, 173

Stockman, H.S., 1978. Pittsburgh Conference of BL Lac Objects, p.149 ed Wolfe, A.M., University of Pittsburgh

Stockman, H.S., Moore, R.L. & Angel, J.R.P., 1984. Ap. J. 279, 485

Strittmatter, P.A., Carswell, R.F., Gilbert, G., & Burbidge, E.M. Ap.J. 190, 509

Tapia, S., Craine, E.R., Gearhart, M.R., Pacht, E. & Kraus, J. 1977 Ap.J.Lett. 215, L71

Tapia, S., Craine, E.R. & Johnson, K., 1976. Ap. J. 203, 291

Valtaoja, E., Lehto, H., Teerikorpi, P., Haarala, S., Korhonen, T., Valtonen, M., Terasranta, H., Salonen, E., Urpo, S., Tiuri, M., Piirola, V., 1982. Turku Univ. Obs. Informo No. 62

Veron, P. & Veron, M.P., 1975. Astron. Astrophys. 39, 281

Vinokur, M., 1965 Ann. D'Astrophys 28, 412

Visvanathan, N.,1969. Ap. J. 155, L133

Visvanathan, N. & Elliot, J.L., 1973. Ap. J. 179, 721

Wardle, J.F.C., 1977. Nature 269, 563

Wardle, J.F.C., 1978. Pittsburgh Conference of BL Lac Objects, p.39, ed. Wolfe, A.M., University of Pittsburgh.

Wardle, J.F.C. & Kronberg, P.P. 1974. Ap. J. 194, 249

Wardle, J.F.C., Roberts, D.H., Potash, R.I. & Rogers, A.E.E., 1984. Bull. Am. Astr. Soc. Vol.16, No.2 35.03

Weiler, K.W. & Johnston, K.J., 1980. Mon. Not. R. astr. Soc. 190, 269

Westfold, K.C. 1959. Ap. J. 130, 241

Wills, B.J., 1976. A.J. 81, 1031

Wills, D. & Wills, B.J., 1976. Ap. J. Supp., 31, 143

Wolstencroft, R.D., Gilmore, G. & Williams, P.M., 1982. Mon. Not. R. astr. Soc., 201, 479

Zekl, H., Klare, G. & Appenzeller, I., 1981. Astron, Astrophys. 103, 342